



UNIVERSITÀ
DEGLI STUDI
FIRENZE

DOTTORATO DI RICERCA IN
SCIENZE CHIMICHE

CICLO XXXI

COORDINATORE Prof. Piero Baglioni

**Glycoconjugated dyes: dye removal and evidence
of self-assembly in solution through spectrophotometric
and scattering techniques**

Settore Scientifico Disciplinare CHIM/06

Dottorando:
Dott. Silvia Fogli

Tutore:
Prof. Roberto Bianchini

Coordinatore:
Prof. Piero Baglioni

Anni 2015/2018

Contents

1	Introduction	1
2	Physico-chemical characterization	7
2.1	Introduction	7
2.2	Glycoconjugated dyes in solution	8
2.3	Solvent mixtures	26
2.4	Interaction between glycoconjugated dyes	32
2.5	GDs interaction with surfactants	41
2.5.1	Reentrant Condensation	53
2.6	Experimental	64
2.6.1	Glycoconjugated dyes	64
2.6.2	Materials	67
2.6.3	UV-Visible spectrophotometry	67
2.6.4	Dynamic Light Scattering	67
2.6.5	Small Angle X-rays Scattering	67
2.6.6	Circular Dichroism	68
2.6.7	Atomic Force Microscopy	68
3	Computational study	71
3.1	Introduction	71
3.2	Molecular Dynamics on GDs monomers	73
3.3	Molecular Dynamics on GDs dimers	76
4	Bioremediation of glycoconjugated dyes	87
4.1	Introduction	87
4.2	Simulated effluents: <i>Funalia trogii</i>	88

CONTENTS

4.3	Real effluents: Activated sludge	103
4.4	Experimental	107
4.4.1	Effluents	107
4.4.2	Bioremediation methodology with <i>Funalia trogii</i>	108
4.4.3	Enzyme activity test	111
4.4.4	Bioremediation procedure with activated sludge	111
4.4.5	Color removal	112
4.4.6	Aromatic Amines	112
4.4.7	Materials	113
4.4.8	UV-Visible spectrophotometry	113
4.4.9	Mass spectrometry	114
5	Conclusion	115
	Bibliography	119

Table of abbreviations

GDs	Glycoconjugated dyes
NR202	Naturalized disperse red dye 202
NB27	Naturalized disperse blue dye 27
NO30	Naturalized disperse orange dye 30
NY42	Naturalized disperse yellow dye 42
NRC1	Naturalized red chromophore synthesized by L. Calugi (Calugi 2018)
MeOH	Methanol
DMSO	Dimethylsulfoxide
EtOH	Ethanol
MIX	Equimolal mixture of NR202, NB27, NO30 and NY42
M1	NR202+NB27 mixture
M6	NY42+NO30 mixture
M8	NB27+NY42+NR202 mixture
M14	NRC1+NO30 mixture
ACFs	Autocorrelation functions
SAXS	Small Angle X-Rays scattering
DLS	Dynamic Light Scattering
(E)CD	Electronic Circular Dichroism
AFM	Atomic Force Microscopy
MS	Mass Spectrometry

CONTENTS

- TX** TritonX-100
- CTAB** Cetil trietilammunium Bromide
- SDS** Sodium Dodecylsulfate
- RC** Reentrant Condensation
 - F** Bioremediation with *F. trogii*
- FG** Bioremediation with *F. trogii* and glucose
- DF** Bioremediation with dead *F. trogii* biomass
- LP** Lactose piperazine
- AS** Activated sludge
- AC** Active carbon
- RE1** Real effluent with composition 80% NY42, 20% NO30
- RE2** Real effluent with composition 5% NR202, 90% NO30, 5% NB27
- RE3** Real effluent with composition 72% NY42, 18% NO30, 10% NB27
- RE4** Real effluent with composition 40% NY42, 10% NO30, 50% NB27
- QM** Quantum Mechanics
- DFT** Density Functional Theory
- MM** Molecular Mechanics
- MD** Molecular Dynamics
 - FF** Force Field

Chapter 1

Introduction

Dyes are everywhere in our everyday life. They are used in textile, leather and paper dyeing as well as in cosmetics, food and drinks. Thus, it is clearly important to fully understand their properties and behavior. In this context, the attention is focused on those dyes used in textile and leather dyeing. In this particular field, several kind of dyes with different characteristics can be employed, depending on the substrate. Reactive dyes are one of these types of compounds and they are chromophores containing a substituent that reacts with OH, SH and NH₂ groups present on the substrate, forming a covalent bond.[15, 33, 79] These dyes are more commonly used in dyeing natural fibers, such as cotton, flax or wool. A second kind of chromophores are Direct dyes. They are water-soluble molecules that adhere to the substrate by non-ionic forces. This dyes usually contain extended aromatic systems that lead to aggregation by hydrophobic effect. Their aggregation allows to set them on substrates, between interstices of fibers.[15, 33, 79] They are typically used in dyeing textiles with high cellulose content, e.g. cotton or viscose rayon. Disperse dyes are yet another kind of substances used in dyeing processes. These molecules have low water solubility and are used in highly dispersed state by action of dispersing agents such as surfactants.[15, 33, 79] Thus, dyeing processes that involve disperse dyes have a high environmental impact, since large quantities of additives are employed. Despite these drawbacks, disperse dyes have very good technical qualities, such as brightness, as well as light and thermal fastness. Therefore, they represent a very appealing candidate for a

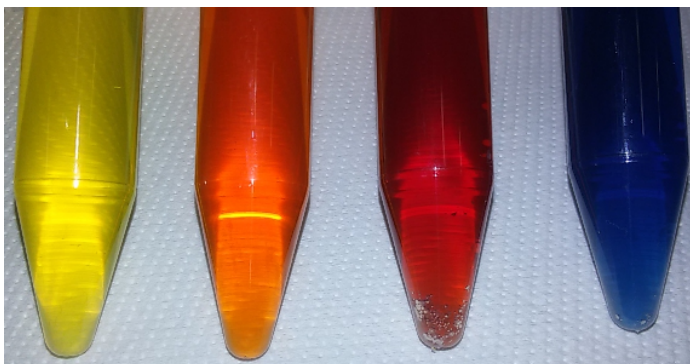


Figure 1.1: GDs 1 mgml^{-1} water solutions.

modification, in order to increase their water solubility and eco-sustainability. Few years ago, Bianchini et al. [6, 7] perfected the glycoconjugation process, that involved the modification of disperse dyes with a sugar, in particular lactose. Chromophores were isolated from commercially available disperse dyes formulations and specifically modified to be conjugated with lactose. Lactose was also modified, inserting a piperazine unity. Among many sugars, lactose was chosen because it is a natural product available at low cost, since it is obtained every day in large amounts as waste product from dairy industry. Therefore, the use of lactose was not only cost effective, but also represented an environment friendly choice, since it allowed to reuse a waste material. From the modification of disperse chromophores with lactose, Bianchini et al. [6, 7] obtained the so called Naturalized or Glycoconjugated Dyes (GDs). These compounds were composed by a hydrophobic core, the chromophore, and a hydrophilic part, lactose, connected by a linker. GDs were able to dissolve in water without the addition of surfactants or salts, as shown in Fig. 1.1, demonstrating the efficacy of sugar conjugation in increasing their affinity with water medium. To verify that the insertion of lactose on the chromophore did not affect its technological qualities, GDs dyeing abilities were tested on a variety of substrates. This trial demonstrated that not only disperse dyes good qualities were maintained in GDs, but also that the substrates they were able to dye had been extended. In fact, GDs efficiently dyed not only polyester and other synthetic fibers, such as nylon, but also natural ones, e.g. wool and hair, as well as leather, as shown in Fig. 1.2. GDs represented very promising



(a) Polyester



(b) Leather



(c) Hair

Figure 1.2: Samples of synthetic and natural fibers, as well as leather, dyed using GDs.

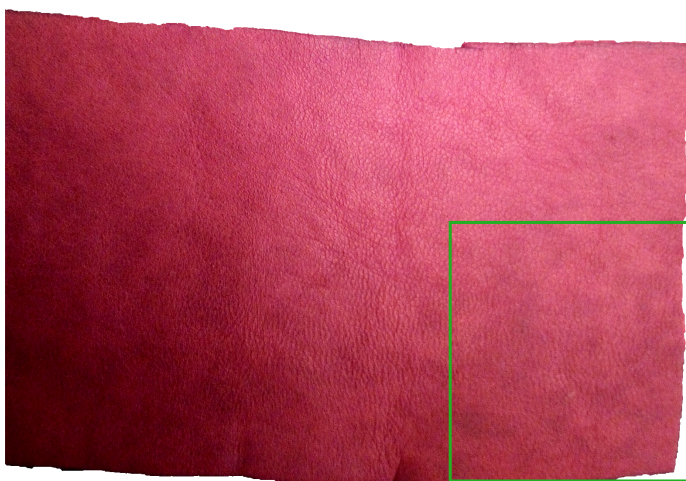


Figure 1.3: Sample of leather dyed with a red GD by Biokimica group s.r.l. for BioNaD LIFE project. Color deposition resulted uneven, as dye accumulated in some areas (green square).

candidates for an industrial application in dyeing. In fact, they were object of an European LIFE project, BioNaD, that involved a scale up of GDs synthesis, leather dyeing tests at semi-industrial scale and dye removal studies on simulated and real effluents, performed by partners: Università di Firenze, CNR-ICCOM, Gruppo Biokimica., Serichim s.r.l. and INESCOP. Tests on a larger scale underlined a variability of dyeing performances between different GDs. A noticeable example was leather dyeing using a red chromophore, that resulted in a non uniform coloring of the substrate. In particular, the dye accumulated in some areas, resulting in a spotted color deposition, as shown in Fig. 1.3. To understand this phenomenon another effect on GDs properties, caused by the conjugation of lactose, had to be taken into account. The presence of both a hydrophilic and a hydrophobic part on the same molecule gave GDs an amphiphilic character, and with it the ability to form aggregates in solution by self-assembly. [70] The presence of aggregates could affect GDs dyeing abilities, therefore it was mandatory to understand their behavior in solution. In this PhD project, GDs were studied from three different point of view, each of which correspond to a section of this work. In the first part, a thorough physico-chemical investigation was performed on five GDs in solu-

tions (NR202, NB27, NO30, NY42, NRC1), whose molecular structures were reported in Fig. 1.4. As can be appreciated from their structures, these five dyes had different nature: NR202 and NO30 were azo dyes, NB27 and NRC1 were anthraquinone dyes and NY42 was an aniline dye. Four of them were object of LIFE project BioNaD, while the fifth, NRC1, was synthesized by L. Calugi during as part of his own PhD project. [12] GDs characterization involved a variety of experimental techniques, including UV-Visible absorption, Light and X-Rays scattering, Electronic Circular Dichroism and Atomic Force Microscopy. The results confirmed the presence of self-assembled aggregates in water and gave some insights on their structure and shape. The influence of solvents and of interaction with other GDs, as well as other species, e.g. surfactants, was also evaluated. GDs behavior and aggregation were further investigated in the second part of this project, using computational tools. In particular, Molecular Dynamics for monomers, dimers and trimers were obtained by Force Fields calculations in vacuum and their conformations were evaluated and classified. Moreover, in light of their possible industrial application in dyeing processes, it was also important to investigate the end of GDs life cycle: their removal from simulated and real dyeing effluents. In fact, leather and textile dyeing are one of the more serious cause of pollution. Not only the remediation of their wastewater is difficult, since they contain a wide variety of pollutants, such as surfactants, inorganic salts and dyes themselves, but also some of their degradation products can be even more dangerous.[36, 39] An example are azo dyes, whose degradation can produce carcinogenic aromatic amines.[49, 59, 67, 68] Therefore, the third and final part of this study consisted in the remediation of GDs effluents using two different biotechnological approaches. The first one, applied on simulated GDs effluents at lab scale, involved a non standard bioremediation procedure using a white-rot fungus, *F. troglia*. The second was a standard bioremediation procedure based on activated sludge and was performed on real GDs leather dyeing effluents, provided by Gruppo Biokimica, that performed large scale dyeing tests for BioNaD LIFE project. It was possible to demonstrate that both standard and non-standard bioremediation procedures could achieve good dye removal performances on GDs effluents.

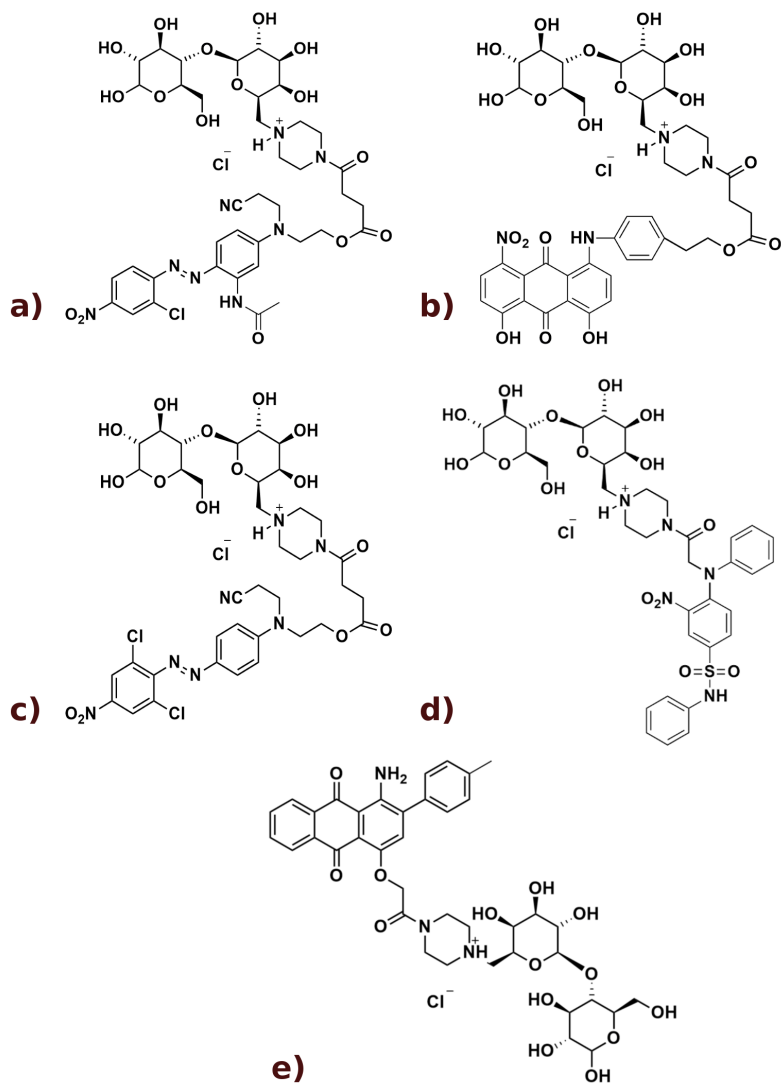


Figure 1.4: Molecular structures of the five GDs object of this work: a) NR202, b) NB27, c) NO30, d) NY42, e) NRC1.

Chapter 2

Physico-chemical characterization

2.1 Introduction

Glycoconjugated dyes (GDs) are a relatively new class of compounds, that have not yet been employed in large scale industrial dyeing processes. Their physico-chemical properties have not been investigated. However, it is important to fully understand the behavior of these systems in solution, since their characteristics and properties are very likely to affect their interaction with substrate and, with that, their dyeing ability. For instance, the amphiphilicity of these molecules allows the formation of self-assembled aggregates in solution and aggregation could interfere with substrate binding, for example making a functional group unavailable. Therefore, GDs physico-chemical characterization was mandatory. A thorough investigation successfully demonstrated the presence of GDs self-assembled aggregates in water solutions, underlining the strong influence of the working conditions. The effects of several parameters on GDs self-assembly were tested. Dye concentration, solvents, interaction with other GDs as well as with surfactants of different nature were all taken into account. The properties of these structures and the influence of each parameter were studied using a variety of methods including UV-Visible absorption, Light and X-Rays scattering, Electronic Circular Dichroism (ECD) and Atomic Force Microscopy (AFM).

2.2 Glycoconjugated dyes in solution

The study of GDs behavior in solution naturally started from their absorption properties in water. Their absorption spectra, reported in Fig. 2.1, were registered at a concentration of 1 mgml^{-1} . All dyes showed broad peaks in the visible region and, in some cases, sharper and more intense peaks at higher energy. The broadness of the peaks in the visible region could be an indication of a very high density of electronic states, due to their aggregation in water.[62] In particular, the presence of a second band at 418 nm for NR202 could be a proof of its aggregation, [10, 63, 74] as well as the tailing at long wavelengths of the main band, that could be caused by the scattering of large suspended objects. Further observations were carried out taking into account the influence of a

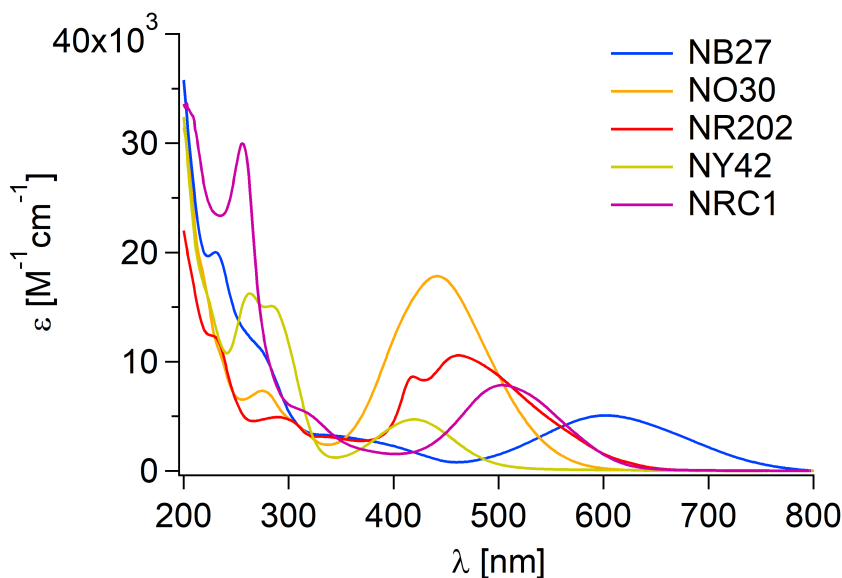


Figure 2.1: Absorption spectra of the five GDs in water at a concentration of 1 mgml^{-1} .

first parameter, their concentration, on GDs absorption. Samples of each dye at five different concentrations ($1, 0.6, 0.3, 0.15, 0.075 \text{ mgml}^{-1}$) were prepared and their absorption measured. The spectra obtained for NB27, NO30, NY42 and NRC1 were reported in Fig. 2.2. It was evident that the decrease in concentration didn't cause any substantial changes in the absorption of these four

dyes. The only variation was a gradual bathochromic shift of 5 nm for NO30 increasing the concentration from 0.075 mgml^{-1} to 1 mgml^{-1} , that could be related to increasing aggregation. On the contrary, the changes induced by

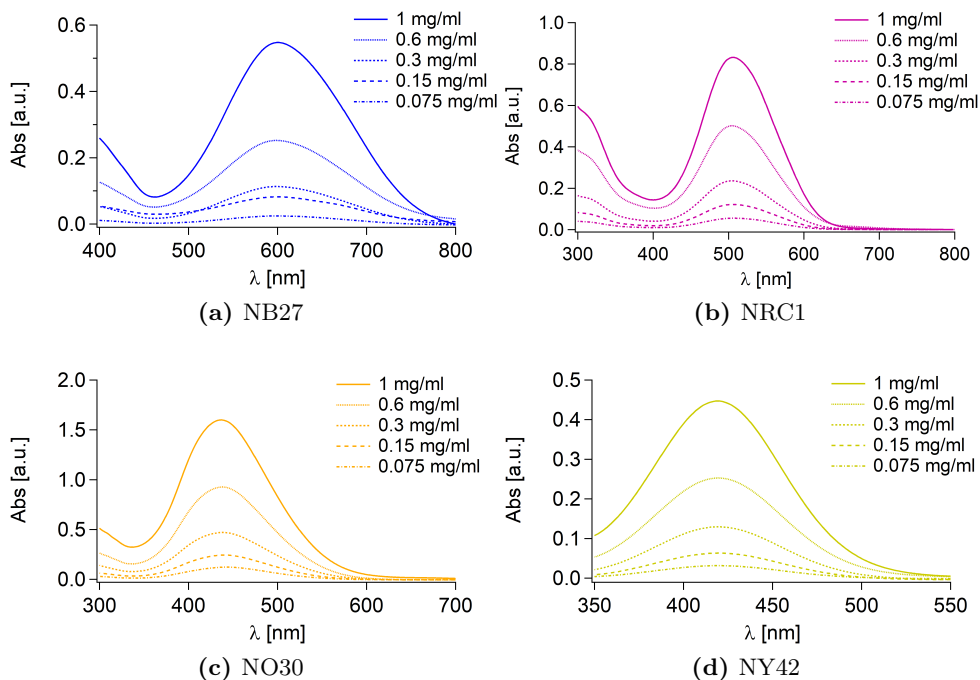


Figure 2.2: Absorption spectra of four GDs (NB27, NRC1, NO30, NY42) at five concentrations: 1, 0.6, 0.3, 0.15 and 0.075 mg/ml.

concentration on NR202 were significant. In fact, the variations were so consistent that five more dye concentrations were taken into account to widen the research: 3.75^{-2} , 1.88^{-2} , 9.38^{-3} and $4.69^{-3} \text{ mgml}^{-1}$. Absorption spectra were normalized to underline the differences between the several concentrations. As can be noticed in Fig. 2.3a, two main changes took place in NR202 at different dye concentration. First of all, the second band at 418 nm increase its intensity with the increase of concentration from $4.69^{-3} \text{ mgml}^{-1}$ to 0.15 mgml^{-1} . This was accompanied by a second variation, consisting in a hypsochromic shift of λ_{max} for the band at 460 nm. However, further increasing dye concentration from 0.15 to 1 mgml^{-1} resulted in a decrease of the intensity of the band at

418 nm, as well as in λ_{max} of the band at 460 nm shifting back to lower energies. Variations between $4.69 \cdot 10^{-3}$ and 0.15 mgml^{-1} could be caused by the intensification of aggregation [3, 9, 10, 20, 44, 63, 74] related to the higher amount of dye in solution. The increase in aggregates dimensions, followed by

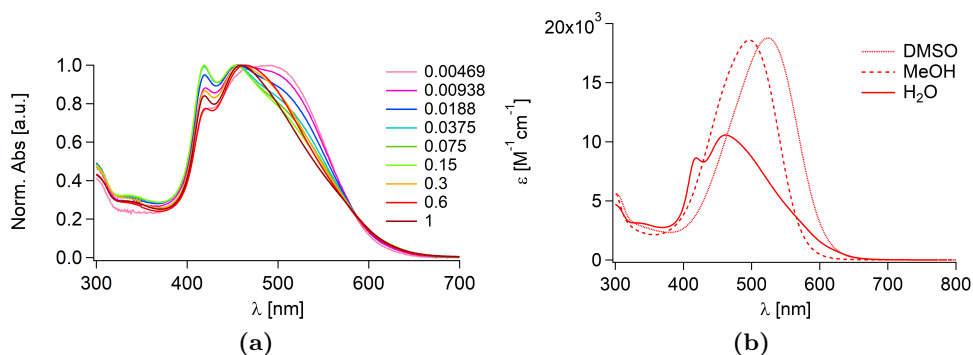


Figure 2.3: a) NR222 normalized absorption spectrain H_2O at several dye concentrations between 1 and $4.69 \cdot 10^{-3} \text{ mgml}^{-1}$. b) Comparison between NR222 absorption spectra in H_2O , MeOH and DMSO at a single concentration: 1 mgml^{-1} .

precipitation could be responsible for the subsequent decrease in the intensity of the aggregation band at 418 nm. To better understand this peculiar behavior, the influence of another important parameter was taken into account: the solvent. Since GDs are amphiphiles, they potentially could behave differently in solvents other than water. Thus, their absorption was measured in two polar organic solvents, one protic and one aprotic, Methanol (MeOH) and Dimethylsulfoxide (DMSO). Results for NR222 (Fig. 2.3b) showed significant variations in terms of ϵ and λ_{max} values, as well as a massive change in the shape of the spectrum. In particular, the peak in the visible region sharpened and lost the band at 418 nm, while λ_{max} consistently shifted at lower energies. The entity of this shift was different in MeOH and DMSO and their exact values were reported in Table 2.1. Moreover, the ϵ value showed a twofold increase from water to organic solvents (Table 2.1). The substantial change in its absorption properties, suggested that MeOH and DMSO were both good solvents for NR222, ensuring its complete dissolution. In analogy, water could be defined as a “poor” solvent for this dye since it promoted dye aggregation.[3, 63, 74] The influence of solvents was tested also on the other four GDs, observing the

Table 2.1: Summary of the λ_{max} and ϵ values for GDs in H₂O, MeOH and DMSO. For GDs in MeOH and DMSO also the shifts in λ_{max} (B: bathochromic, H: hypsochromic) and the percent increase in ϵ are reported, using values registered in water as reference.

H₂O						
	NR202	NB27	NO30	NY42	NRC1	
$\lambda_{max}(nm)$	457	601	442	419	506	
ϵ (cm ⁻¹ M ⁻¹)	10200	4900	17000	4400	7800	
MeOH						
	500	609	415	411	516	
$\lambda_{max}(nm)$	20400	8200	20000	4300	11200	
ϵ (cm ⁻¹ M ⁻¹)	Shift (nm)	(B) 43	(B) 8	(H) 27	(H) 8	(B) 10
+ $\epsilon\%$	101.1	68.3	17.7	-	42.8	
DMSO						
	523	610	431	421	518	
$\lambda_{max}(nm)$	19500	9000	18000	4400	11000	
ϵ (cm ⁻¹ M ⁻¹)	Shift (nm)	(B) 66	(B) 9	(H) 11	-	(B) 12
+ $\epsilon\%$	92.3	84.2	6.02	(B) 2	39.2	

variations of their absorption properties induced by MeOH and DMSO. In both organic solvents, NB27, NO30 and NRC1 showed sharper peaks, increased ϵ values and more or less significant shift in λ_{max} (Table 2.1). In analogy with NR202 case, these variations could indicate that MeOH and DMSO completely dissolved these GD, at variance with water, in which they could aggregate. For NY42, the changes in λ_{max} in DMSO and in ϵ in both cases were negligible (Fig. 2.4c). All GDs but NY42 showed an increase in ϵ values in both the organic solvents compared to water. The entity of this increase was not the same for all dyes, reaching the highest value for NR202 and the lowest for NO30. The shift in λ_{max} were both bathochromic and hypsochromic, depending on the dye taken into account. NR202, NB27 and NRC1 all showed bathochromic shifts of different consistency, both in DMSO and MeOH. On the contrary, NO30 and NY42 gave hypsochromic shifts, even though NY42 in DMSO did not show a significant one. Changes in concentration and solvent particularly affected NR202 behavior in solution. A bathochromic shift took place for either a decrease in concentration or a change in solvent. Both these variations seemed to favor a different transition in the spectrum, one at lower energy than that taking place at high NR202 concentrations in water. This contribution at longer wavelengths could probably be ascribed to the isolated dye molecule.

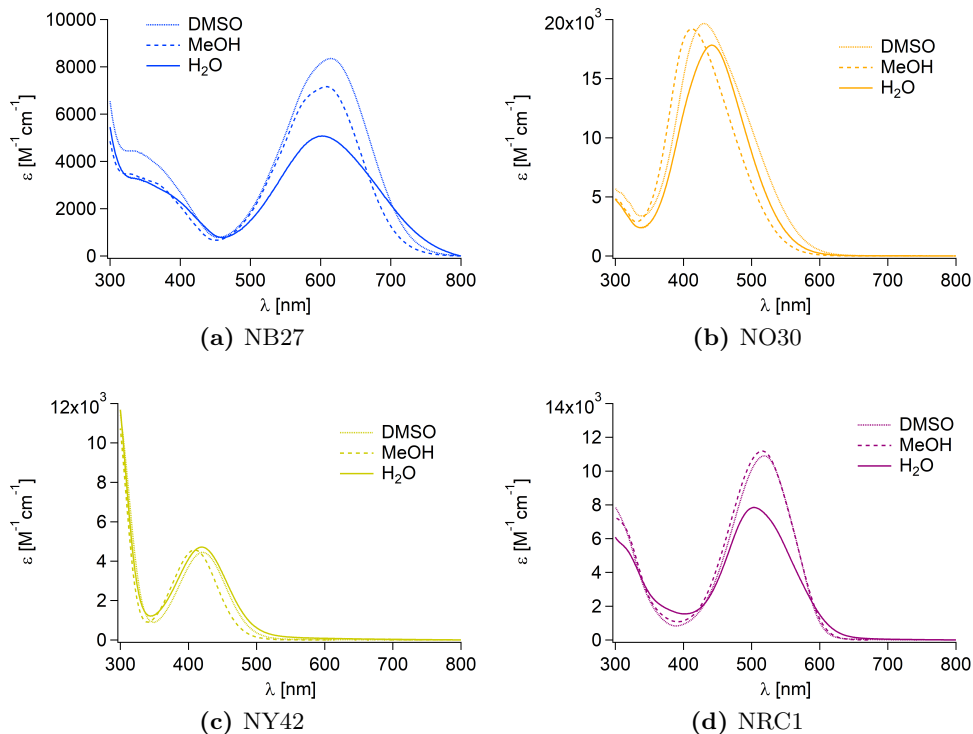


Figure 2.4: Comparison between the absorption spectra of the five GDs in H_2O , MeOH and DMSO at a concentration of 1 mgml^{-1} .

In fact, this would be the only contribution in a non-aggregated system, like a very diluted water solution or a good solvent solution. Since all GDs share the same amphiphilic character, it was possible to hypothesize that all of them aggregated in water, but not in organic solvents. This hypothesis was further investigated by DLS, SAXS and ECD investigations, as well as absorption studies on mixed solvents, reported in Section 2.4. The formation of self-assembled aggregates in water was confirmed using Dynamic Light Scattering. Samples of each dye at a concentration of 0.1 mgml^{-1} were studied. Since the two laser lines we used were at $\lambda = 532$ and 633 nm , a lower dye concentration was used in this case, to avoid an excess of absorption of the beam light. Autocorrelation functions (ACFs) were registered for NR202, NO30, NY42 and NRC1 (Fig.

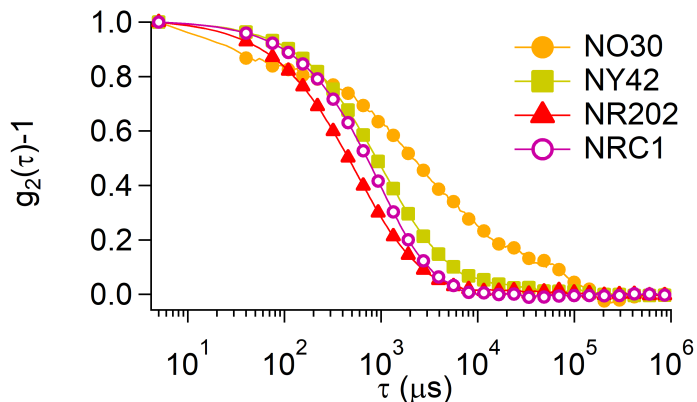


Figure 2.5: Autocorrelation functions for NR202, NO30, NY42 and NRC1 in water at a concentration of 0.1 mgml^{-1} .

2.5), but not for NB27, because for this dye the absorption was still too high to obtain a reliable function. However, since a small amount of absorption was present for all the GDs, these results must be intended as an indication. The ACFs were analyzed by CONTIN,[60] obtaining information on the hydrodynamic diameter of the objects in solution, as well as on their polydispersity. For all of them, the very high polydispersity indicated the presence of aggregates having very different diameters, from a few nanometers up to a micron. This was confirmed by diameters distributions of the objects in solution, reported in Fig. 2.6. These distributions underlined the presence of at least two populations for each of the four GDs. The dimensions of the aggregates were different for each dye. NR202 and NRC1 (Fig. 2.6a-2.6d) both had one population of objects with dimensions around 100 nm and another one around 500 nm. NO30 (Fig. 2.6b) had a small amount of object of about 10 nm and a population of aggregates with average diameter 100 nm. However, considering both the average diameter obtained by CONTIN [60] analysis and its ACF, NO30 it was likely to possess very big aggregates, with dimensions over the μm . This objects could not be taken into account since their diameter was higher than the experimental sensibility of this technique. Finally, NY42 (Fig. 2.6c) had one population with diameters around 250 nm and another one of over 800 nm, that probably comprehended some objects with dimensions over the μm . Average hydrodynamic diameters of all GDs and their polydispersity

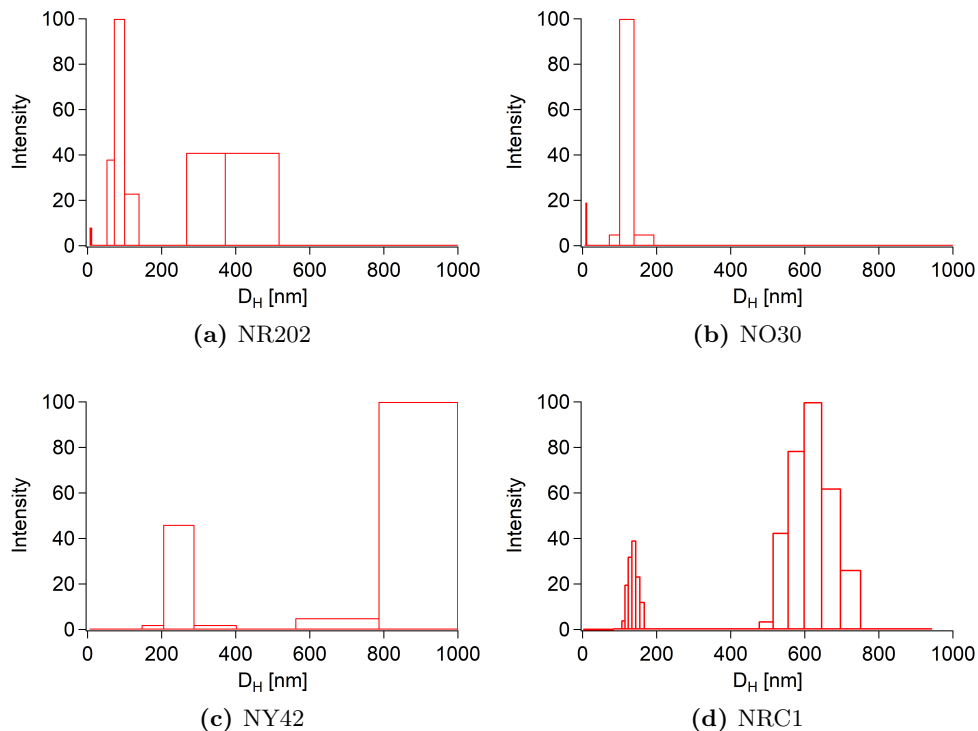


Figure 2.6: Size distribution of the aggregates present in GDs 1 mgml^{-1} water solutions reported as a function of scattering intensity.

Table 2.2: Summary of the information obtained by DLS and SAXS analysis. For each dye are reported: hydrodynamic diameter (D_H) and polydispersity (PDI) extrapolated by CONTIN [60] analysis on DLS ACFs; radius, length and number of aggregation of the aggregates in solution obtained fitting SAXS curves where possible.

DLS	NR202	NB27	NO30	NY42	NRC1
D_H (nm)	205.3 ± 4.2	–	352.9 ± 195.2	382.0 ± 14.9	312.7 ± 3.5
PDI	0.350 ± 0.005	–	0.388 ± 0.036	0.341 ± 0.014	0.310 ± 0.012
SAXS					
radius (nm)	2.8	3.7	3.6	–	–
length (nm)	28	–	–	–	–
n° agg.	241	18	17	–	–

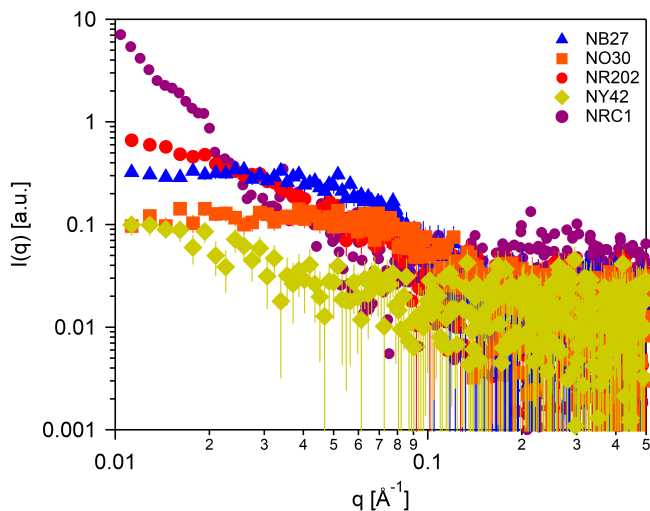


Figure 2.7: Comparison between the SAXS curves of the five GDs in water at dye concentration 1mgml^{-1}

were reported in Table 2.2. The same light scattering study was also performed on all GDs in MeOH and DMSO, but no ACFs could be registered. Moreover, SAXS investigation on the same GDs solutions in both organic solvents, at the same dye concentration, could not reveal the presence of aggregates. These specific results provided unquestionable proof of the absence of GDs aggregation in organic solvents. Thus, the initial hypothesis, according to which GDs self-assembled only in water, was confirmed. GDs water solutions were further characterize using SAXS. This technique is complementary to DLS since two techniques work in different dimensional range. In particular, SAXS analyses objects with dimensions in the 0.5-50 nm range, while DLS covers bigger objects, with diameters up to $1\ \mu\text{m}$. However, a direct comparison with DLS could not be performed because of the low X-ray scattering of $0.1\ \text{mgml}^{-1}$ sample. SAXS analysis on $1\ \text{mgml}^{-1}$ water solutions, underlined the presence of aggregates for all GDs, including NB27, for which an ACF could not be registered by DLS. A comparison between the five curves registered for water solutions (Fig. 2.7) underlined that the region at low q for these curves were different, implying that GDs formed different aggregates in water. In particular, NO30 and NB27 had a Guinier region at low q , suggesting the presence

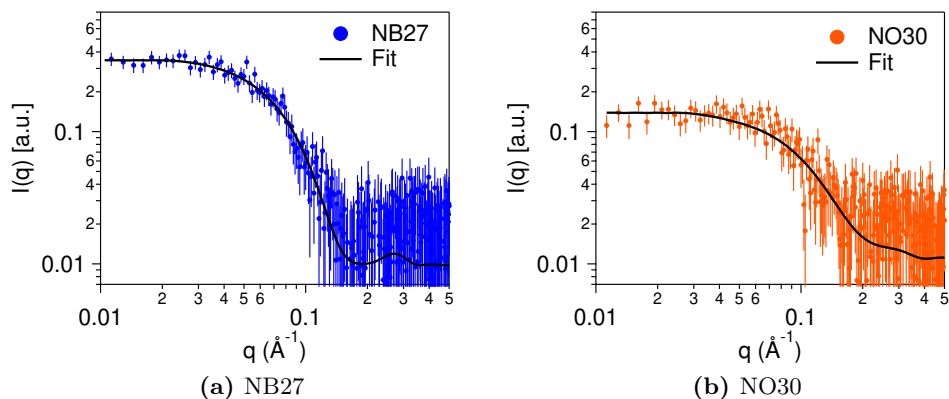


Figure 2.8: SAXS curves of 1mgml^{-1} a) NB27 and b) NO30 water solutions and their fitting.

of spheroidal aggregates. On the contrary, NR202, NY42 and NRC1 all had negative slope in these q region indicating objects dimensions above the limit of the instrument (>70 nm). However, these slopes had different values for the three dyes. Power-law fitting of this region of the curves revealed that NR202 and NY42 had a slope of -1 , showing the typical profile of elongated objects (e.g. cylinders or ellipsoid). The same analysis on NRC1 linear region between 0.01 and 0.06 \AA^{-1} revealed a -3 slope. Each curve was then fitted using the appropriate function. NB27 (Fig. 2.8a) and NO30 (Fig. 2.8b) were fitted using the Core-Shell Sphere function and through this analysis it was possible to obtain the dimension of the aggregates, as well as their number of aggregation (Table 2.2). The curves registered for NR202 and NY42 were fitted using a Core-Shell Cylinder function. It was possible to obtain radius, length and number of aggregation for NR202 (Table 2.2 from the fitting but this analysis was not possible for NY42, because the sample had a very poor scattering and, as a result, the curve was very noisy. NRC1 was instead fitted with a power law function. Its slope in the Guinier region was -3 could be, according to the literature, an indication of macroscopic aggregation.[11, 19] Moreover, considering NRC1 molecular structure, it was hypothesized that dye molecules would arrange in H-aggregates, in analogy with what observed by Dirian et al.[19]. Since lactose is a chiral structure, its conjugation to the chro-

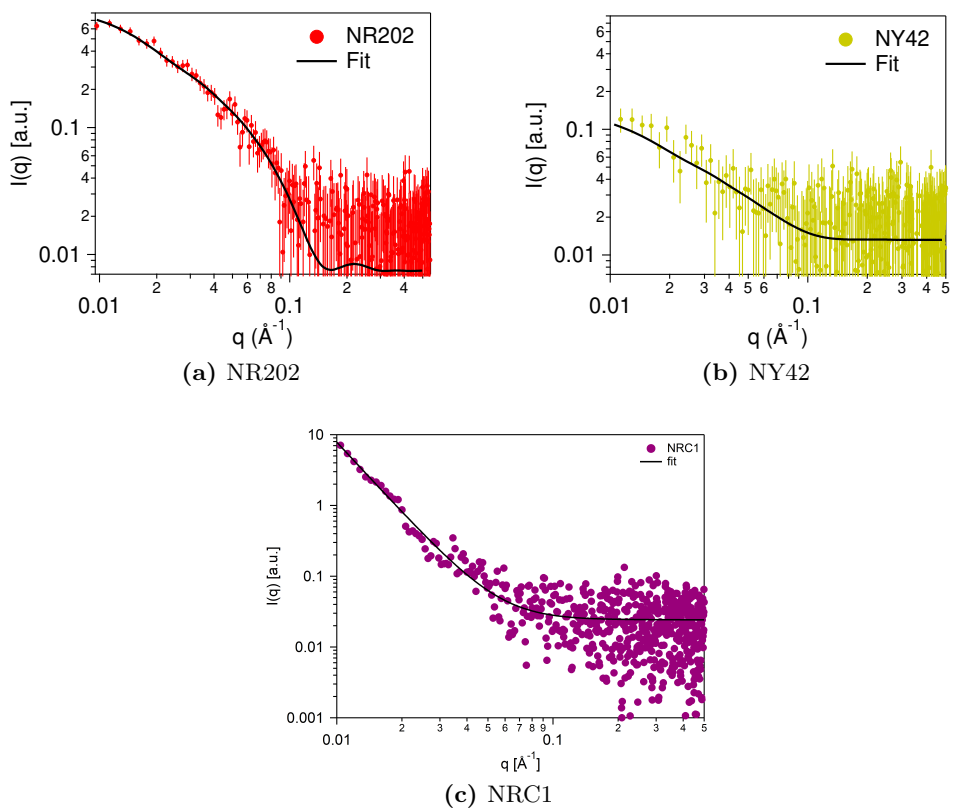


Figure 2.9: SAXS curves of 1mgml^{-1} a) NR202, b) NY42 and c) NRC1 water solutions and their fitting.

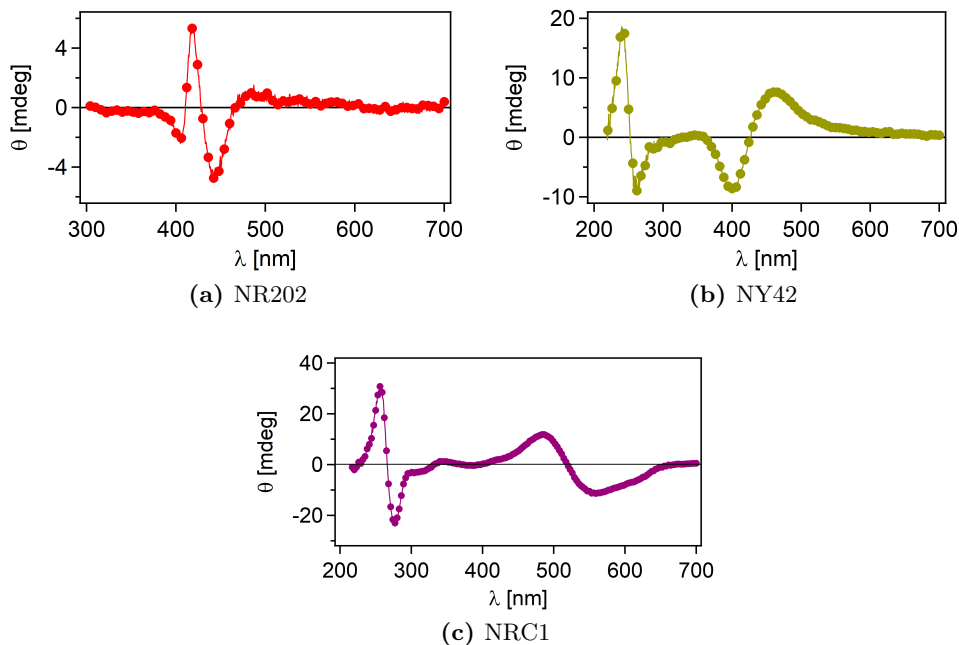


Figure 2.10: CD spectrum for NR202, NY42 and NRC1 in water at a concentration of 1 mgml^{-1} .

mophore could have some non negligible implications on both the conformation of the single chromophoric unit and the structure of the formed aggregates. A planar, cofacial interaction between the chromophores could be, in this scenario, twisted in a locally skewed arrangement, the sense of which selected by the influence of lactose central chirality. Therefore, GDs solutions were also studied by Electronic Circular Dichroism (ECD). CD analysis were performed on GDs solutions at 1 mgml^{-1} dye concentration in water, MeOH and DMSO. For all dyes in both organic solvents, no detectable CD signal was observed. This piece of information revealed that for the isolated molecule the central chirality of lactose, several atoms away from the chromophore, was not able to impart a significant chiral perturbation. On the contrary, for water samples of NR202, NY42 and NRC1, the presence of optical activity (Fig. 2.10 not only confirmed their chirality, but also provided more information about the structure of NY42 and NRC1 aggregates in solution. These last two samples

showed an exciton-coupled spectrum, suggesting that two or more non conjugated chromophores were near in space to one another.[5, 54]. In general, considering the chemical structures of these dyes (Fig. 1.4), that includes a rather flat hydrophobic core (more or less flat, depending on the dye) and an hydrophilic side chain, intermolecular interactions between dye molecules were likely to take place mainly through stacking interactions. Therefore, several molecules would probably pile up to form H or J-aggregates.[54]. This kind of structure was in agreement with both ECD and SAXS analysis. NY42 and NRC1 had two contributions to their ECD spectrum, one at short wavelengths and the other in the visible region. Both these signals were exciton couplets ascribable to GDs aggregates. The couplet at longer wavelengths concerned the primary structure of said aggregates, while the one at higher energies pertain to their secondary structure and was of no interest in this case. NRC1 exciton couplets (Fig. 2.10c) were centered at 266 nm and 518 nm. Thus, they both presented a bathochromic shift compared to λ_{max} of the correspondent absorption peaks. The negative sign of the exciton couplets indicated a left-handed screw sense of rotation of the supramolecular structure itself.[54] NY42 (Fig. 2.10b) showed an exciton couplet centered at 420 nm, in correspondence with its visible absorption, whose positive sign indicated a right-ended screw sense of rotation for the supramolecular structure.[54] The couplets at lower energies for both NRC1 and NY42 were rather symmetrical, indicating conservative transitions.[51, 55, 63] NR202 spectrum (Fig. 2.10a) was complex, as it was not a clear exciton couplet, but it appeared to be the result of multiple transitions balancing out. This consideration was supported by its behavior toward absorption (Fig. 2.3a), since its spectrum was not only broad, but its shape also changed with concentration. These data all suggested the presence of multiple transitions in that range of wavelengths. At variance with what observed for the other GDs, NB27 and NO30 water solutions did not show any detectable CD signal. Thus, it could be concluded that their aggregate were not chiral. However, the formation of H or J-aggregates could not be excluded, since both dyes presented a non negligible shift in their absorption with respect to the monomer UV-Visible absorption (Table 2.1), where the absorption in MeOH could be considered as that of the monomer. In particular, NB27 was characterized by a hypsochromic shift (Fig. 2.4a) while NO30 by a bathochromic one (Fig. 2.4b). This behavior suggested that NB27 and NO30 formed respectively H and a J aggregates.[54] It was peculiar that NO30 did

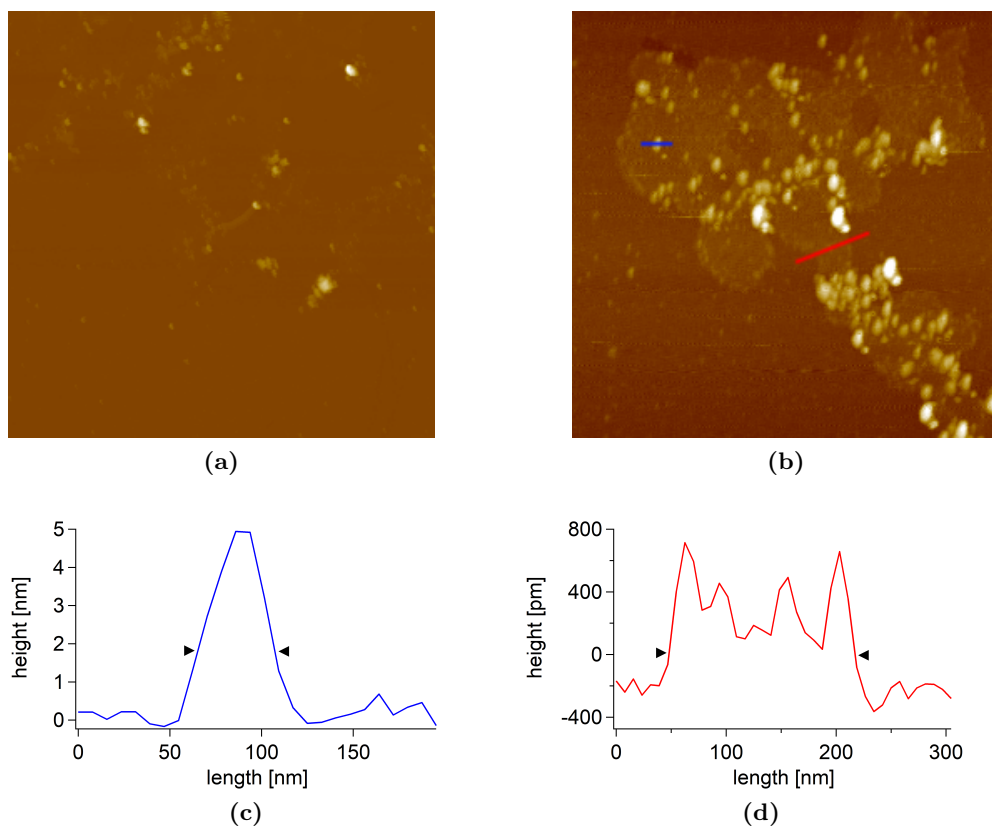


Figure 2.11: a) $10\ \mu\text{m} \times 10\ \mu\text{m}$ and b) $2\ \mu\text{m} \times 2\ \mu\text{m}$ AFM images of NR202 $1\ \text{mgml}^{-1}$ water solution. Analysis of the cross section of a) a flat zone (red line) and b) an aggregate (blue line). The cursors in line profiles indicate the height at which the length of each object was measured.

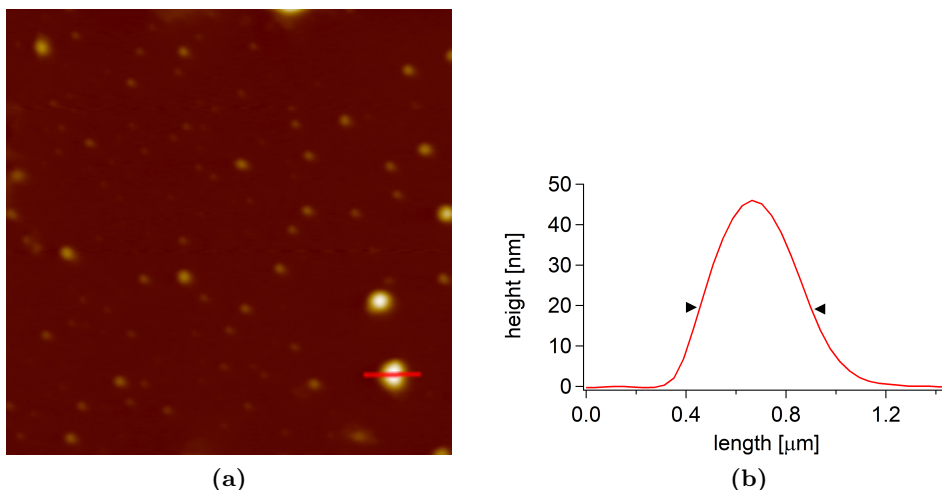


Figure 2.12: a) AFM image $10\ \mu\text{m} \times 10\ \mu\text{m}$ of NY42 $1\ \text{mgml}^{-1}$ water solution. b) Analysis of the cross section of one big aggregate (red line). The cursors in the line profile indicate the height at which the length of the object was measured.

not show any optical activity, since its molecular structure was very similar to that of NR202. Therefore, NR202 dichroic activity could be ascribed to the presence of the acetamide, that has the ability to form H bonds. Therefore, this group was probably involved in the formation of the supramolecular aggregate. Water solutions $1\ \text{mgml}^{-1}$ for NR202, NY42 and NRC1 were studied by AFM in an attempt to observe GDs aggregates. However, it had to be considered that, since this technique works on dry samples, the images could potentially represent aggregates in a different state with respect to that of the dye in solution. The objects retraced in each sample were analyzed to understand their dimensions from their line profiles. In the attempt to reduce biases due to a flattening of the aggregates on the mica surface, the length of the objects was measured at half height, in correspondence of the cursors reported in each profile. NR202 images at different scale, $10 \times 10\ \mu\text{m}$ (Fig. 2.11a) and $2 \times 2\ \mu\text{m}$ (Fig. 2.11b), showed the presence of aggregates. In particular spheroidal aggregates of different dimensions were identified in both Fig. 2.11a and 2.11b. Two objects present in Fig. 2.11b were analyzed: one spheroidal aggregate (blue line) and a rather flat zone (red line). The line profile (Fig. 2.11c) of the aggregate showed that its height and length were approximately 5 nm and

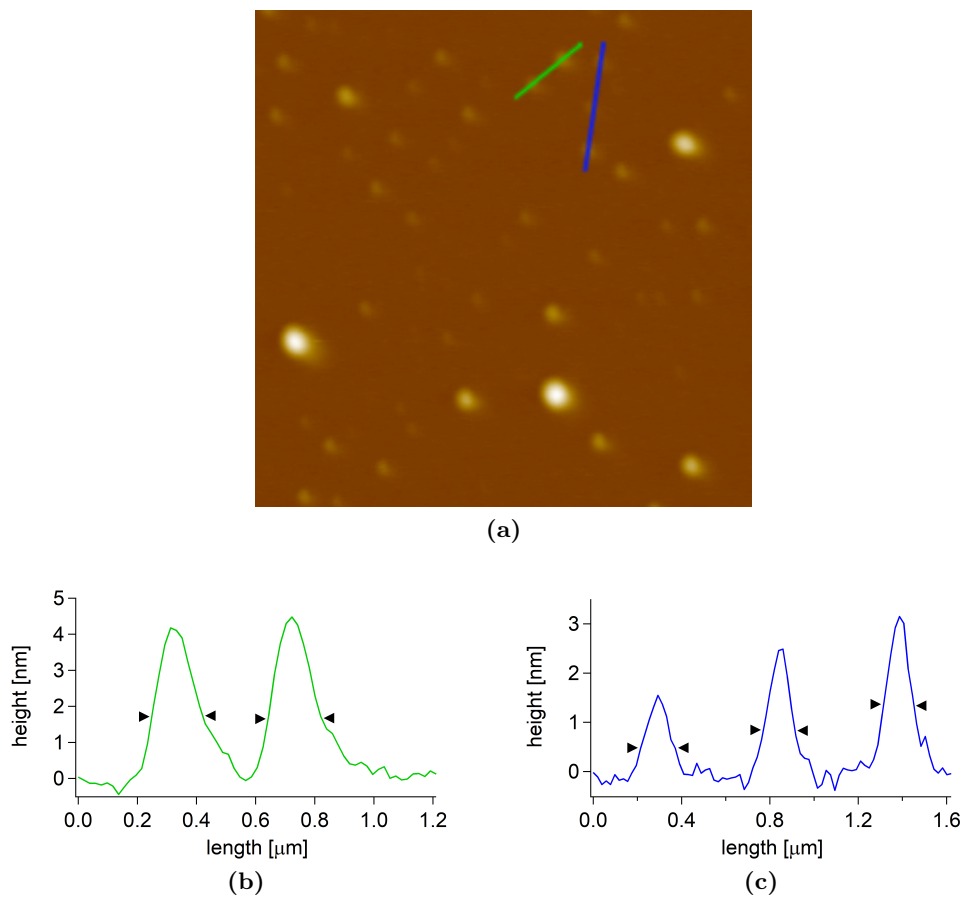


Figure 2.13: a) AFM image $5 \mu\text{m} \times 5 \mu\text{m}$ of NY42 1 mg ml^{-1} water solution. Analysis of the cross section of b) two (green line) and c) three (blue line) aggregates spatially close. The cursors in line profiles indicate the height at which the length of each object was measured.

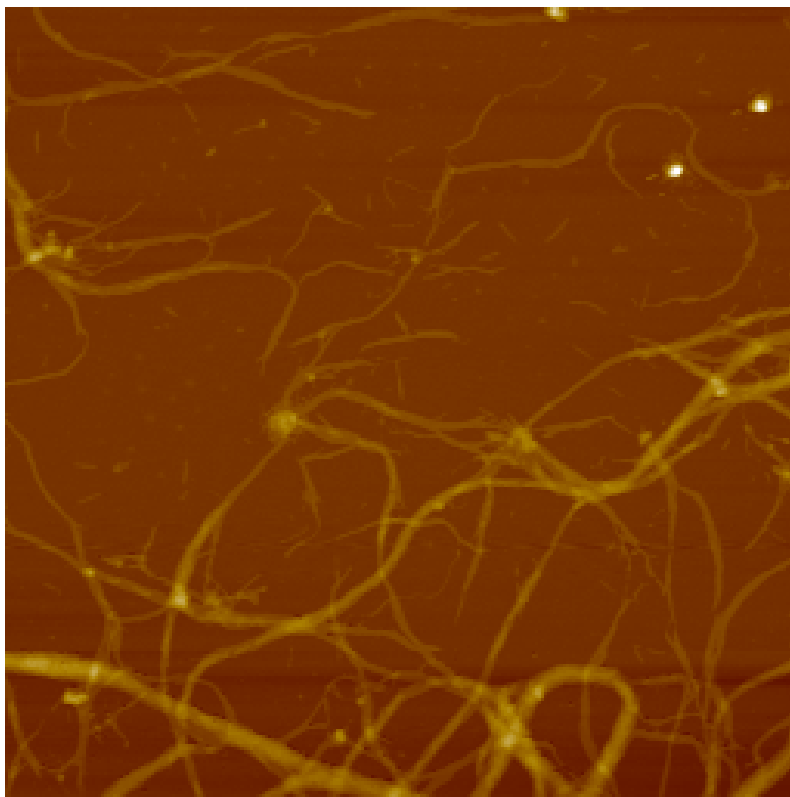
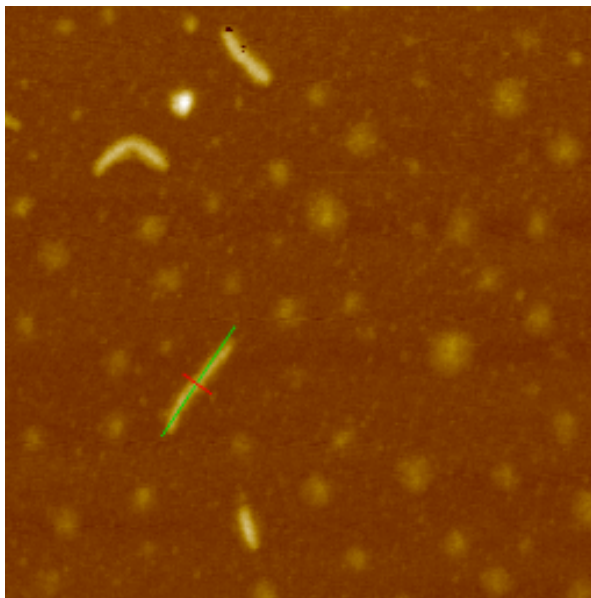
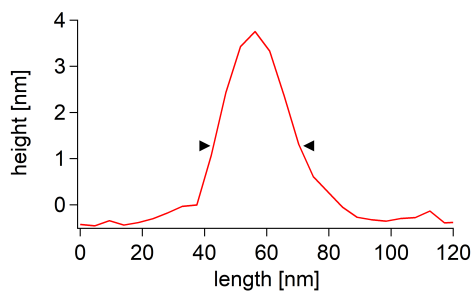


Figure 2.14: AFM image $5 \times 5 \mu\text{m}$ of fibrils formed by NRC1 at 1 mgml^{-1} .

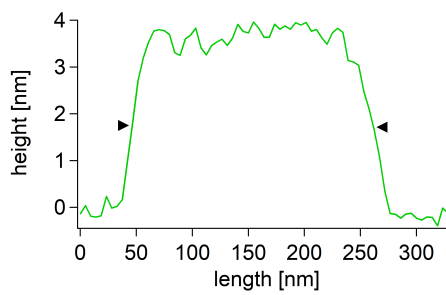
40 nm, while for the flat zone (Fig. 2.11d) height and length were respectively about 700 pm and 170 nm. Images of NY42 at two different scales, $10 \times 10 \mu\text{m}$ (Fig. 2.12a) and $5 \times 5 \mu\text{m}$ (Fig. 2.13a) revealed the presence of spheroidal aggregates, in analogy with what observed for NR202. Also in this case, some of the objects were analyzed to find out their size. The line profile of one big aggregate in Fig. 2.12a (red line) showed that its height and cross section were respectively around 45 nm and 400 nm (Fig. 2.12b). In Fig. 2.13a two groups of aggregates were analyzed, the first composed by 2 objects (green line) and the second by three (blue line). This analysis was performed on more than one object to find out if their dimensions were different or if most of them had the same size. The line profile of the first two aggregates (Fig. 2.13b) showed



(a)



(b)



(c)

Figure 2.15: a) AFM image $1.25 \mu\text{m} \times 1.25 \mu\text{m}$ of NRC1 1 mg/ml – 1 water solution. Analysis of one elongated aggregate: b) Cross section (red line) and c) length (green line). The cursors in line profiles indicate the height at which the length of the object was measured.

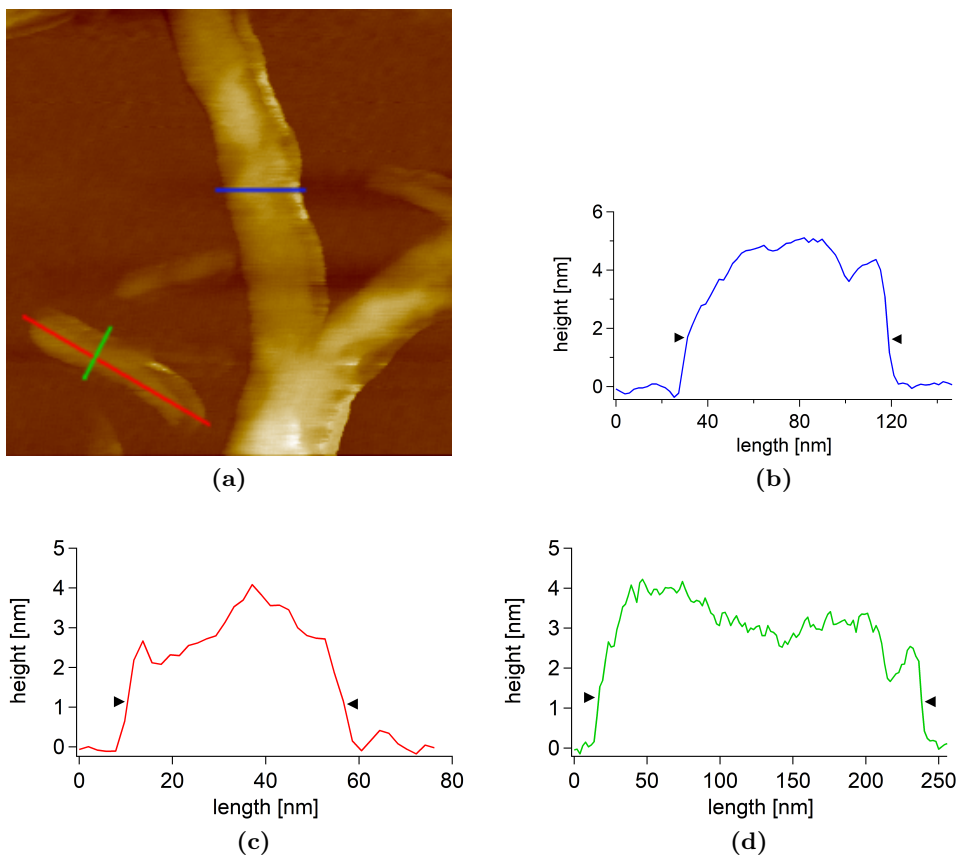


Figure 2.16: a) AFM image 500 nm \times 5 nm of NY42 1 mgml $^{-1}$ water solution. Analysis of b) the cross section of a big fibril (blue line), c) cross section (green line) and length (red line) of an elongated aggregate. The cursors in line profiles indicate the height at which the length of each object was measured.

that their height and cross section were approximately the same and were respectively 4 nm and 200 nm. On the contrary, the profile analysis for the three aggregates (Fig. 2.13c) revealed they all had different height, 1.5 2.5 and 3 nm, but approximately the same cross section, 150 nm. Images of NRC1 at three different scales, $5 \times 5 \mu\text{m}$ (Fig. 2.14) $1.25 \times 1.25 \mu\text{m}$ (Fig. 2.15) and $500 \times 500 \text{ nm}$ (Fig. 2.16), confirmed the presence of elongated objects in this sample. In particular, as can be appreciated in Fig. 2.14, this dye formed very long fibrils that were in perfect agreement with the previous results obtained by SAXS and ECD, that suggested the presence of massive aggregation and columnar aggregates. Smaller elongated objects as well as little spheroidal aggregates were also found in this sample, as shown in Fig. 2.15a. The spheroidal objects were likely to be formed by isolated dye molecules that got together during the drying process. In analogy with what was done for NR202 and NY42, one of these aggregates was analyzed and its line profiles were reported in Fig. 2.15b and 2.15c. This object height, cross section and length were approximately 3.5 nm, 30 nm and 215 nm. Finally in Fig. 2.16a, the scale allowed to appreciate a fibril and a smaller elongated aggregate next to each other. Both these objects were analyzed. The line profile for the fibril (Fig. 2.16b) showed height and cross section of approximately 5 nm and 90 nm. The line profiles of the smaller object (Fig. 2.16c and 2.16d) revealed that its height, cross section and length were approximately 4 nm, 45 nm and 220 nm. These dimensions were comparable with those found for the previously analyzed elongated object in Fig. 2.15.

2.3 Solvent mixtures

In the previous section the effects of some parameters on GDs behavior in solution were investigated. It became clear that solvent had a crucial influence on the self-assembly of these dyes. In fact, no evidence of aggregation could be found for GDs in organic solvents, suggesting that these molecules were entirely dissolved in both MeOH and DMSO. To study more in detail the disruption process of aggregates formed in water, absorption profiles of all GDs were registered upon progressive addition of a good solvent (MeOH and DMSO). The same study was performed adding a non solvent for GDs, EtOH, to water samples. Solutions 1 mgml^{-1} of all GDs were prepared with 9 different

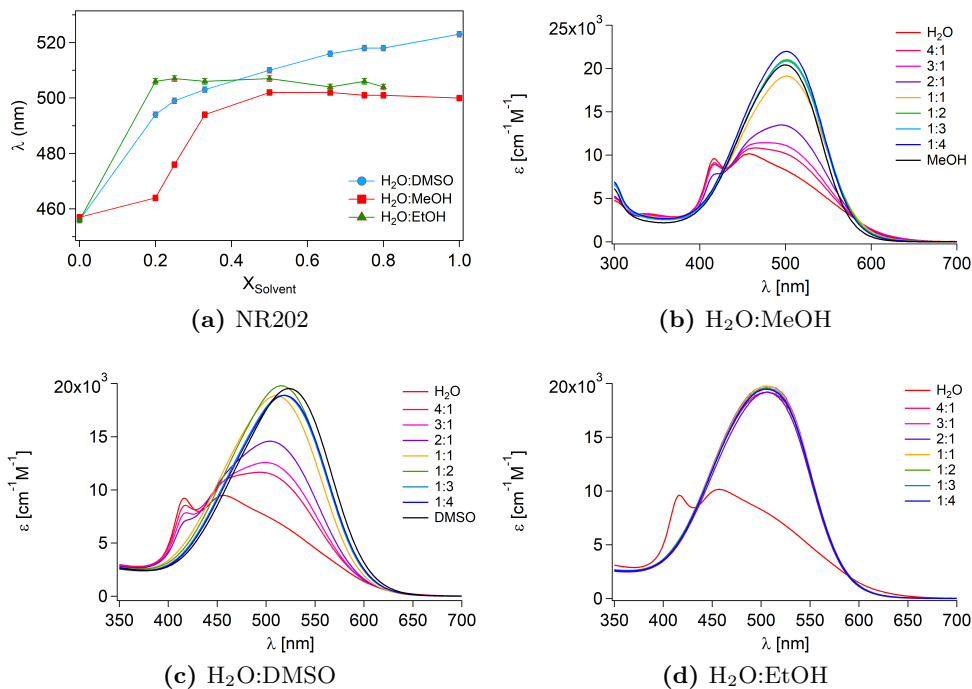


Figure 2.17: a) Variation of λ_{max} for NR220 as a function of organic solvent molar fraction: DMSO (●), MeOH (■) and EtOH (▲). NR220 absorption spectra for different ratio of b) H₂O: MeOH c) H₂O:DMSO and d) H₂O: EtOH combinations.

H₂O: organic solvent ratios: 1:0, 4:1, 3:1, 2:1, 1:1, 1:2, 1:3, 1:4, 0:1. However, a small amount of water was necessary in EtOH to avoid dye precipitation, thus the last sample was missing for this solvents combination. The changes in absorption and λ_{max} for all samples were studied as a function of the organic solvent molar fraction. NR220 absorption spectrum changed radically increasing organic solvent molar fraction, showing a considerable bathochromic shift (Fig. 2.17a). However, the progression was different for the three organic solvents. Increasing MeOH molar fraction lead to a slow, gradual disappearance of the peak at 418 nm, accompanied by the increase of the contribution at MeOH λ_{max} (Fig. 2.17b). Since GDs were completely dissolved in MeOH, the hypsochromic shift that took place increasing the amount of H₂O was probably caused by a stiffening of the system due to aggregation.[3, 63, 74] Disruption

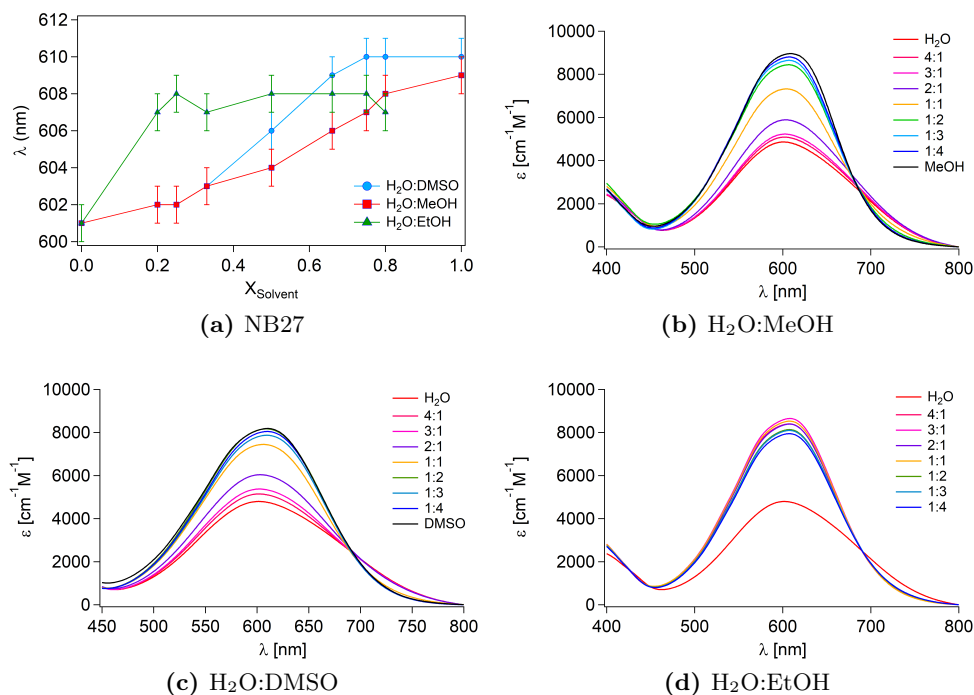


Figure 2.18: a) Variation of λ_{max} for NB27 as a function of organic solvent molar fraction: DMSO (●), MeOH (■) and EtOH (▲). NB27 absorption spectra for different ratio of b) H₂O: MeOH c) H₂O:DMSO and d) H₂O: EtOH combinations.

of NR202 aggregates increasing the amount of good solvent was confirmed by the progressive disappearance of the aggregation band at 418 nm.[3, 63, 74] These observations were in agreement with the results obtained for NR202 at different dye concentrations (Fig. 2.3a). The same considerations were valid also for H₂O:DMSO combination, since also DMSO was a good solvent for these molecules. The only difference was that DMSO influence on absorption was higher than for MeOH. In fact, the shift was faster, as can be appreciated in Fig. 2.17a, and the changes in absorption more consistent at low DMSO molar fractions (Fig. 2.17c). Interestingly, upon addition of non solvent EtOH, NR202 absorption changed abruptly at low solvent molar fraction (Fig. 2.17a) and both λ_{max} and the spectrum (Fig. 2.17c) remained unchanged after that. This piece of information suggested that EtOH, even if it was not a good

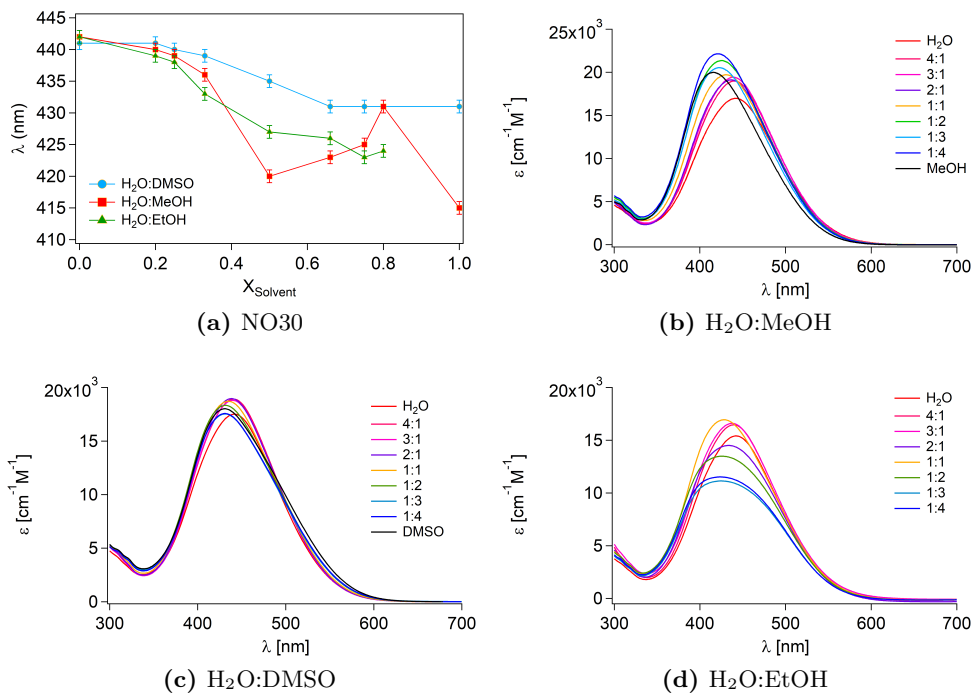


Figure 2.19: a) Variation of λ_{max} for NO30 as a function of organic solvent molar fraction: DMSO (●), MeOH (■) and EtOH (▲). NO30 absorption spectra for different ratio of b) H₂O: MeOH c) H₂O:DMSO and d) H₂O: EtOH combinations.

solvent, probably favored an immediate disruption of dyes aggregates, stabilizing a situation in which the molecule was isolated or poorly associated. The same considerations could be made for both the good solvents, DMSO and MeOH, in the case of NB27. Increasing the amount of organic solvent, λ_{max} gradually shifted at lower energies (Fig. 2.18a) while ϵ increased (Fig. 2.18b and 2.18c). These variations indicated a progressive disruption of aggregates in solution until NB27 was mainly dissolved.[62] For H₂O:EtOH combination, in analogy with what seen for NR202, absorption (Fig.2.18d) and λ_{max} (Fig. 2.18a) changed abruptly and remained constant, indicating a strong and immediate influence of EtOH on aggregation. NO30 absorption, upon increase of organic solvent molar fraction, gave an hypsochromic shift, as shown in Fig. 2.19a. This shift was consistent for H₂O:MeOH combination and was accom-

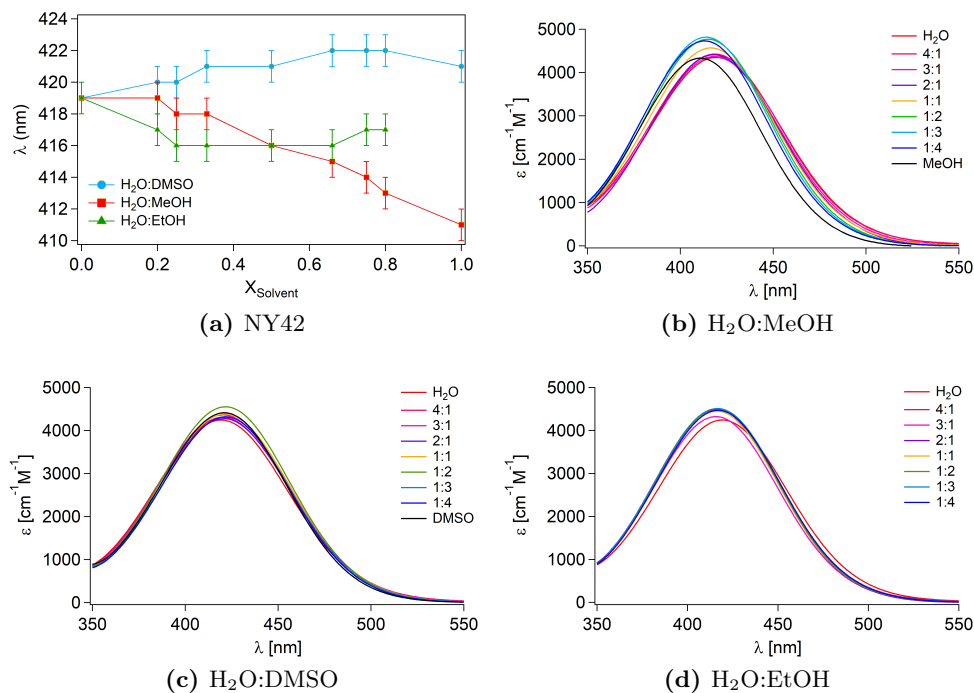


Figure 2.20: a) Variation of λ_{max} for NY42 as a function of organic solvent molar fraction: DMSO (●), MeOH (■) and EtOH (▲). NY42 absorption spectra for different ratio of b) H₂O: MeOH c) H₂O:DMSO and d) H₂O: EtOH combinations.

panied by a rather significant increase in ϵ (Fig. 2.19b). At variance with what observed for NR202 and NB27, progressive addition of DMSO showed a smaller shift, as well as less pronounced variations in its absorption spectrum (Fig. 2.19c). Nevertheless, for MeOH and DMSO, results indicated a gradual disruption of the aggregates.[62] Addition of non solvent EtOH had a different effect on NO30, compared to previous cases. In fact, above 50% of EtOH in solution resulted in a decrease in absorbance accompanied by a broadening of the peak (Fig. 2.19d). This could be an indication of a destabilization of NO30 in solution that, consequently, started to precipitate. Therefore, it could be concluded that the addition of a non solvent had a higher influence on NO30 aggregation than on NR202 and NB27. Addition of both good solvent DMSO and non solvent EtOH, caused negligible changes on NY42 λ_{max} (Fig. 2.20)

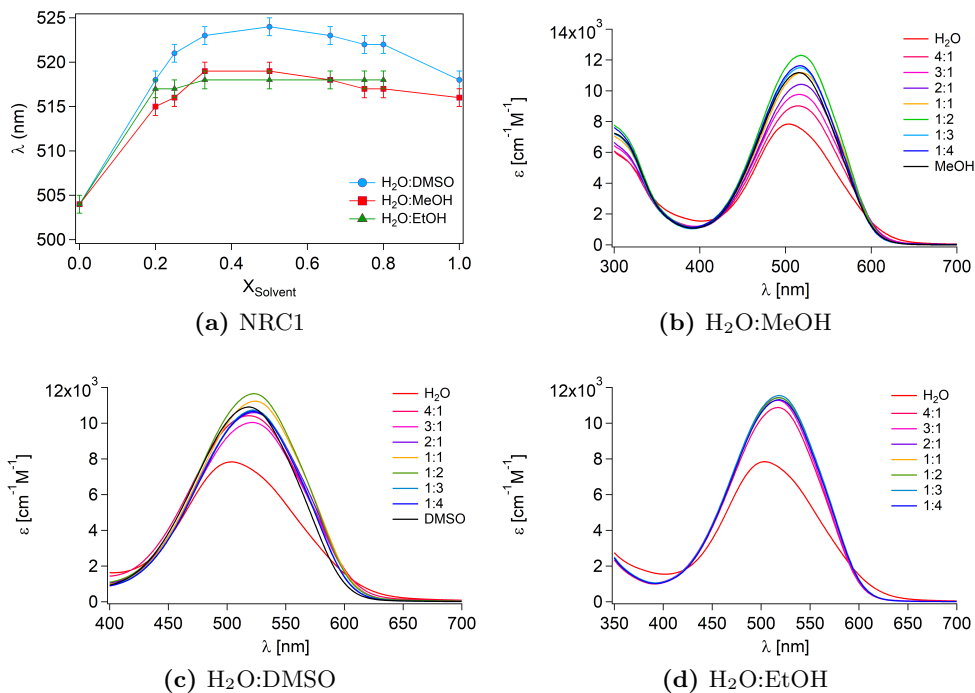


Figure 2.21: a) Variation of λ_{max} for NRC1 as a function of organic solvent molar fraction: DMSO (●), MeOH (■) and EtOH (▲). NRC1 absorption spectra for different ratio of b) H₂O: MeOH c) H₂O:DMSO and d) H₂O: EtOH combinations.

and absorption (Fig. 2.20c and 2.20d with the increase of their molar fractions. The only noticeable variation was the hypsochromic shift of λ_{max} in H₂O:MeOH combination, accompanied by a slight increase in ϵ (Fig. 2.20b). These alterations seemed to be caused by a small solvatochromic effect rather than by a real change in aggregation, even if the absence of self-assembly in organic solvents had been verified by scattering techniques. Even if NRC1 and NB27 were both anthraquinone, the two dyes behaved differently in solvents mixtures. This dye had a more extended hydrophobic part compared to the other GDs (Fig. 1.4), thus it seemed to have lower affinity for water, despite the presence of lactose. In fact, in all three water-solvent combinations, the effect of organic solvents was immediate and strong, in spite of their being good or non solvents. This was testified by the consistent shift in λ_{max} in presence

of 20% of organic solvents. NRC1 λ_{max} changed abruptly at low organic solvent molar fractions for both MeOH and EtOH combinations, reaching what could be defined a plateau (Fig. 2.21a). However, while for EtOH absorption variation was sudden and permanent as in previous cases (Fig. 2.21d), for MeOH the change was more gradual, as can be appreciated in Fig. 2.21b. H₂O:DMSO combination showed the highest bathochromic shift in λ_{max} accompanied by a fast variation in ϵ (Fig. 2.21c). Looking at Fig. 2.21a, it was possible to appreciate that λ_{max} for NRC1 in DMSO shifted back at higher energies. This could be an effect due to the dielectric constant. Since these dyes were all cations, the polarity of their solvent played a role in their behavior in solution. The final hypsochromic shift could indicate a decrease in NRC1 solubility in DMSO compared to a case in which both water and DMSO were present. As already pointed out, this dye had an extended hydrophobic core. Thus, the presence of organic solvent tended to stabilize it in solution, even if the amount of solvent was small. However, for higher concentrations of DMSO the effect of the dielectric constant became more and more important, since this molecule was charged. This meant that a more stable situation for NRC1 was that when at least a small amount of water was present in solution. This effect was not noticed for the other dyes because the presence of a longer linker chain between their hydrophobic core and lactose (Fig. 1.4) guaranteed more degrees of freedom to the structure, probably resulting in a stabilization of the molecule.

2.4 Interaction between glycoconjugated dyes

GDs, as already pointed out, were designed to be used in industrial leather and textile dyeing. In dyeing processes is necessary to mix two or more dyes to obtain certain colors and shades, such as light or dark green, golden yellow or black. Therefore, to provide an investigation as thorough as possible, the influence of interaction between GDs on their behavior in solution was also studied. Mixtures of the five GDs were investigated first by UV-Visible absorption and ECD to identify the more interesting ones. Then these mixtures were analyzed by DLS and SAXS. However, the scattering study was only performed on mixtures of NR202, NB27, NO30 and NY42, without NRC1. In fact, since NRC1 has been synthesized by L. Calugi as part of his PhD

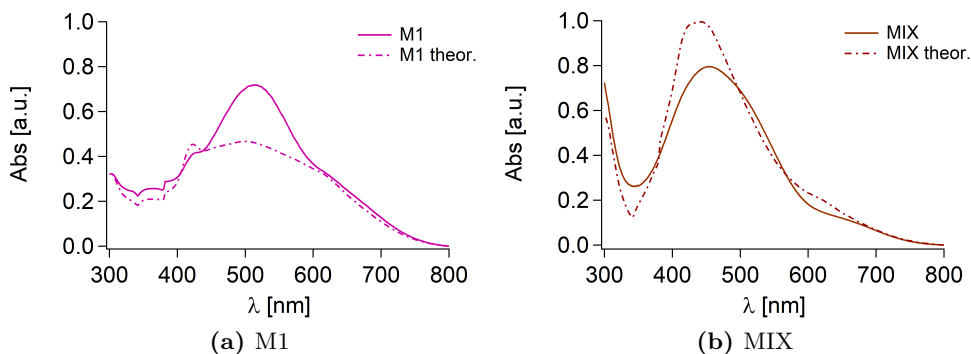


Figure 2.22: Comparison between experimental and theoretical absorption for two GDs mixtures a) M1 and b) MIX in water solution.

project[12], the properties of this dye were studied at a later time than those of other GDs. Thus, there was not enough time to perform these particular experiments on its mixtures. First of all, UV-Visible absorption spectra were registered for all the possible equimolar combinations of NR202, NB27, NO30 and NY42. In order to highlight any possible interaction between dyes, experimental absorption for each combination was compared to its theoretical one, obtained summing the spectra of the single components at the concentration they had in the mixture. Two of these combinations clearly showed evidence of interaction: M1, binary combination of NR202 and NB27, and MIX, the equimolar mixture of the four GDs. As can be appreciated in Fig. 2.22, experimental and theoretical absorption of both M1 and MIX were consistently different. M1 experimental absorption (Fig. 2.22a) showed an increase in absorption intensity at 512 nm, approximately the λ_{max} of isolated NR202. This could be an indication of an interaction between the two dyes resulting in the disruption of their aggregates, possibly to form new and different ones. On the contrary, MIX experimental spectra (Fig. 2.22b) had a lower absorption than expected and a broader peak, indicating the presence of aggregates. Moreover, in the experimental spectrum NR202 contribution to absorption seemed comparable to that of NO30, suggesting that the interaction with NB27 took place, resulting in disruption of its aggregates and, consequently, in its higher intensity, in analogy with M1. M1 and MIX were also studied in MeOH and DMSO, to characterize GDs mixture behavior in organic solvents. It was ev-

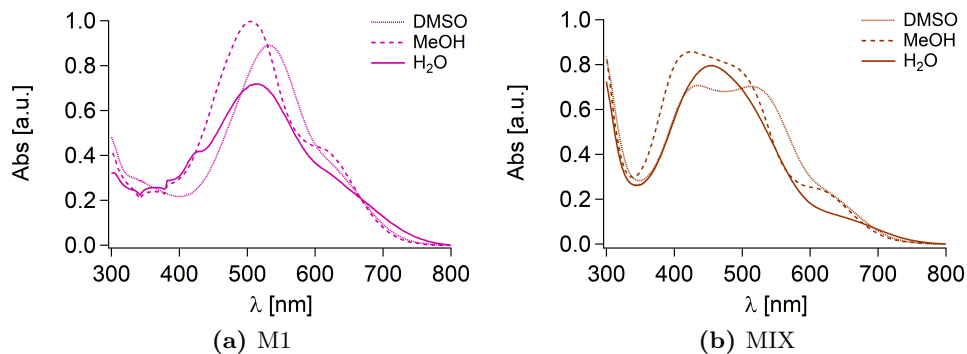


Figure 2.23: Comparison between absorption spectra of H₂O, MeOH and DMSO solutions for the two GDs mixtures a) M1 and b) MIX.

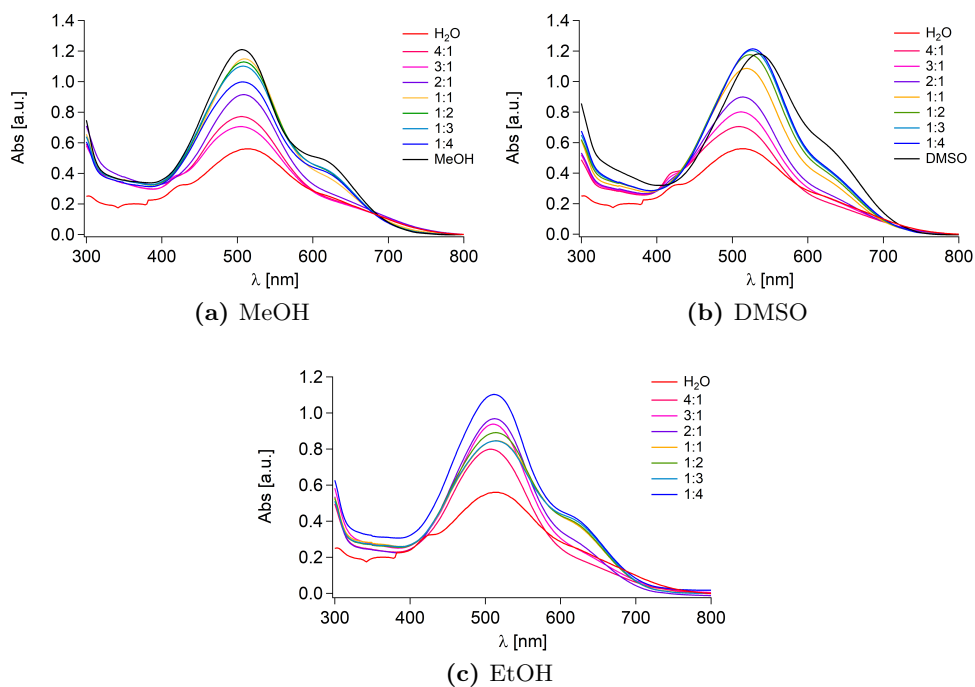


Figure 2.24: M1 absorption spectra for different ratio of a) H₂O: MeOH b) H₂O:DMSO and c) H₂O: EtOH combinations.

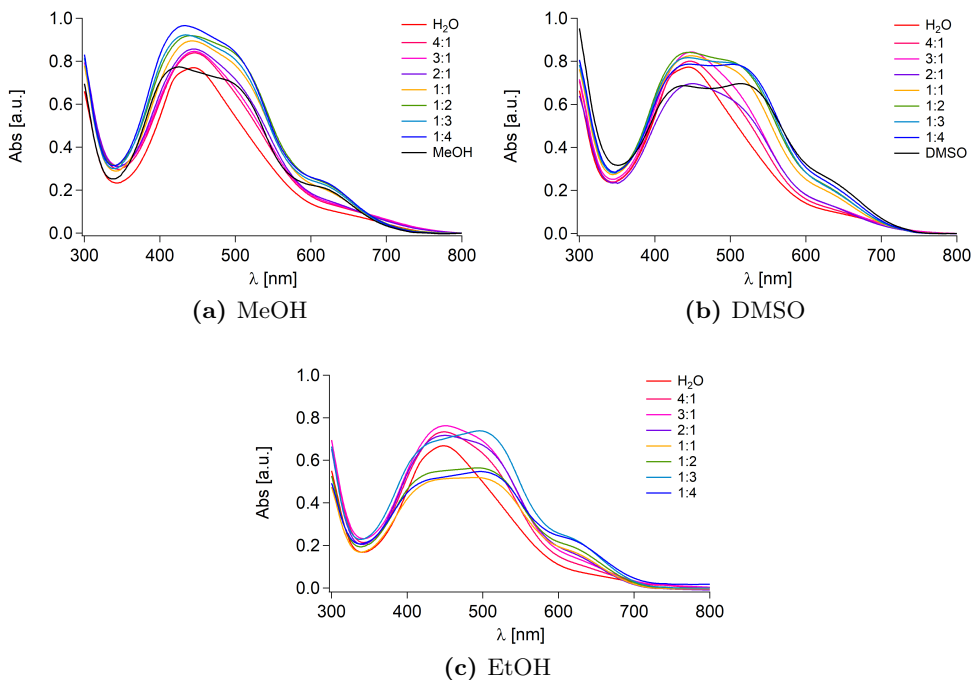


Figure 2.25: MIX absorption spectra for different ratio of a) H₂O: MeOH b) H₂O:DMSO and c) H₂O: EtOH combinations.

ident that in organic solvents mixtures of GDs, as well as single GDs, were not aggregated, since in both M1 (Fig. 2.23a) and MIX (Fig. 2.23b) the peaks were not broad as in water, but the absorption of each dye was sharper and separated. To verify that the influence of organic solvents on GDs mixtures was the same as on single dyes solutions, absorption profile for M1 and MIX were studied progressively adding good solvents (MeOH and DMSO). In analogy with what reported in Section 2.4, changes in M1 and MIX spectra were observed as a function of organic solvent molar fraction for H₂O:MeOH, H₂O:DMSO and H₂O:EtOH combinations at the same 9 water-solvent ratios. M1 absorption spectra changed gradually for H₂O:MeOH (Fig. 2.24a) and H₂O:DMSO (Fig. 2.24b) increasing organic solvent molar fraction. The same was observed upon addition of EtOH (Fig. 2.24c), even if absorption changed faster in this case. For all these three solvents combinations was possible to

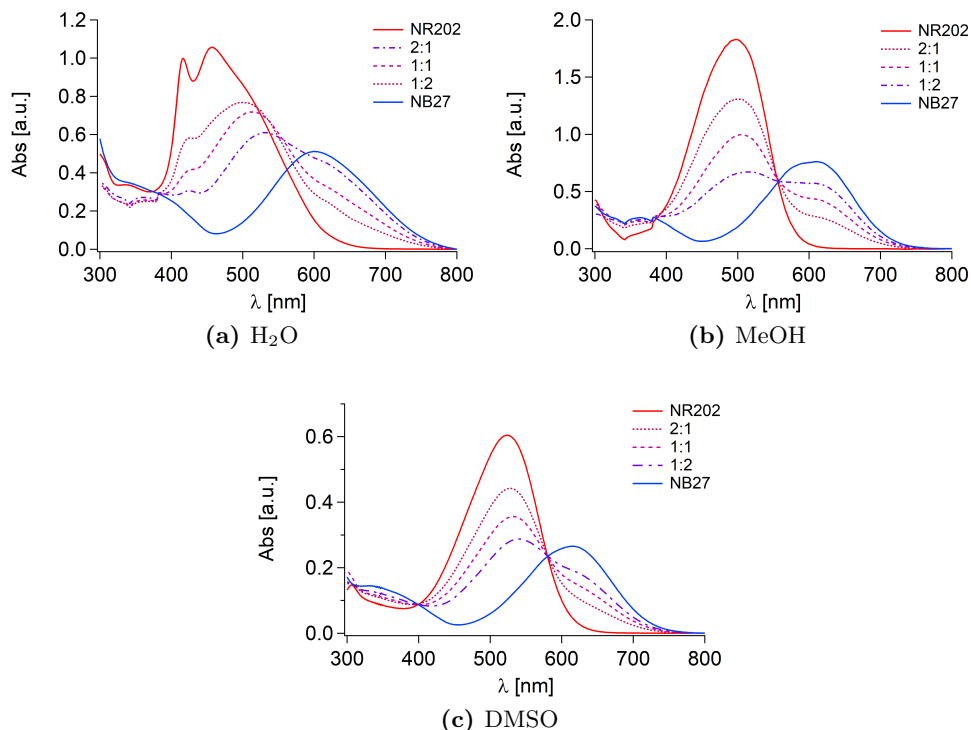


Figure 2.26: M1 absorption spectra at different NR202:NB27 ratios in three different solvents: a) H₂O, b) MeOH, c) DMSO.

observe the progressive increase in NR202 contribution at 512 nm, probably corresponding to disruption of NR202 aggregates caused by organic solvents. It was possible to follow the disruption of GDs aggregates in MIX as well, as the organic solvent molar fraction increased. But, as already observed in Fig. 2.23b, the absorption intensity decrease in presence of organic solvent. The gradual separation of single GDs contribution to MIX absorption, resulting in a lower intensity took place upon addition of both good solvents, MeOH (Fig. 2.25a) and DMSO (Fig. 2.25b). The addition of EtOH (Fig. 2.25c) caused the same consistent broadening and decrease in intensity of absorption already seen for NO30 (Fig. 2.19d). This suggested that, in analogy with NO30 case, GDs in mixture were destabilized by the presence of more than 50% of EtOH

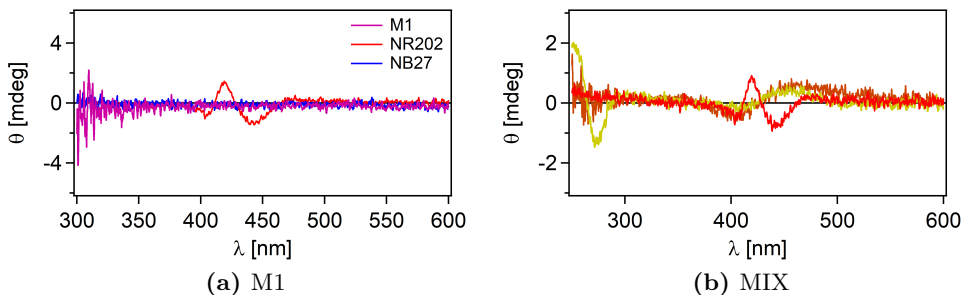


Figure 2.27: ECD spectra for water solutions of a) M1 and b) MIX in comparison with those of their single components.

and probably started to precipitate. Since M1 was a binary and simple system, the ratio between its two components (NR202 and NB27) was varied to observe how it affected its absorption. This study was performed on GDs solutions in water, MeOH and DMSO. For each solvent, five M1 solutions were prepared at different NR202:NB27 ratios: 1:0, 2:1, 1:1, 1:2, 0:1. Absorption spectra for the five M1 aqueous solutions were reported in Fig. 2.26a. The interaction between NR202 and NB27 was evident, since these spectra did not have an isosbestic point. On the contrary, the presence of an isosbestic point for both M1 solutions in MeOH (Fig. 2.26b) and DMSO (Fig. 2.26c) indicated that the two GDs did not interact and were the only species in solution. M1 and MIX solutions in H₂O, MeOH and DMSO were then studied by ECD. In analogy with what seen for single dye solutions in Section 2.2, GDs mixtures in organic solvents did not have optical activity. In (Fig. 2.27a) the ECD spectrum for M1 1 mgml⁻¹ water solution was reported in comparison with those of NR202 and NB27 at 0.5 mgml⁻¹, the concentration they had in the mixture. M1 did not show any detectable activity, confirming that the same interaction between NR202 and NB27 took place, canceling NR202 dichroic activity. The signal detected for MIX 1 mgml⁻¹ water solution (Fig. 2.27b) was very similar to that of NY42. This result provided two pieces of information. First, NR202 and NB27 interacted also in presence of other GDs, as already suggested by UV-Visible absorption of MIX (Fig. 2.22b). Second, NY42 seemed to interact only with itself, since its dichroic activity was preserved. An ECD investigation on all other combinations of GDs confirmed both these hypotheses. Two

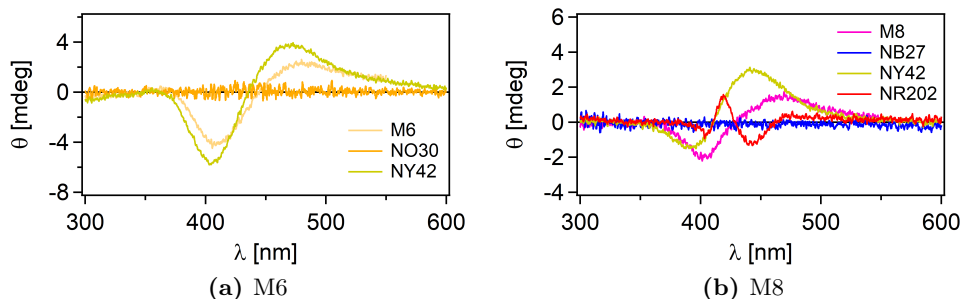


Figure 2.28: ECD spectra for 1 mgml^{-1} water solution of the two GDs combinations a) M6 and b) M8, reported in comparison with those of their single components.

of these spectra were reported in Fig. 2.28 as an example. M6 combination showed that NO30 and NY42 did not interact with each other, since the change of intensity for NY42 exciton couplet was negligible (Fig. 2.28a). The same could be observed for NY42 couplet in M8 ternary combination, whose signal also confirmed the interaction between NB27 and NR202, since the activity of the latter was canceled in the mixture (Fig. 2.28b). As anticipated at the beginning of this Section, M1 and MIX were further investigated by DLS. ACFs were registered for M1 and MIX (Fig. 2.29) and their CONTIN[60] analysis provided size distributions for both of them (Fig. 2.29b and 2.29c), as well as hydrodynamic diameters and polydispersities, reported in Table 2.3. Both M1 and MIX had very high polydispersities, as well as single GDs solutions. Moreover, their ACFs had a second relaxation time, ascribable to very big objects in solution that fell out of the experimental range of this technique (Fig. 2.29). M1 and MIX 1 mgml^{-1} water solution were also studied by SAXS to have some indications about the shape of their aggregates. SAXS curves for both samples had a Guinier region at low q (Fig. 2.30), probably indicating the presence of spheroidal aggregates in solution. Both curves were fitted using a Core-Shell Spheres function and radius values obtained from this fitting were reported in Table 2.3. Analyses of NRC1 binary combinations with the other four dyes were also performed, using UV-Visible absorption and ECD. None of the four mixtures showed any evidence of interaction between GDs in their absorption spectra. However, ECD study underlined that an interaction was indeed present between NRC1 and NO30. No significant differences could be

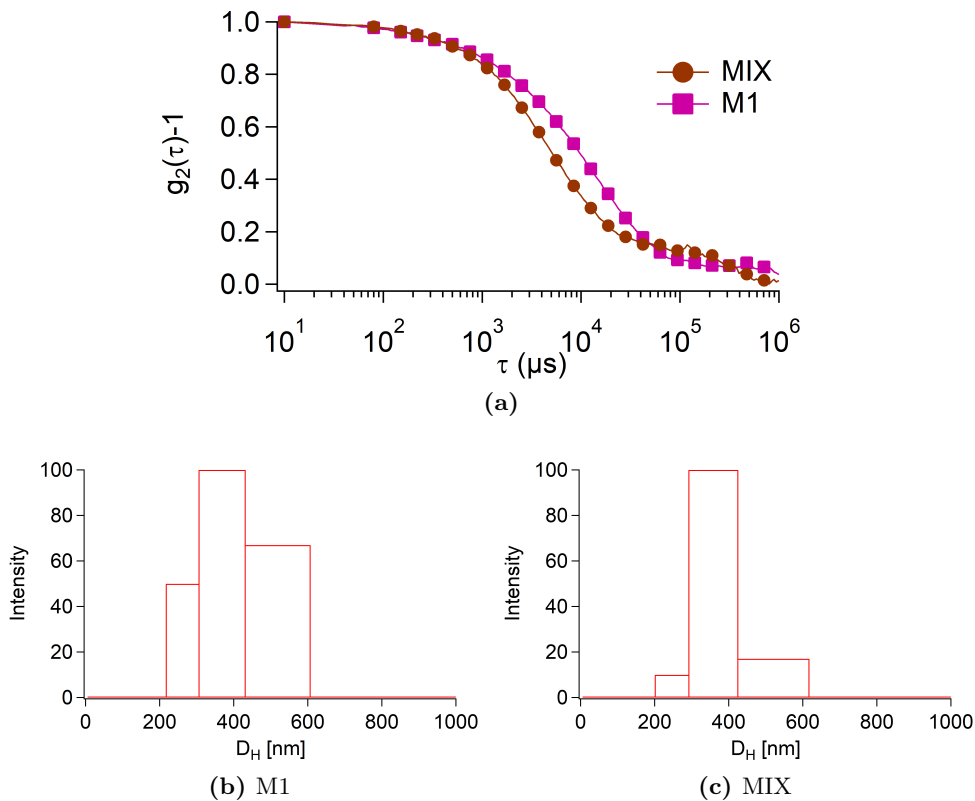


Figure 2.29: a) Normalized dynamic light scattering ACFs for the two 0.1 mgml^{-1} GDs mixtures M1 and MIX water solutions. b) M1 and c) MIX size distributions of the aggregates present in solution reported as a function of scattering intensity.

Table 2.3: Hydrodynamic diameters (D_H) and polydispersities (PDI) obtained by CONTIN[60] analysis for the two 0.1 mgml^{-1} GDs combinations M1 and MIX in water solution; radius of the aggregates obtained by SAXS fitting for M1 and MIX 1 mgml^{-1} water solutions.

	M1	MIX
D_H (nm)	333.5 ± 2.7	375.8 ± 4.9
PDI	0.359 ± 0.027	0.362 ± 0.031
radius (nm)	3.3	2.8

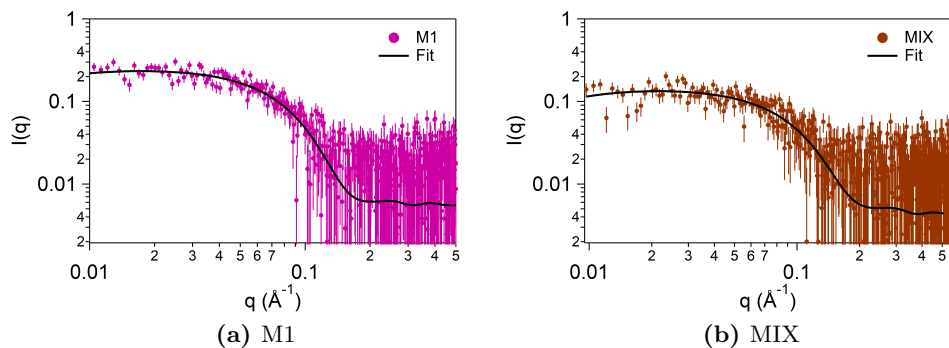


Figure 2.30: SAXS analysis of two GDs mixtures a) M1 and b) MIX in water at 1 mgml^{-1} . In graphic are reported the fit for each sample, obtained with Schultz spheres function.

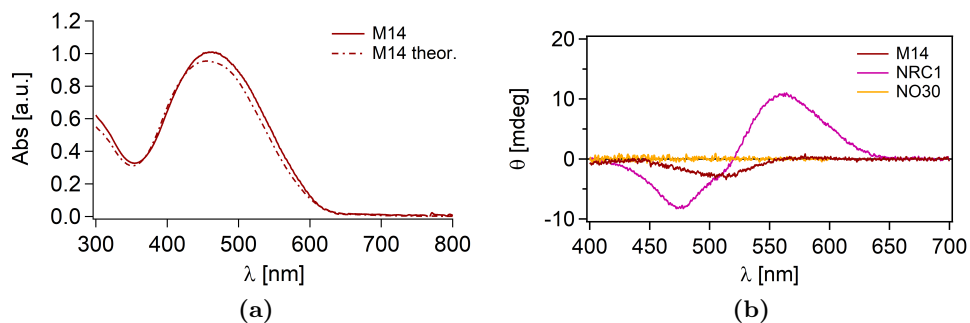


Figure 2.31: a) Absorption and b) ECD spectra for M14 1 mgml^{-1} water solution.

observed comparing M14 experimental spectra with its theoretical one (Fig. 2.31a). On the contrary, the optical activity of this mixture was very different from that of NRC1 at the same concentration, reported in Fig. 2.31b as a reference. While NRC1 ECD spectrum in the visible region consisted of an exciton couplet, M14 showed a central chirality instead.

2.5 GDs interaction with surfactants

In light of GDs application in industrial leather and textile dyeing, one last parameter was taken into account: their behavior in presence of surfactants. This was an important aspect to consider for two main reasons. First of all, because industrial dyeing processes could employ surfactants. Secondly, be-

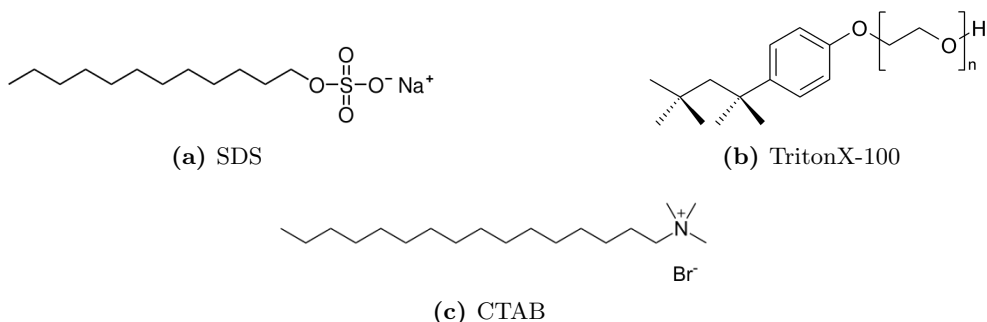


Figure 2.32: Molecular structures of the three surfactants studied in interaction with GDs: a) SDS b) TX c) CTAB.

cause dyed substrates, being them leather or any kind of textiles, will come in contact with different classes of surfactants that can be found in all detergent formulations. In both cases, the surfactants in question could be anionic, non ionic or cationic, therefore the behavior of GDs was studied in presence of three different surfactants, one for each class: Sodium Dodecylsulfate (SDS), TritonX-100 (TX) and Cetrimonium Bromide (CTAB), whose molecular structures were reported in Fig. 2.32. The interaction of these three molecules with GDs was studied to observe their influence on the self-assembly of the dyes. Surfactants are known to have the ability to disrupt membranes and lipid dou-

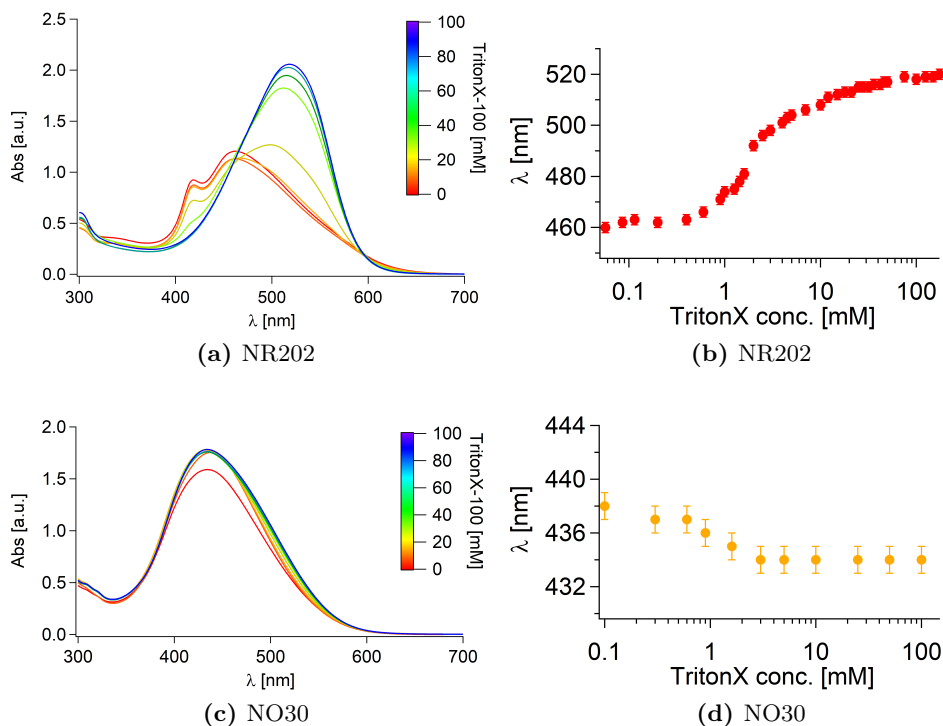


Figure 2.33: Effect of the addition of increasing concentration of non ionic TX between 0.1-100 mM to 1 mgml⁻¹ solutions of the two azo dyes: NR202 and NO30. Variation of a-c) NR202 and NO30 absorption spectra and b-d) their λ_{max} as a function of surfactant concentration.

ble layers. [18, 27, 45, 52] GDs aggregates were different from liposomes, and even more so from a complex system like a membrane. However, since GDs were amphiphiles as well as surfactants, their interaction was highly probable, consequently leading to disruption of GDs self-assembled aggregates in water. Increasing concentrations of surfactants, in the range between 0.1 and 150 mM, were added to GDs 1 mgml⁻¹ water solutions. Absorption spectra were registered for each concentration of the three surfactans (SDS, CTAB, TX) and their comparison underlined more or less significant variations for each dye in terms of ϵ values and λ_{max} . All λ_{max} shifts for each dye, induced by the interactions with the TX, CTAB and SDS, were summarized in Table 2.4. First of all, the influence of non ionic TX was observed on GDs solutions. The two

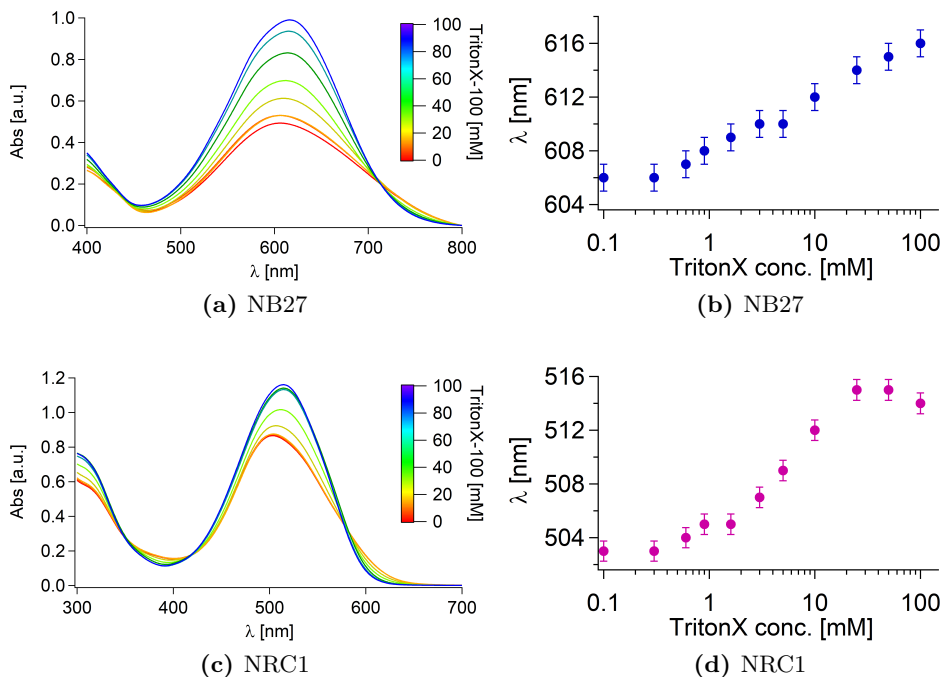


Figure 2.34: Effect of the addition of increasing concentration of non ionic TX between 0.1-100 mM to 1 mgml^{-1} solutions of the two anthraquinone dyes:NB27 and NRC1. Variation of a-c) NB27 and NRC1 absorption spectra and b-d) their λ_{max} as a function of surfactant concentration.

azo dyes, NR202 and NO30 behaved very differently in presence of the non ionic surfactant TX. As already observed in Section 2.4, when the influence of solvents was presented, NR202 absorption spectrum (Fig. 2.33a) changed not only in terms of λ_{max} and ϵ , but also in terms of its shape. Increasing TX concentration the aggregation peak at 418 nm gradually disappeared while the contribution at lower energies intensified. The bathochromic shift was very consistent (Fig. 2.33b) and the main change happened abruptly between 0.9 and 4 mM of TX, over the surfactant's CMC. NO30 showed much more moderate changes both in its absorption (Fig. 2.33c), that after the initial small variation remained the same, and in its hypsochromic λ_{max} shifts (Fig. 2.33d). The two anthraquinone dyes NB27 and NRC1 behaved similarly upon addition

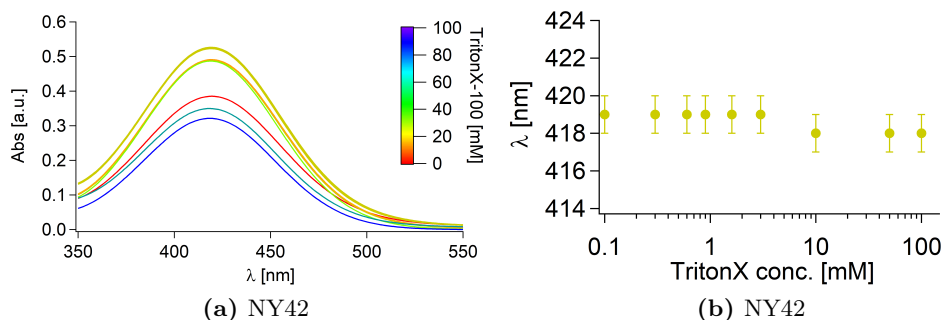


Figure 2.35: Effect of the addition of increasing concentration of non ionic TX between 0.1-100 mM to 1 mgml⁻¹ solutions of NY42. Variation of a) NY42 absorption spectrum and b) λ_{max} as a function of surfactant concentration.

of TX. Their absorption gradually changed, accompanied by a sharpening of the peak and an increase in its intensity, as shown in Fig. 2.34a and 2.34c. NB27 λ_{max} variation was not abrupt but progressive (Fig. 2.34b) while for NRC1 the change was slightly more sudden (Fig. 2.34d) and its final shift was more consistent (see Table 2.4). For NRC1 the more considerable change in λ_{max} took place in TX concentration range between 1.6 and 10, well above the surfactant CMC. The addition of TX to NY42 water solution only caused variability in absorption intensity (Fig. 2.35a), but it was not followed by a shift in λ_{max} , that remained unchanged in the entire range of surfactant concentrations. Then, the influence of the cationic surfactant CTAB on GDs solutions was studied. In analogy with TX case, NR202 and NO30 behaved in a consistently different way. NR202 absorption spectra massively changed, with the fast disappearance of the aggregation peak at 418 nm and the increase in intensity at lower energies (Fig. 2.36a). Its bathochromic shift was considerable (Fig. 2.36b), of approximately the same entity as that observed for TX addition (see Table 2.4). The more consistent changes in λ_{max} took place around a CTAB concentration of 0.95 mM, that corresponds to its CMC. No shift took place for NO30 upon addition of CTAB (Fig. 2.36d) and in agreement with what observed for TX, its absorption did not changed but slightly (Fig. 2.36c). NB27 and NRC1 behaved similarly to the previous case. Their absorption changed progressively its intensity (Fig. 2.37a and 2.37c), but again NB27 shifted more gradually towards lower energies (Fig. 2.37b) while NRC1 changed its λ_{max}

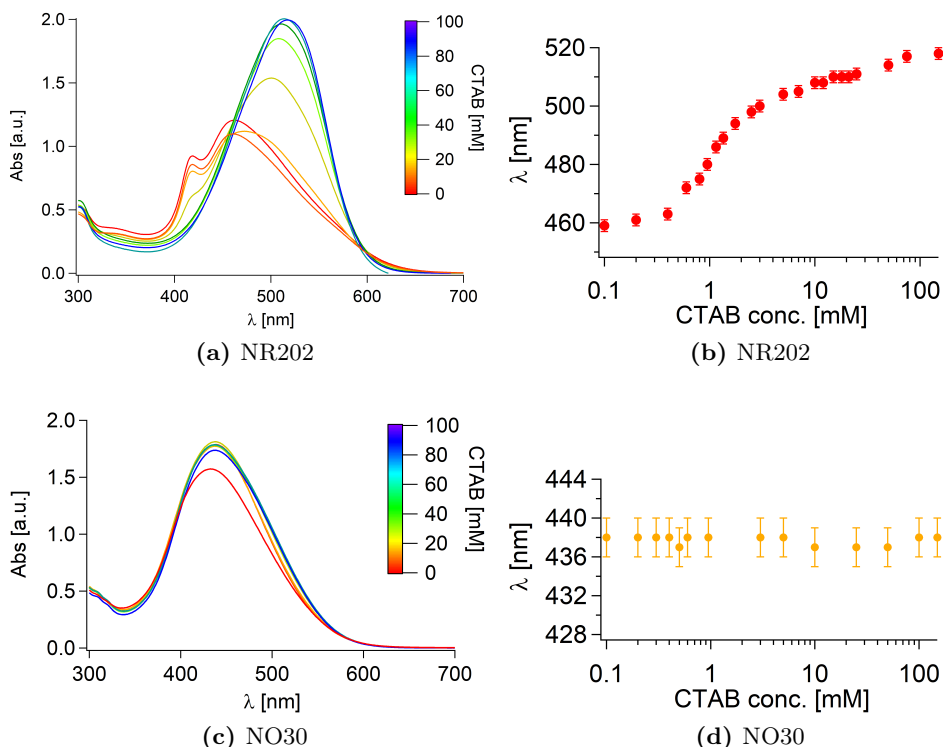


Figure 2.36: Effect of the addition of increasing concentration of cationic CTAB between 0.1-100 mM to 1 mgml^{-1} solutions of the two azo dyes: NR202 and NO30. Variation of a-c) NR202 and NO30 absorption spectra and b-d) their λ_{max} as a function of surfactant concentration.

more abruptly (Fig. 2.37d). For NB27 the shift began at CTAB CMC, around 1mM, while for NRC1 the more consistent shift happened before the surfactant CMC, between 0.3 and 0.95 mM. Nevertheless, the final shift of these two anthraquinone dyes had the same consistency (Table 2.4). Finally, NY42 absorption changed its intensity as soon as 0.1 mM of surfactant was added, remaining the same also for higher concentrations (Fig.2.38a). However, λ_{max} did not varied accordingly (Fig. 2.38a). These results showed that, even if GDs are positively charged, the effects on their absorption after the interaction with the cationic surfactant CTAB were approximately the same as the ones caused by presence of the non ionic TX. The interaction of SDS with GDs solutions

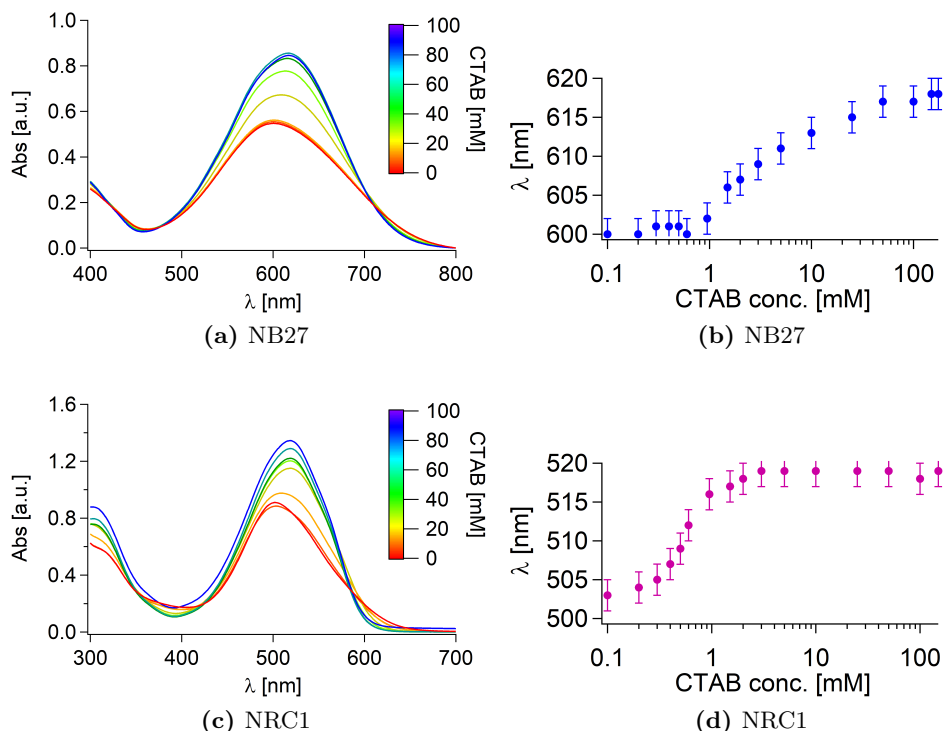


Figure 2.37: Effect of the addition of increasing concentration of cationic CTAB between 0.1-100 mM to 1 mgml⁻¹ solutions of the two anthraquinone dyes: NB27 and NRC1. Variation of a-c) NB27 and NRC1 absorption spectra and b-d) their λ_{max} as a function of surfactant concentration.

not only resulted in a change of absorption and in a shift of λ_{max} , but also led to unexpected results. In fact, the presence of anionic surfactant at specific concentrations induced the precipitation of all GDs, a phenomenon known as reentrant condensation (RC).[8, 75] This specific topic will be treated more in details in Section 2.5.1. The range of SDS concentrations at which GDs precipitated was represented as a gray area in graphics reporting λ_{max} variations as a function of surfactant concentration. The range of SDS concentrations at which GDs precipitated changed from one dye to the other and did not seem related to their molecular structures. NR202, NRC1 and NB27 had the wider precipitation ranges (approximately between 0.2 and 1.2 mM), while NO30

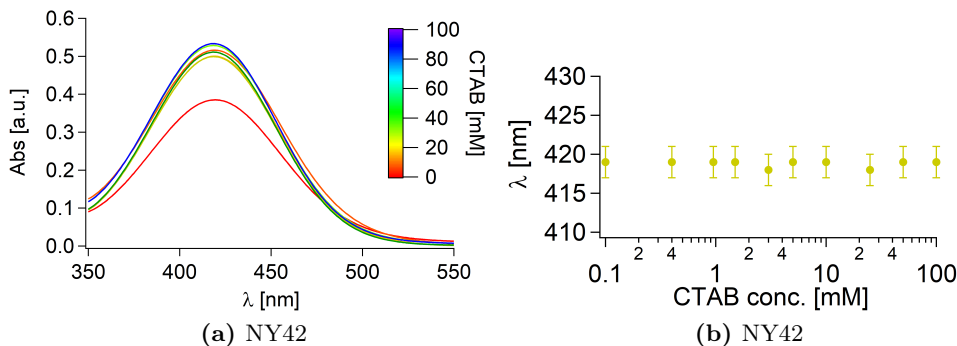


Figure 2.38: Effect of the addition of increasing concentration of cationic CTAB between 0.1-100 mM to 1 mgml⁻¹ solutions of NY42. Variation of a) NY42 absorption spectrum and b) λ_{max} as a function of surfactant concentration.

an azo dye just like NR202, had the smaller one (between 0.5 and 1 mM). NY42 precipitated between 0.4 and 1.2 mM of SDS. The azo dyes NR202 and NO30 once again showed different behaviors in presence of surfactant. Electrostatic interactions probably played a strong role in the major changes of NR202 absorption (Fig. 2.39a). In fact, for SDS 0.5 and 3 mM a contribution at 445 nm, that was never observed before, dominated the spectrum. Since this concentrations were approximately the limits of the RC range, one hypothesis could be that this peak was ascribable to a dye-surfactant aggregate. For higher concentrations of SDS, NR202 absorption variations were analogous to TX and CTAB cases. The changes in its absorption spectrum induced once more a bathochromic shift in λ_{max} (Fig. 2.39b), whose value varied mostly around 5 mM of SDS, before its CMC. The influence of dye-SDS aggregation induced some modifications on NO30 absorption too, even if less evident (Fig. 2.39c). In this case, absorption of SDS 0.5 and 3 mM samples showed a decrease in intensity that could be probably related to the association of NO30 with the surfactant. This hypothesis was supported by the peak broadening for these samples. In analogy with NR202 case, samples at higher SDS concentrations behaved similarly to previous cases. As shown in Fig. 2.39d, λ_{max} variation was more complicated. In fact, after an initial strong hypsochromic shift, ascribable to dye precipitation, λ_{max} increased again and then reached a plateau. NB27 absorption gradually changed, as a function of SDS concentration, increasing its intensity and sharpening its peak (Fig. 2.40a). This was

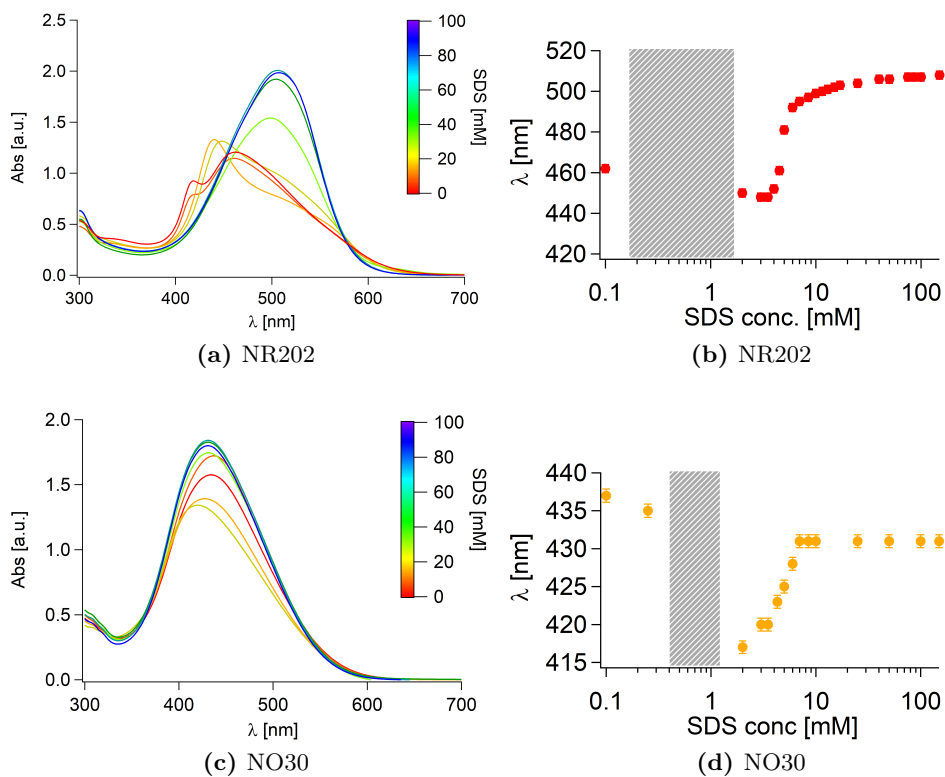


Figure 2.39: Effect of the addition of increasing concentration of anionic SDS between 0.1-100 mM to 1 mgml⁻¹ solutions of the two azo dyes:NR202 and NO30. Variation of a-c) NR202 and NO30 absorption spectra and b-d) their λ_{max} as a function of surfactant concentration. The gray areas in b) and d) correspond to the range of SDS concentration at which the reentrant condensation takes place and the dyes precipitate.

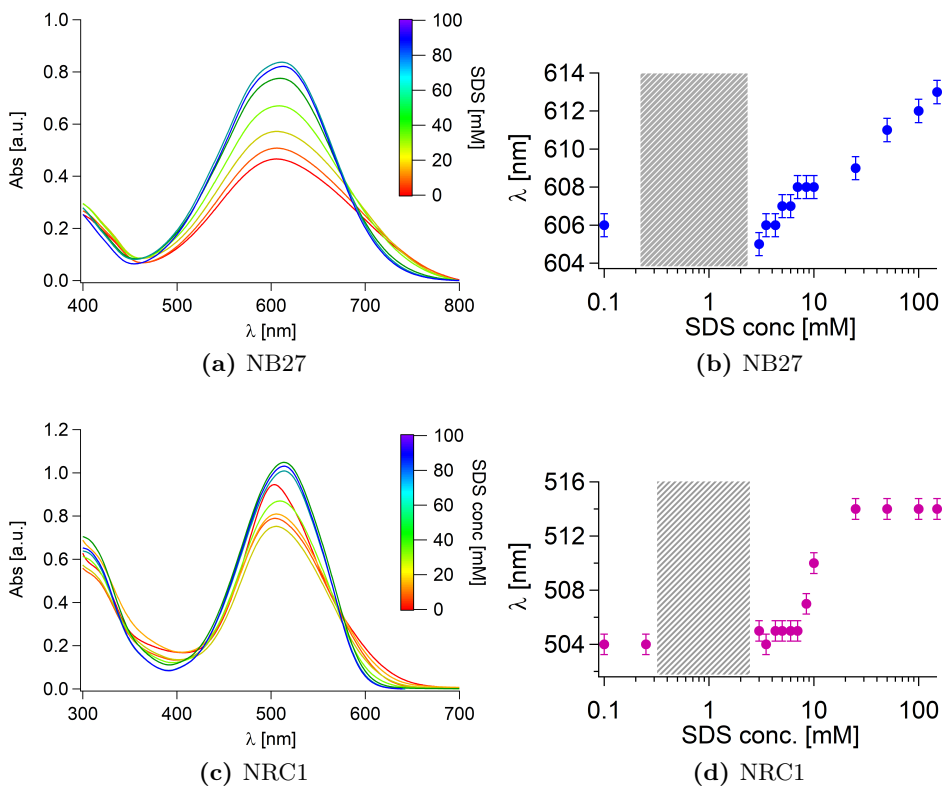


Figure 2.40: Effect of the addition of increasing concentration of anionic SDS between 0.1-100 mM to 1 mg ml^{-1} solutions of the two anthraquinone dyes: NB27 and NRC1. Variation of a-c) NB27 and NRC1 absorption spectra and b-d) their λ_{max} as a function of surfactant concentration. The gray areas in b) and d) correspond to the range of SDS concentration at which the reentrant condensation takes place and the dyes precipitate.

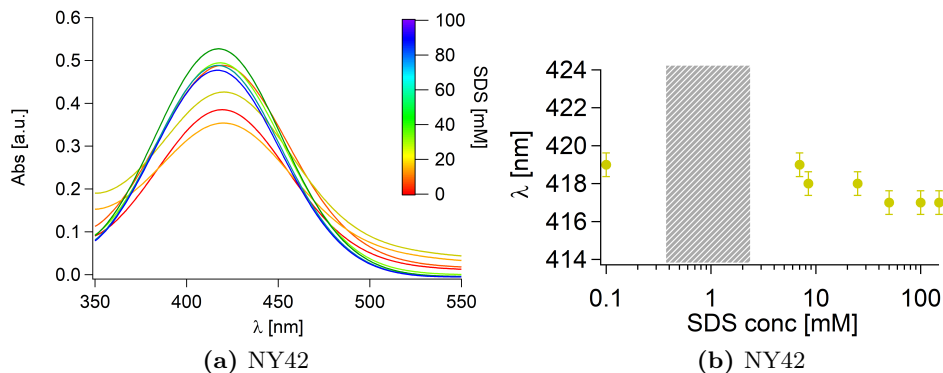


Figure 2.41: Effect of the addition of increasing concentration of anionic SDS between 0.1-100 mM to 1 mgml⁻¹ solutions of NY42. Variation of a) NY42 absorption spectrum and b) λ_{max} as a function of surfactant concentration. The gray area in b) corresponds to the range of SDS concentration at which the reentrant condensation takes place and the dye precipitates.

accompanied by a progressive bathochromic shift of its λ_{max} after the reentrant condensation range (Fig. 2.40b). In analogy with what observed for NR202 and NO30, NRC1 absorption seemed to be influenced by the presence of reentrant condensation. For concentrations of SDS between 0.1 and 3 mM, absorption

Table 2.4: Summary of the final λ_{max} shifts induced by three surfactants: non ionic TX, cationic CTAB and anionic SDS. For each shift was specified if it was bathochromic (B) or hypsochromic (H).

	NR202	NB27	NO30	NY42	NRC1
TX	(B) 60	(B) 10	(H) 4	–	(B)11
CTAB	(B) 58	(B) 18	–	–	(B) 16
SDS	(B) 48	(B) 7	(H) 6	–	(B) 10

intensity decreased (Fig. 2.40c). However, since the peak got sharper in this case, instead of broadening as seen for NO30 (Fig.2.39c), this variation was probably caused by the beginning of dye precipitation. The spectrum changes for SDS over 10 mM were analogous to TX and CTAB previous cases. NRC1 bathochromic shift was significant and the major changes in λ_{max} took place around SDS 10 mM (Fig. 2.40d), which is the surfactant CMC. Small variations in absorption intensity for NY42 (Fig. 2.41a) were the only evidence

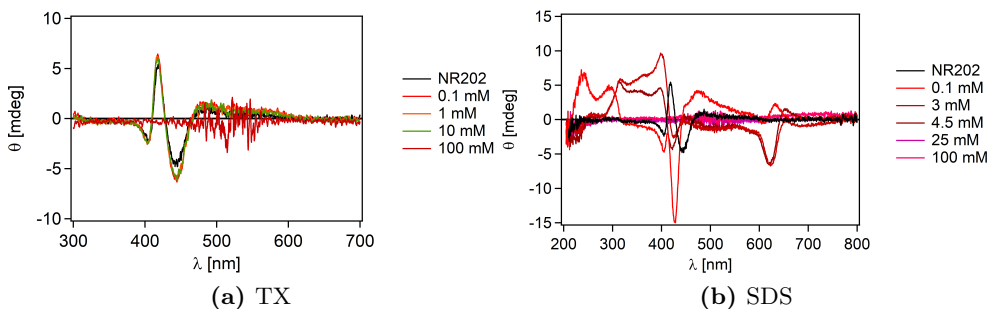


Figure 2.42: Influence of increasing concentration of a) non ionic TX and b) anionic SDS on the optical activity of 1 mgml^{-1} solutions of NR202.

of its interaction with SDS, except for the presence of reentrant condensation. The shift in λ_{max} was not significant (Fig. 2.41b). Samples of the three optically active GDs (NR202, NY42, NRC1) at selected concentrations of TX and SDS were analyzed using ECD. However, ECD measurements were not performed on GDs in presence of CTAB, because it would not have been possible to determine if the probable effects on the optical activity of NR202, NY42 and NRC1 were induced by electrostatic interaction due to CTAB positive charge or to a different kind of interaction. First of all, the influence of the two surfactants on NR202 was tested. The addition of TX did not have a strong effect on NR202 optical activity, that was maintained up to 10 mM of TX and was canceled at 100 mM (Fig. 2.42a). The influence of SDS was stronger, as shown in Fig. 2.42b. Since SDS clearly disrupted NR202 aggregates, the ECD spectrum in presence of surfactant was the result of many contributions due to several species, probably partially disrupted, each of which had its own transitions. Therefore, this spectrum was not easy to understand. TX decisively affected NY42, since its exciton couplet already disappeared at 0.1 mM of surfactant (Fig. 2.43a). The same results were observed upon addition of SDS, that succeeded in canceling NY42 optical activity at 0.1 mM as well (Fig. 2.43b). This behavior probably indicated NY42 higher susceptibility to disrupt its own aggregates to associate with both surfactants. TX and SDS. The results obtained from the addition of surfactants to NRC1 solutions were more interesting. As already reported in the previous section, NRC1 in water formed left-handed helical aggregates (Fig. 2.10c). Upon addition of TX,

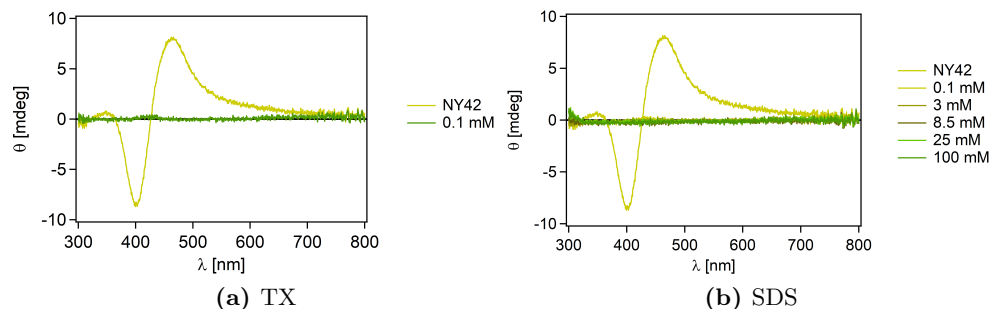


Figure 2.43: Influence of increasing concentration of a) non ionic TX and b) anionic SDS on the optical activity of 1 mgml^{-1} solutions of NY42.

NRC1 exciton couplet inverted its sign and became positive, as soon as TX 0.1 mM (Fig. 2.44a). This indicated an inversion of the helicity of aggregates in solution, that resulted in a right-handedness of NRC1 aggregates. Helicity inversion is a well known phenomenon that can take place both in natural or synthetic systems. It can be triggered by many factors, like modifying building block structure[41, 42] or applying external stimuli, such as light,[21, 37, 56] temperature,[32, 77] solvent,[24, 30, 31, 35, 38, 61] or ion coordination.[1, 65] In this case, NRC1 handedness changed after the addition of surfactant. The switch between the two forms of NRC1 aggregate could take place either by its disruption followed by the formation of a different aggregate more stable in that environment, or by loosening of intermolecular interactions. The presence of a surfactant would be crucial in both cases: to stabilize the monomer in the first one, since NRC1 was very hydrophobic, and unlocking the structure in the second one. The disruptive effect of TX on NRC1 aggregates could be appreciated observing the decrease of exciton couplet intensity at the increase of concentration (Fig. 2.44a). Since there was an isosbestic point for these curves, the optical activity for samples at 0.1 , 1 and 10 mM of surfactant was due to NRC1 residual aggregates in the initial form. Helicity inversion of NRC1 aggregate took place also upon addition of SDS to its solutions (Fig. 2.44b). At variance with TX case, the intensity of NRC1 exciton couplet decreased more quickly and, more importantly, at 8.5 mM the couplet disappeared and was replaced by a single negative signal. The disappearance of the exciton couplet indicated that NRC1 aggregates were disrupting or already disrupted. The

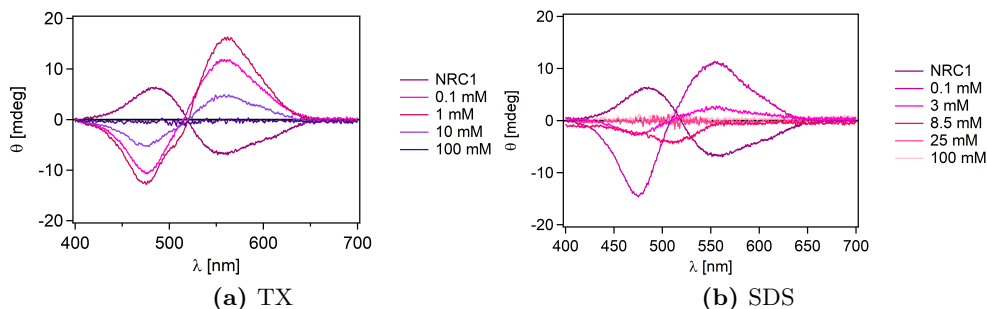


Figure 2.44: Influence of increasing concentration of a) non ionic TX and b) anionic SDS on the optical activity of 1 mgml^{-1} solutions of NRC1.

presence of the negative signal, among other possibilities, could be induced by a perturbation of the chromophore by lactose chiral centers. In analogy with TX case, the optical activity for 0.1 and 3 mM SDS samples had to be referred to residual aggregates with original conformation. The higher disruptive efficacy for SDS compared to TX was testified by the quicker decrease in exciton couplet intensity. The results obtained from this ECD investigation could suggest the presence of two forms of NRC1 aggregates in solution. The dye initially assembled in left-handed aggregates. However, the equilibrium was easily shifted towards a right-handed analogous structure even after the addition of surfactant, even at a concentration as low as 0.1 mM. That could indicate that these two structures possessed similar energy. The presence of a second form of NRC1 aggregates was confirmed analyzing the same 1 mgml^{-1} dye solution after a long time interval. After three months, NRC1 ECD spectrum presented the same exciton couplets, but at this point the helicity of the system had changed and their sign was positive. This inversion indicated that aggregates in solution had switched to a more stable right-handed helical structure.

2.5.1 Reentrant Condensation

In the previous section the behavior of GDs in presence of surfactants was reported. The interaction of these cationic dyes with anionic surfactant SDS

led to the precipitation of GDs in a specific range of SDS concentrations. This phenomenon is known as reentrant condensation (RC) and takes place when a polyion is condensed by addition of ions of opposite charge.[8, 75] The counterions complex the polyelectrolyte, reducing its surface charge to nearly zero. In this situation, short-range attraction prevail on Coulomb repulsion, resulting in polyelectrolyte condensation.[29, 75] This phenomenon is widely represented in literature, mainly as a tool for condensation of DNA and proteins,[4, 66, 69, 76] but also of more complex systems, such as virus nanoparticles.[2] The presence of SDS triggered the same condensation process for GDs aggregates, resulting in their precipitation. The range of surfactant concentrations in which RC took place (0.1-3 mM) was investigated more in details by light and X-Rays scattering for all the five dyes. Evidences of GDs condensation and precipitation were obtained by DLS, that revealed a massive increase of aggregates dimension in solution in a limited range of SDS concentrations for all dyes. Information on the shape of aggregates in the samples at the limits of RC region were obtained by SAXS, as well as on the structure of each precipitate. For each GD, the precipitate was collected from those sample at which there was maximum precipitation. Moreover, GDs precipitation could also be appreciated visually, therefore, for each dye a picture of its samples in RC range was reported, showing solutions at increasing SDS concentration from 0.1 to 3 mM from left to right. First of all, NR202 was analyzed. As shown in Fig. 2.45c, D_H of aggregates in solution increase for those SDS concentrations at which NR202 precipitated. CONTIN [60] analysis also allowed to appreciate how the size distribution of objects in solution varied with increasing SDS concentration. In Fig. 2.45b were reported four size distributions, the first of NR202 before SDS addition, and the other three at significant surfactant concentrations: 0.1 mM, 0.9 mM and 3 mM. 0.1 and 3 mM were the first and last points of RC range, while 0.9 mM was the concentration at which NR202 precipitated more. Diameters distribution for NR202 in water and in presence of 0.1 mM SDS were very similar, having a small population of objects with dimensions around 100 nm and another having D_H of approximately 500 nm. At 0.9 mM SDS NR202 was precipitating, thus only a small population of aggregates of 300 nm could be detected, since its other aggregates were too big and fell out of the experimental limit. 0.1, 0.9 and 3 mM SDS samples were also studied by SAXS. Power-law fitting showed that 0.1 mM SDS NR202 sample (Fig. 2.45d) had low q slope of -1, indicating the presence of one-dimensional scatterers in

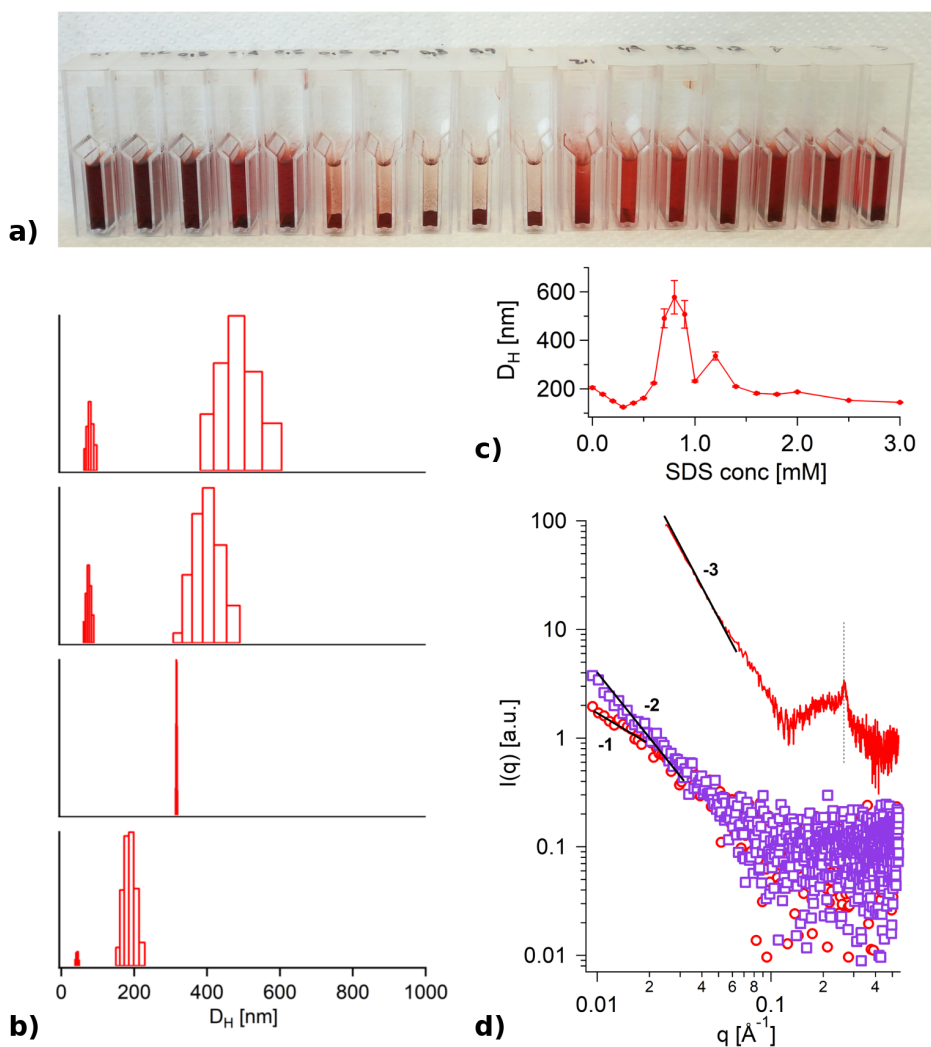


Figure 2.45: a) Picture of NR202 RC range. Variation of NR202 a) aggregates size distribution for (from top down) 0, 0.1, 0.9 and 3 mM of SDS and c) hydrodynamic diameter of its assemblies in the entire RC range (0.1 -3 mM). d) SAXS analysis of SDS 0.1 mM (\circ), 3 mM (\square) and 0.9 mM (red line) NR202 samples. SAXS curves were reported vertically offset for clarity.

solution. Two-dimensional scatterers were retraced in 3 mM SDS sample, as testified by a slope of -2 in the low q region. Finally, the linear region between 0.02 and 0.06 \AA^{-1} for the precipitate obtained at 0.9 mM SDS was analyzed by Power-law, showing a low q slope of -3, indicating the presence of three dimensional scatterers. More importantly, it also had a peak at higher q values. This peak could suggest that NR202 precipitated forming a crystalline phase. Dye precipitation occurred in a much smaller range of surfactant concentrations for NO30, as could be appreciated both visually (Fig. 2.46a) and experimentally by light scattering investigation (Fig. 2.46c). Four size distributions for NO30 at different SDS concentrations were reported in Fig. 2.46b: 0, 0.2, 1 and 3 mM. As in NR202 case, 0.2 and 3 were the limits of RC range, while 1 mM was the SDS concentration at which maximum precipitation for this dye took place. As already pointed out, NO30 in solution formed very big and polydisperse aggregates, that could be retraced by CONTIN [60] analysis also in its size distribution, together with a very small population of objects of about 10 nm in diameter. Adding 0.2 mM SDS to NO30 led to a decrease in objects dimension. In this case there were two populations: the first having average D_H around 200 nm and the second one composed by very small aggregates of about 10 nm. Also at 1 mM SDS two populations were detected: one centered around 30 nm and the other one around 300 nm. This was at variance with what observed for NR202 at SDS concentration of maximum condensation (Fig. 2.45b), but it was consistent with what could be appreciated visually (Fig. 2.46a). In fact, the condensation range was narrower and, even if the dye precipitated, there was a higher amount of residual NO30 in the solution. This could suggest that NO30 was less affected by the presence of SDS compared to NR202, which was in agreement with the small changes observed in its absorption upon addition of the surfactant (Fig. 2.39c). At 3 mM SDS a reduction in aggregates diameters was observed, as well as in NR202 case, leading to two populations of aggregates with average diameters of 20 and 90 nm respectively. SAXS measurements were performed on 0.1, 1 and 3 mM SDS samples. The curve registered for 0.1 mM SDS sample had higher scattering intensity compared to that of NO30 solution (Fig. 2.8b), but was not significantly different in other aspects. On the contrary, for 3 mM SDS sample the curve had two different slopes at $q < 0.1 \text{\AA}^{-1}$, -2 and -1 respectively at intermediate and low q . This could indicate the presence of objects in the shape of ellipsoidal or large cylinder. The 1 mM precipitate curve had

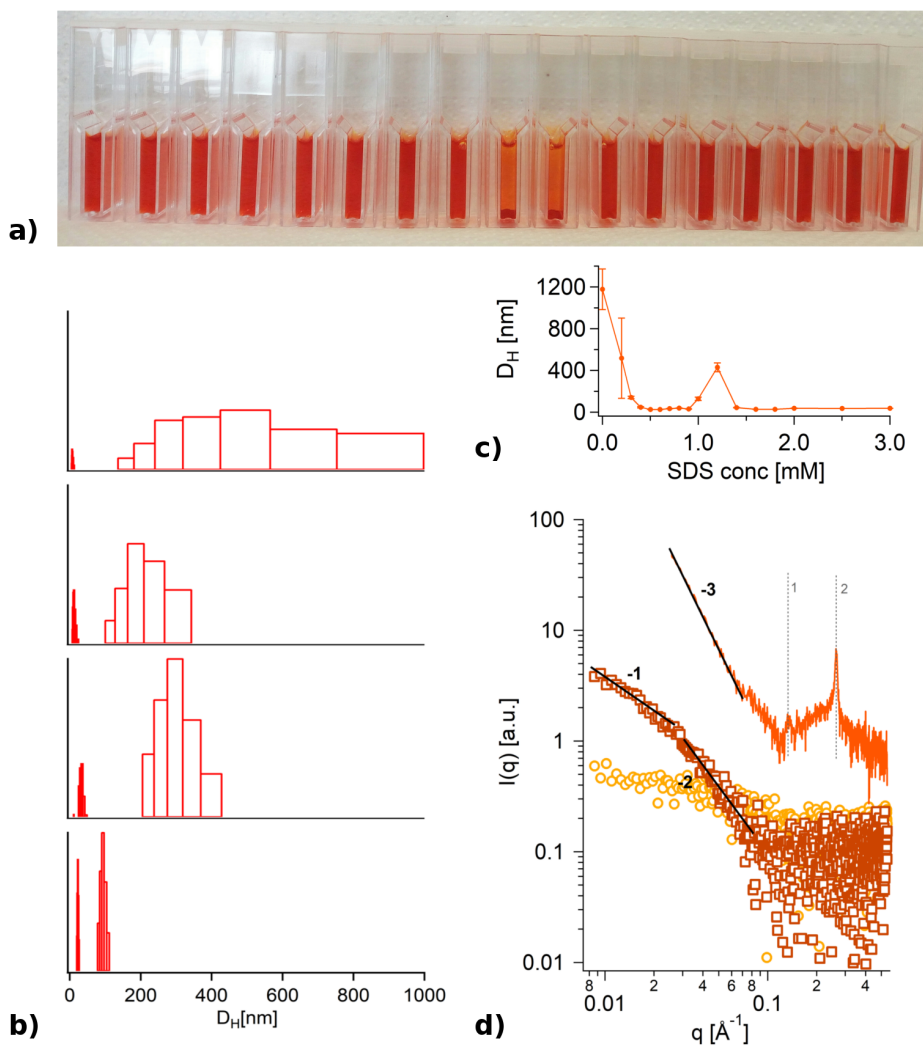


Figure 2.46: a) Picture of NO30 RC range. Variation of NO30 a) aggregates size distribution for (from top down) 0, 0.1, 1 and 3 mM of SDS and c) hydrodynamic diameter of its assemblies in the entire RC range (0.1 -3 mM). d) SAXS analysis of SDS 0.2 mM (\circ), 3 mM (\square) and 1 mM (orange line) NO30 samples. SAXS curves were reported vertically offset for clarity.

a -3 slope at low q , between 0.02 and 0.06 \AA^{-1} and two peaks of different intensity at $q > 0.1$, respectively at 0.13 and 0.26 \AA^{-1} . The presence of more than one peak could probably be caused by an ordered phase. The two peaks occurred in sequence 1, 2 that could suggest a lamellar morphology.[26] The intensity of these peaks was, however, unusual, since that at higher q , that would correspond to a higher order peak, was more intense than the other, possibly indicating a particular kind of lamellar aggregate. The next dye that was analyzed was NB27. Visual (Fig. 2.47a) and DLS (Fig. 2.47c) analysis both confirmed that dye precipitation occurred in a rather large range of SDS concentrations. Also in this case four size distribution obtained from CONTIN [60] analysis were reported in comparison, to demonstrate the variations that took place in solution increasing surfactant concentration. For NB27 these four concentrations were 0, 0.1, 0.7 and 3 mM SDS (Fig. 2.47b) were 0.7 mM was NB27 maximum precipitation concentration for the entire RC range. NB27 without added surfactant showed a broad population with diameters between 200 and 800 nm, plus a very small population under 10 nm. At 0.1 mM SDS, objects size increased and became more polydisperse, while a third population having average D_H around 100 nm appeared. At 0.7 mM only very big objects were detected, in agreement with the ongoing massive precipitation. At 3 mM SDS, three populations were again detected: two very small ones at 50 nm and under 10 nm, and a third composed by objects with average size of 300 nm. 0.1, 3 and 0.7 mM SDS samples were then analyzed by SAXS (Fig. 2.47d). 0.1 and 3 mM had similar curves, with double slope at $q < 0.1 \text{\AA}^{-1}$. In analogy with what reported for 3 mM SDS NO30 sample (Fig. 2.46d), this could indicate the presence of structures that possess one- and two- dimensional scattering, such as ellipsoidal or large cylinders. The curve for 0.7 mM SDS precipitate presented a -3 slope at $q < 0.08 \text{\AA}^{-1}$ and two peaks at $q > 0.1 \text{\AA}^{-1}$, at 0.115 and 0.23 \AA^{-1} respectively. The sequence at which these two peaks occurred was 1, 2, as in NO30 case. However, this curve was more similar to that of a typical lamellar morphology. These two peaks, united to the -3 slope at low q probably suggested a lamellar crystalline aggregate,[26] where the slope at low q could be an indication of the presence of a network-like structure on a larger length scale.[28] NRC1 behaved differently from the other four GDs. Its precipitate, obtained between 0.3 and 0.8 mM SDS, appeared as a flocculate to visual inspection. Moreover, at 0.2 mM and between 0.9 and 1.4 mM, it also formed a spatially self-organized gel-like structure, as shown in Fig. 2.48a. For

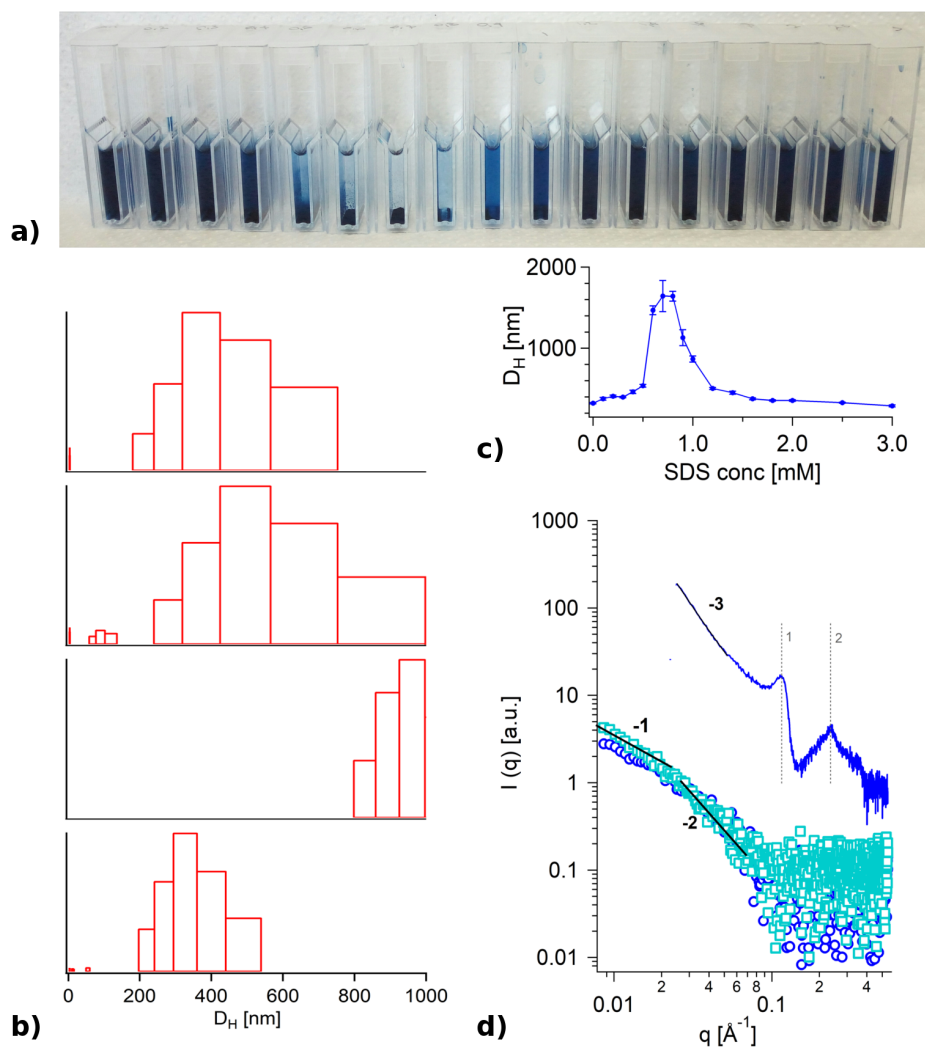


Figure 2.47: a) Picture of NB27 RC range. Variation of NB27 a) aggregates size distribution for (from top down) 0, 0.1, 0.7 and 3 mM of SDS and c) hydrodynamic diameter of its assemblies in the entire RC range (0.1 -3 mM). d) SAXS analysis of SDS 0.1 mM (\circ), 3 mM (\square) and 0.7 mM (blue line) NB27 samples. SAXS curves were reported vertically offset for clarity.

SDS concentrations between 1.8 and 3 mM, NRC1 appeared homogeneously dispersed in solution. The increase of aggregates dimensions between 0.3 and 1 mM, as a consequence of dye-SDS complexes aggregation and precipitation was verified by DLS (Fig. 2.48c). Four size distribution obtained by CONTIN [60] analysis were reported for four significant concentrations: 0.1, 0.5, 1.2 and 3 mM SDS (Fig. 2.48b). In this case the solution of NRC1 without surfactant was not reported, in order to show the two concentrations at which the precipitate and the gel-like phase formed, respectively 0.5 and 1.2 mM, as well as RC limit SDS concentrations. At 0.1 mM SDS, NRC1 showed three populations: one around 60 nm, a second, broader, around 200 nm and a third distributions of objects with D_H above 400 nm. At 0.5 mM only a polydisperse distribution of objects with dimensions between 200 and 600 nm was identified. At 1.2 mM, four distributions were detected. Two very small populations with dimensions under 10 nm and around 20 nm, one around 150 nm and a distribution of very big objects. For 3 mM SDS sample. the size distribution was similar to that for 0.1 mM: one small population around 20 nm, one around 150 nm and big aggregates with diameters over 400 nm. 0.5, 1.2 and 3 mM SDS samples were studied by SAXS (Fig. 2.48d). 3 mM sample curve, in analogy with those for NO30 and NB27 (Fig. 2.46d and 2.47d), showed a double slope for intermediate and low q values, -2 and -1 respectively, probably indicating the formation of ellipsoidal or large cylindrical aggregates. The precipitate and the gel-like phases revealed the presence of an ordered structure, the latter being less ordered. Several peaks were present at $q > 0.1 \text{ \AA}^{-1}$, with occurring sequence $1, \sqrt{2}, \sqrt{3}, \sqrt{4}, \sqrt{6}, \sqrt{8}$. The SAXS curve for the gel-like structure showed reflections peaks, although only partially corresponding to that of the precipitate. This suggested that the zero-charged ordered structure found in the precipitate was progressively disrupted by an excess of SDS. This was also confirmed by the gradual color recovery for SDS concentration > 0.5 mM. Hamley et al. reported a similar pattern in WAXS/XRD curves for protein hydrogels containing β -sheets,[25] for which signals in sequence $1, \sqrt{2}, \sqrt{3}, \sqrt{4}$ were detected. This suggested the possibility of β -sheets organization also for NRC1. In the oligopeptide presented by Hamley et al., the small dimensions of the molecules/functional groups responsible for H-bonding along the peptide chain determined the presence of this signal pattern in the WAXS q -range. In this case, the same pattern is unusually found in the SAXS region, probably because of the wider spatial extension of lactose residues, as well as SDS being

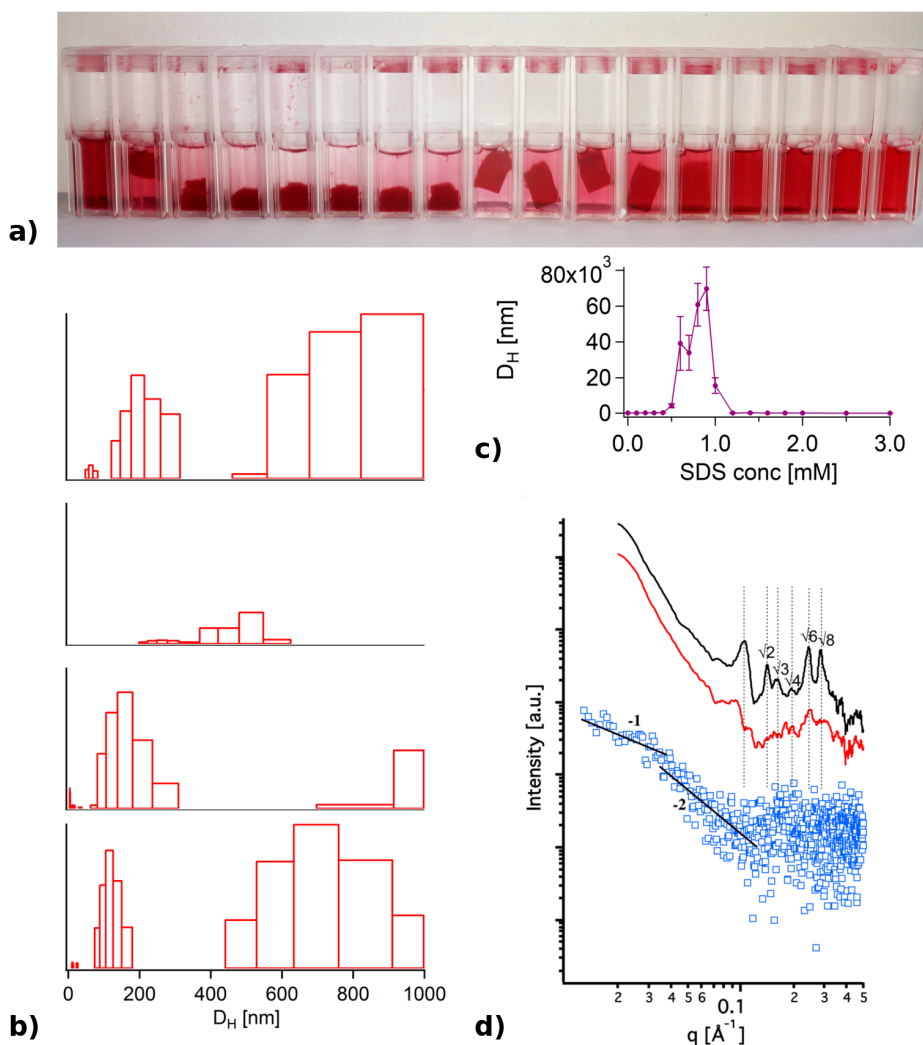


Figure 2.48: a) Picture of NRC1 RC range. Variation of NRC1 a) aggregates size distribution for (from top down) 0.1, 0.5, 1.2 and 3 mM of SDS and c) hydrodynamic diameter of its assemblies in the entire RC range (0.1 -3 mM). d) SAXS analysis of SDS 3 mM (\square), 0.5 mM (black line) and 1.2 mM (red line) NRC1 samples. SAXS curves were reported vertically offset for clarity.

a part of the structure. However, further investigations are required to confirm the hypothesis of β -sheets morphology for NRC1 precipitate. Finally, NY42 was analyzed. From both visual inspection (Fig. 2.49a) and DLS analysis (Fig. 2.49c) it was verified that massive dye precipitation occurred only at three SDS concentrations. In Fig. 2.49b were reported size distributions for 0, 0.1, 0.9 and 3 mM, obtained by CONTIN [60] analysis. Again, 0.1 and 3 mM were reported because they were RC SDS concentration limits while 0.9 mM was SDS concentration for maximum dye condensation. NY42 in absence of SDS size distribution showed three populations: two around 80 and 200 nm and a distribution of objects with dimensions above 700 nm. Three distributions were detected also in presence of 0.1 mM: one small distribution around 40 nm, one around 150 nm and a third broad one for bigger objects with D_H above 500 nm. In presence of massive NY42 precipitation at 0.9 mM, only a few objects of 300 nm in size were detected, as reported for NR202 (Fig. 2.45b). At 3 mM SDS, two populations were identified, a smaller one with average D_H around 150 nm and a broader, bigger one, composed by aggregates with dimensions between 400 and 800 nm. Finally, 0.1, 0.9 and 3 mM SDS samples were analyzed by SAXS (Fig. 2.49d). 0.1 mM curve was identical to that of NY42 (Fig. 2.9b), thus it gave no clear information on the aggregate structure. In analogy with 3 mM SDS samples for the previous GDs, except for NR202, this curve for NY42 presented a double slope at intermediate and low q values of -2 and -1 respectively. Also in this case this could be ascribable to formation of ellipsoidal or large cylindrical aggregates. The precipitate obtained at 0.9 mM SDS concentration showed a -3 slope for q between 0.02 and 0.06 \AA^{-1} and two very sharp peaks at $q > 0.1 \text{\AA}^{-1}$, respectively at 0.14 and 0.28 \AA^{-1} , with equal and very high intensity. Since these two peaks occurred with sequence 1,2, they could probably be related to the formation of a crystalline lamellar morphology,[26] even if these peculiar signals could also indicate a particular kind of lamellar structure. Further investigations are required to assign a certain morphology to all GDs-SDS precipitate.

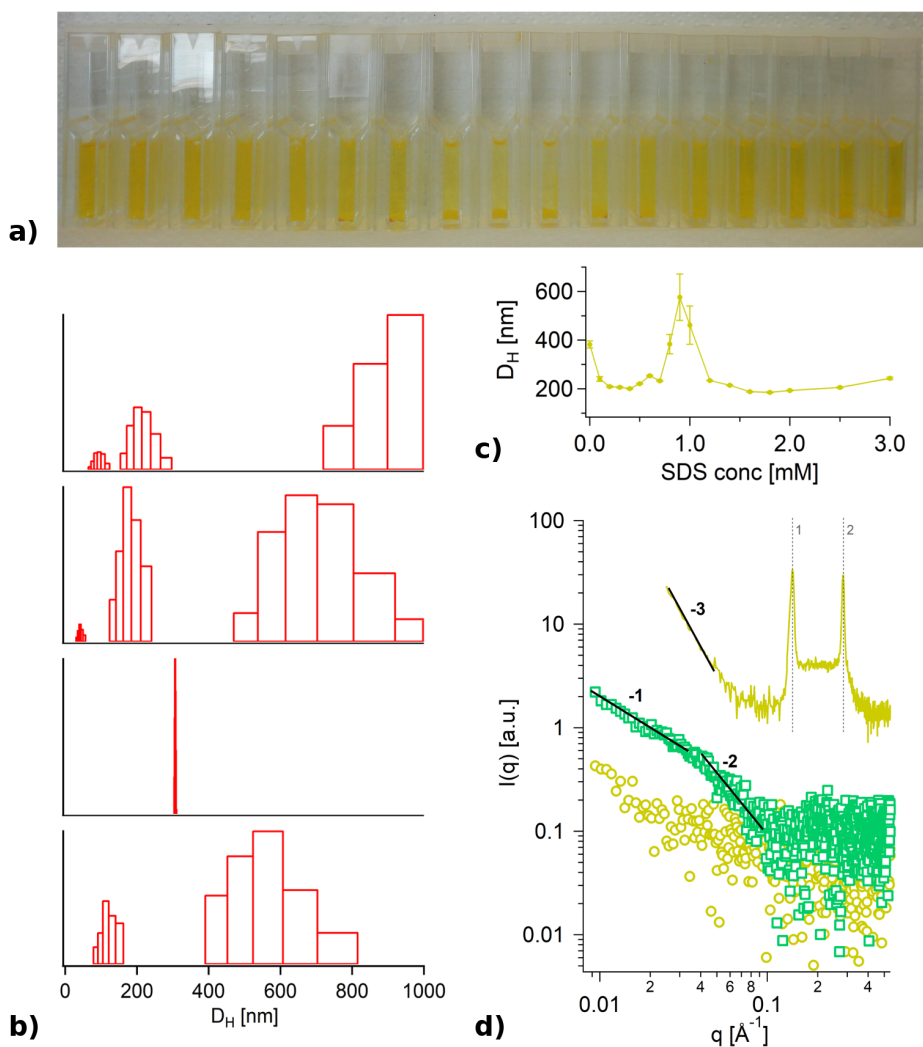


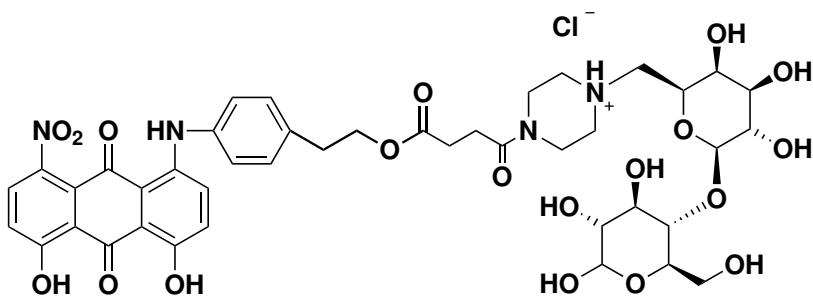
Figure 2.49: a) Picture of NB27 RC range. Variation of NY42 a) aggregates size distribution for (from top down) 0, 0.1, 0.9 and 3 mM of SDS and c) hydrodynamic diameter of its assemblies in the entire RC range (0.1 -3 mM). d) SAXS analysis of SDS 0.1 mM (\circ), 3 mM (\square) and 0.9 mM (yellow line) NY42 samples. SAXS curves were reported vertically offset for clarity.

2.6 Experimental

2.6.1 Glycoconjugated dyes

The five glycoconjugated dyes, NR202, NB27, NO30, NY42 and NRC1, were synthesized in our laboratories. [6, 7, 12] Their complete characterization was reported here.

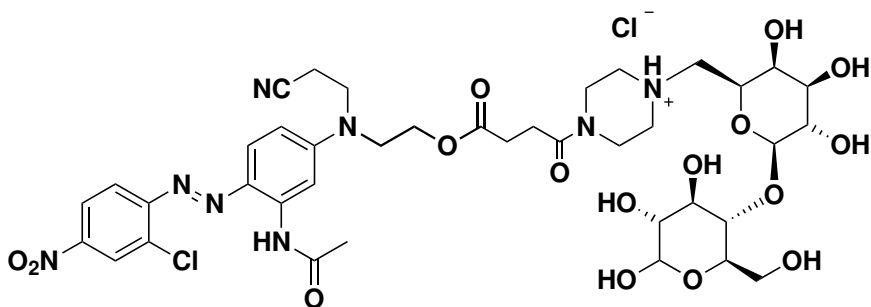
Analytical data: 3- {4- [(2R, 3R, 4S, 5R, 6S)- 6- ((2R, 3S, 4R, 5R)- tetrahydro- 4, 5, 6- trihydroxy- 2- (hydroxymethyl)- 2H- pyran- 3- yloxy)- tetrahydro- 3, 4, 5- trihydroxy- 2H- pyran- 2- yl) methyl] piperazin- 1- yl}- 3- oxopropyl 3- [4- (9, 10- dihydro- 4, 5- dihydroxy- 1- nitro- 9, 10- dioxoanthracen- 8- ylamino) phenyl] propanoate hydrochloride (NB27).



Dark blue solid, mp 160-185°C (dec.); λ_{max} (ϵ) (H₂O): 600 nm (4800 M⁻¹cm⁻¹); δ H (300 MHz, DMSO-d₆): 8.07 (1H, d, J 8.8 Hz), 7.64 (1H, d, J 9.9 Hz), 7.47 (1H, d, J 8.8 Hz), 7.42-7.23 (6H, m), 4.96-4.29 (5H, m), 4.284.19 (4H, m), 4.18-3.65 (16H, m), 3.64-3.41 (4H, m), 3.39-2.83 (5H, m), 2.72-2.37 (4H, m); ESI (m/z, +c): 913.6 (100%) [M+H]⁺.

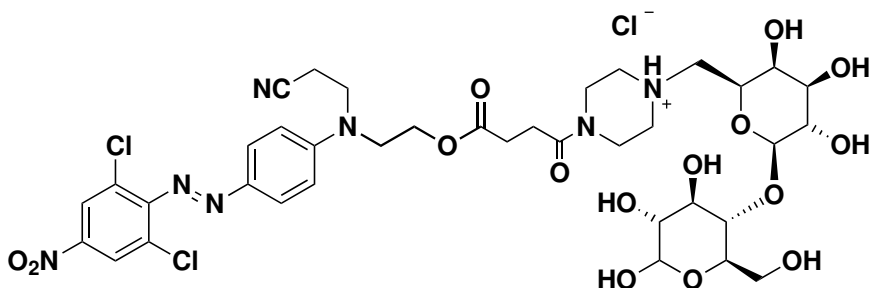
Analytical data: {2- [(2- cyanoethyl)- (3- acetylamino- 4- ((E)- (2- chloro- 4- nitrophenyl) diazenyl) phenyl) amino] ethyl} - 4- {4- [(2R, 3R, 4S, 5R, 6S)- 6- ((2R, 3S, 4R, 5R)- tetrahydro- 4, 5, 6- trihydroxy- 2- (hydroxymethyl)- 2H- pyran- 3- yloxy)- tetrahydro- 3, 4, 5- trihydroxy- 2H- pyran- 2- yl) methyl] piperazin- 1- yl}- 4- oxobutanoate hydrochloride (NR202).

Dark red solid, mp 170-177°C (dec.); λ_{max} (ϵ) (H₂O): 425 nm (12900 M⁻¹cm⁻¹); δ H (300 MHz, DMSO-d₆): 11.05 (1H, s), 8.44 (1H, d, J 2.7 Hz), 8.25 (1H, dd, J



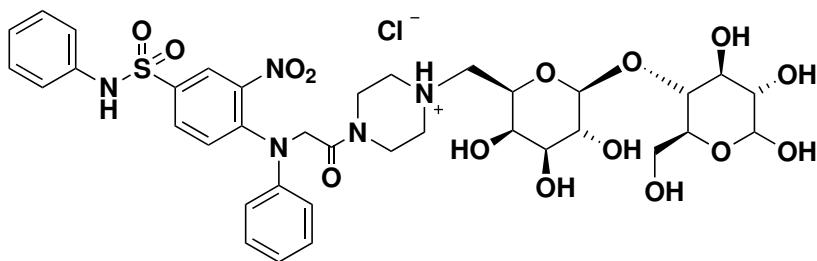
2.4 and J' 9.0 Hz), 8.05 (1H, d, J 9.0 Hz), 7.99 [1H, d (br), J 2.7 Hz], 7.79 (1H, d, J 9.0 Hz), 6.87 (1H, dd, J 9.0 and J' 2.4 Hz), 4.93-4.22 (6H, m), 4.14-3.54 (7H, m), 3.533.39 (5H, m), 3.38-3.36 (4H, m), 3.362.96 (12H, m), 2.92-2.87 (3H, m), 2.72-2.54 (2H, m), 2.53-2.40 (3H, m), 2.24 (3H, s); ESI (m/z, +c): 923.4 (100%) [M+H]⁺, 925.3 (40%) [M+H]⁺.

Analytical data: {2- [(2- cyanoethyl)- (4- ((E)- (2, 6- dichloro- 4- nitrophenyl) diazenyl) phenyl) amino] ethyl]- 4- {4- [((2R, 3R, 4S, 5R, 6S)- 6- ((2R, 3S, 4R, 5R)- tetrahydro-4, 5, 6- trihydroxy-2- (hydroxymethyl)- 2H- pyran- 3- yloxy)- tetrahydro- 3, 4, 5 - trihydroxy- 2H- pyran- 2- yl) methyl] piperazin- 1- yl]- 4- oxobutanoate hydrochloride (NO30).



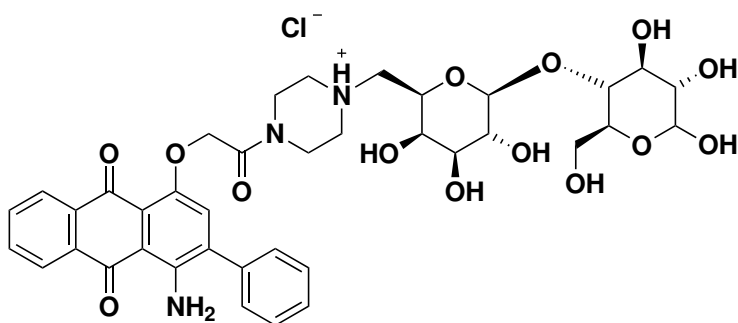
Dark orange solid, mp 174-183°C (dec.); λ_{max} (ϵ) (H₂O): 441 nm (16300 M⁻¹cm⁻¹); δ H (300 MHz, DMSO-d₆): 8.44 (2H, s), 7.85 (2H, d, J 9.3 Hz), 7.06 (2H, d, J 9.3 Hz), 5.13-4.52 (8H, m), 4.43-4.21 (4H, m), 4.143.95 (2H, m), 3.93-3.40 (13H, m), 3.37-2.92 (11H, m), 2.90-2.82 (2H, s), 2.70-2.60 (1H, m), 2.582.53 (1H, s); ESI (m/z, +c): 900.2 (100%) [M+H]⁺, 902.3 (89%) [M+H]⁺, 904.0 (43%) [M+H]⁺, 922.3 (18%) [M+Na]⁺, 924.2 (12%) [M+Na]⁺.

Analytical data: 1-{4- [(2R, 3R, 4S, 5R, 6S)- 6- ((2R, 3S, 4R, 5R)- tetrahydro-4, 5, 6- trihydroxy- 2- (hydroxymethyl)-2H-pyran-3-yloxy) -tetrahydro- 3, 4, 5- trihydroxy- 2H- pyran- 2-yl) methyl]piperazin- 1-yl} -2- {N- [4- (phenylaminosulfonyl)- 2- nitrophenyl]- N- phenylamino} ethanone hydrochloride (NY42).



Yellow-orange solid, mp 180-195°C (dec.); λ_{max} (ϵ : 420 nm ($4200 \text{ M}^{-1}\text{cm}^{-1}$); δH (300 MHz, CDCl_3): 9.89 [1H, s (br)], 8.318.25 (1H, m), 7.72-7.61 (1H, m), 7.56-7.45 (2H, m), 7.457.21 (8H, m), 7.14 (1H, d, J 9.3 Hz), 5.23-4.52 (10H, m), 4.44-4.18 (2H, m), 4.14-3.96 (2H, m), 3.95-3.65 (3H, m), 3.643.54 (3H, m), 3.53-3.42 (2H, m), 3.41-2.81 (10H, m); ESI (m/z, +c): 820.5 (100%) $[\text{M}+\text{H}]^+$, 842.4 (12%) $[\text{M}+\text{Na}]^+$.

Analytical data: 4- O- [6- (4- {[4- amino- 9, 10- dioxo- 3- phenyl- 9, 10- dihydroanthracen- 1- yl) oxy] acetyl} piperazin- 1- ium- 1- yl) -6- deoxy- b- D- galactopyranosyl] - D- xylo- hexopyranose (NRC1).



Dark purple solid, mp °C (dec.), λ_{max} (ϵ : 504 nm ($7800 \text{ M}^{-1}\text{cm}^{-1}$); ESI (m/z, +c): 802 (100%) $[\text{M}+\text{H}]^+$, 816 $[\text{M}+\text{OCH}_2+\text{Na}]^+$; HRMS (ESI-Orbitrap): calculated for $\text{C}_{39}\text{H}_{46}\text{N}_3\text{O}_{14}$ $[\text{M}-\text{H}]^+$ 78.2974; found 780.2964

2.6.2 Materials

Dimethylsulfoxide, Ethanol and Methanol were purchased from Sigma-Aldrich (St. Louis, MO). Dodecyl sulfate sodium was provided by Merck (Germany). N, N, N- Trimethyl hexadecan- 1- aminium bromide was purchased from Fluorochem (Hartfield, UK). Polyethylene glycol mono- 4- octyl phenyl ether was provided by Tokyo Chemical Industry (Tokyo, Japan).

2.6.3 UV-Visible spectrophotometry

UV-Visible measurements were carried out with a Perkin-Elmer Lambda EZ 201 (Waltham, Massachusetts, USA) in 0.1 cm quartz cuvettes. Spectra were registered in the wavelength range 200-800 nm.

2.6.4 Dynamic Light Scattering

Dynamic Light Scattering measurements were carried out with a Brookhaven Instruments apparatus (BI 9000AT correlator and BI 200 SM goniometer). The signal was detected by an EMI 9863B/350 photomultiplier. The light source were a second harmonic of a diode Nd:YAG laser, $\lambda=532$ nm Coherent Inova, linearly polarized in the vertical direction and a HeNe laser, 633 nm JAS Uniphase, linearly polarized in the vertical direction.

2.6.5 Small Angle X-rays Scattering

SAXS measurements were carried out with a HECUS SWAX-camera (Kratky) equipped with a position-sensitive detector (OED 50 M) containing 1024 channels of width 54 m. Cu K_{α} radiation of wavelength 1.542 Å has been obtained using an X-ray generator (Seifert ID-3003), operating at a maximum power of 2 kW. A 10 m thick W filter was used to remove the primary Cu K_{α} radiation. The volume between the sample and the detector was kept under vacuum ($P < 1$ mBar) during measurements to minimize scattering from air. The liquid samples were filled into 1 mm quartz capillary and then sealed. Semi-solid samples were placed in a sample holder cell between two Kapton windows.

Measurements were done at 25°C and temperature was controlled by a Peltier element, with an accuracy of 0.1°C. All scattering curves were corrected for the solvent contribution. SAXS measurements were carried out on a S3-MICRO SAXS/WAXS instrument (HECUS GmbH, Graz, Austria) which consists of a GeniX microfocus X-ray sealed Cu K α source (Xenocs, Grenoble, France) power 50 W which provides a detector focused X-ray beam with $\lambda = 0.1542$ nm Cu K α line. The instrument is equipped with two one-dimensional (1D) position sensitive detectors (HECUS 1D-PSD-50 M system), each detector is 50 mm long (spatial resolution 54 m/channel, 1024 channels) and cover the SAXS q-range ($0.003 < q < 0.6 \text{ \AA}^{-1}$). The temperature was controlled by means of a Peltier TCCS-3 Hecus.

2.6.6 Circular Dichroism

Circular Dichroism measurements were performed on a JASCO J-600 spectropolarimeter, in the 800-200 nm range, using Hellma 1 mm pathlength quartz cuvettes, scanning speed 50 nm/min, response 1 sec, 5 accumulations per sample.

2.6.7 Atomic Force Microscopy

Atomic force microscopy (AFM) images were collected with a XE7 system (Park System Corp., Korea). NR202 and NY42 images were acquired in non-contact mode using PointProbe[®] Plus PPP-NCHR 10M tips with guaranteed radius of curvature < 10 nm, a nominal force constant of 42 N m^{-1} , and a resonance frequency of 296 kHz (drive =77%). Measurements were performed in air in both high- voltage and low-voltage mode. Low-voltage mode measurements were performed for scan areas of $2 \mu\text{m}^2$. NRC1 images were acquired in non-contact mode using SSS-NCHR 10M AFM tips with a guaranteed radius of curvature of 5 nm, a nominal force constant of 42 N m^{-1} , and a resonance frequency of 292 kHz (drive =40%). Measurements were performed in air in both high- voltage and low-voltage mode. Low-voltage mode measurements were performed for scan areas of 500 nm^2 . Set point value is 12.4 nm. The samples investigated was obtained by deposition of a drop of 1 mgml^{-1} water solution of NR202, NY42 and NRC1 on a mica support. The solution was

left on the support for 10 seconds to allow the adherence of a low quantity of sample to the mica. Then, the support was quickly dipped in clean water to remove the excess of substance and avoid a too concentrated sample. The sample was left to dry under hood overnight.

Chapter 3

Computational study

3.1 Introduction

Glycoconjugated dyes have a rather complex molecular structure and a high number of degrees of freedom. Thus, their behavior in solution is very difficult to understand since they are very sensitive to any change in their environment. Their physico-chemical characterization demonstrated the presence of self-assembly in water, probably triggered by hydrophobic and stacking interactions. However, it was not possible to fully understand how these molecules interact in solution. To have a description of the interactions that take place at atomistic level, GDs were studied using computational tools. Two computational approaches could be used to study these molecules: quantum mechanics (QM) based methods (e.g. Density Functional Theory, DFT) or classical mechanics based ones (e.g. Molecular Mechanics, MM, Molecular Dynamics, MD). DFT is a QM method that computes energy and other properties for a system based on its electron density (ρ). In general, QM methods are powerful and versatile and their use is widespread. They can be used to calculate energies and optimize structures, as well as to calculate molecular properties.[46] However, their computational cost makes them difficult to use to study large molecular systems. MM methods are also largely spread in molecular modelling. They utilize a set of molecules (represented as balls -atoms- and springs -bonds) to derive rules and parameters for a more general use, e.g. Force Fields, FF.

Thanks to the approximations they use, these methods are more efficient and have a lower computational cost than QM ones. Since GDs are quite large molecules, with more than 100 atoms each, they were studied by MM methods, in particular FF. The following equation describes a typical force field equation (AMBER [16]), that represents the potential energy function of the system:

$$\begin{aligned}
 V_{AMBER} = & \sum_i^{n_{bonds}} b_i(r_i - r_{i,eq})^2 + \sum_i^{n_{angles}} a_i(\theta_i - \theta_{i,eq})^2 + \sum_i^{n_{dihedrals}} \sum_n^{n_{i,max}} (V_{i,n}/2) \\
 & [1 + \cos(n\phi_i - \gamma_{i,n})] + \sum_{i<j}^{n_{atoms}'} \left(\frac{A_{ij}}{r_{ij}^{12}} - \frac{B_{ij}}{r_{ij}^6} \right) + \sum_{i<j}^{n_{atoms}'} \frac{q_i q_j}{4\pi\epsilon_0 r_{ij}}
 \end{aligned}
 \tag{3.1}$$

The potentials due to bond distances, bond angles and dihedral angles are included in the first three terms of Eq. 3.1, the bonded terms. The last two terms of the equation, the non-bonded terms, takes into account Lennard-Jones and Coulombic terms for dispersion-repulsion and electrostatic effects. It is possible to calculate a trajectory using Newton’s law of movement in order to develop a dynamic view of a molecular system (Molecular Dynamic, MD) and Force Fields, based on classical mechanics, can be used to determine the energy of the system along the trajectory. The specific parameter used to study GDs were chosen from General AMBER Force Field library [71] using AMBER tools, with the exception of atomic charges in each molecule, which were calculated by DFT. In particular, DFT calculations were performed using ORCA [47, 48] and PBE functional,[53] from which Mulliken atomic charges were obtained. In this work, the behavior of the five GDs, NR202, NB27, NO30, NY42 and NRC1, was studied by FF. For simplicity, only the core of each dye was taken into account, neglecting lactose piperazine and part of the linker. The molecular structures of these cores were reported in Fig. 3.1. This investigation was performed using LAMMPS [57] to perform a MD at 300 K, with timestep of 0.5 fs. In the first 50000 fs of MD a thermalization using a thermostat was performed on each system, followed by an acquisition run of 50 ns in the NVE ensemble. A conformational search was performed on each GD core in vacuum and was later extended to same-dye dimers and trimers. These data represent a preliminary study. A perspective investigation should

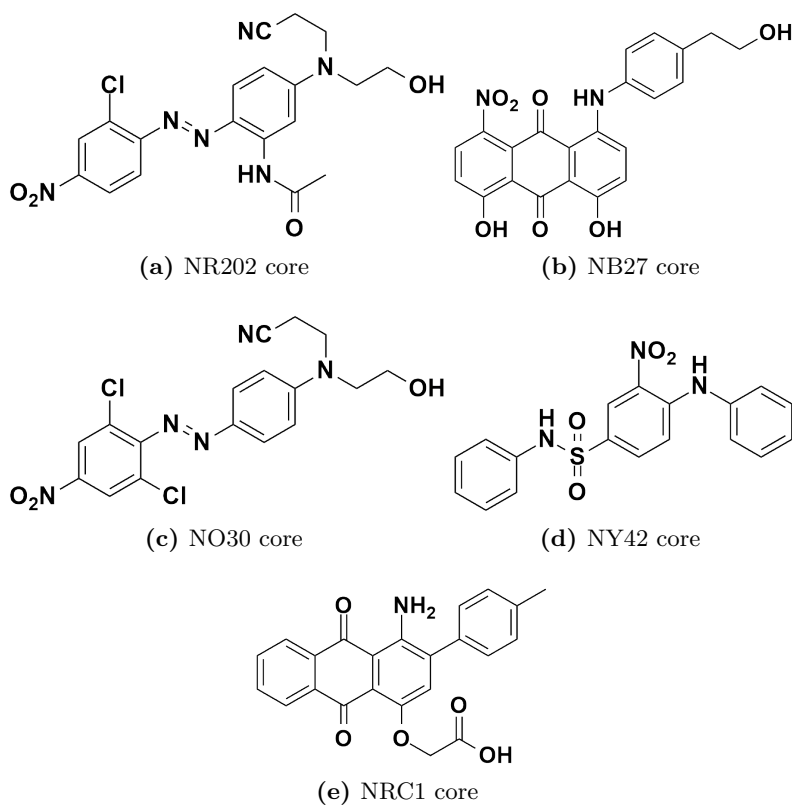


Figure 3.1: Molecular structures of the five GDs, limited to the core, used as basis for FF.

include computational modeling of GDs entire molecules, including lactose and a TD-DFT study of these systems in water, to fully consider the influence of the solvent and obtain simulated UV-Visible and ECD spectra.

3.2 Molecular Dynamics on GDs monomers

The first step on this conformational search was performing a MD on single GDs cores, reported in Fig. 3.1. NR202 core structure assumed only one significant conformation in MD, reported in Fig. 3.2a. This was consistent with

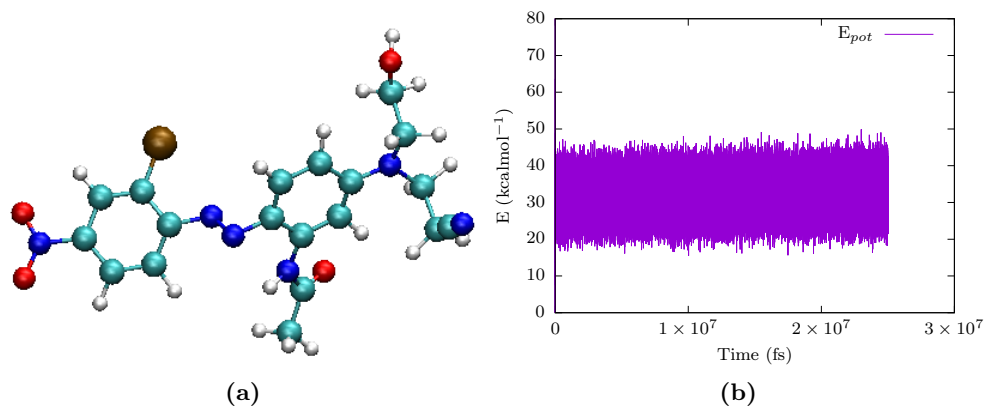


Figure 3.2: NR202 core a) principal conformation and b) E_{pot} profile obtained by FF MD in vacuum.

its Potential Energy profile during the entire MD, that did not underline important variations and constantly oscillated between 40 and 20 kcalmol⁻¹ (Fig. 3.2b). Since their molecular structure was very similar, the behavior of NO30, the second azo dye, was very similar to that observed for NR202. In fact, also in this case, the molecule assumed only one conformation. This conformation was reported in Fig. 3.3a. Its E_{pot} remained between 20 and 0 kcalmol⁻¹, showing no significant variations. NB27 had a more rigid structure compared to azo dyes, since its core consisted in an anthraquinone molecule. Therefore, it had few conformational degree of freedom, consisting mainly on rotation around C-C bond for the side chain and around C-N bond for the phenyl group. This reflected on its preferential conformation (Fig. 3.4a), in which the phenyl was mainly tilted with respect to the anthraquinone, and on its E_{pot} profile, shown in Fig. 3.4b. The energy was maintained between 70 and 40 kcalmol⁻¹ for the entire MD. NRC1 anthraquinone dye, in analogy with NB27, had also a more rigid core structure compared to azo dyes. It preferentially assumed just one conformation, reported in Fig. 3.5a, in which lateral phenyl was slightly tilted with respect to anthraquinone. Its E_{pot} constantly oscillated between 60 and 30 kcalmol⁻¹ for all the MD. The presence of three separated aromatic rings gave NY42 the highest conformational freedom of all five GDs. In fact, these molecule assumed not one, but three preferential conformations. The first one

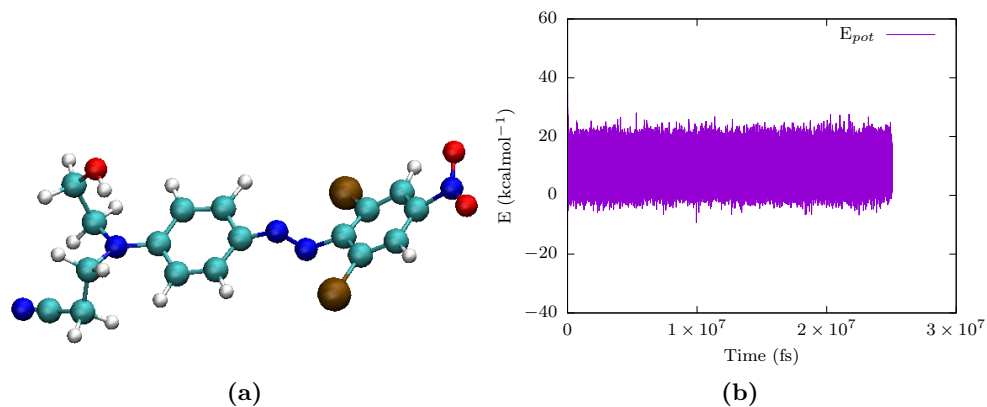


Figure 3.3: NO30 core a) principal conformation and b) E_{pot} profile obtained by FF MD in vacuum.

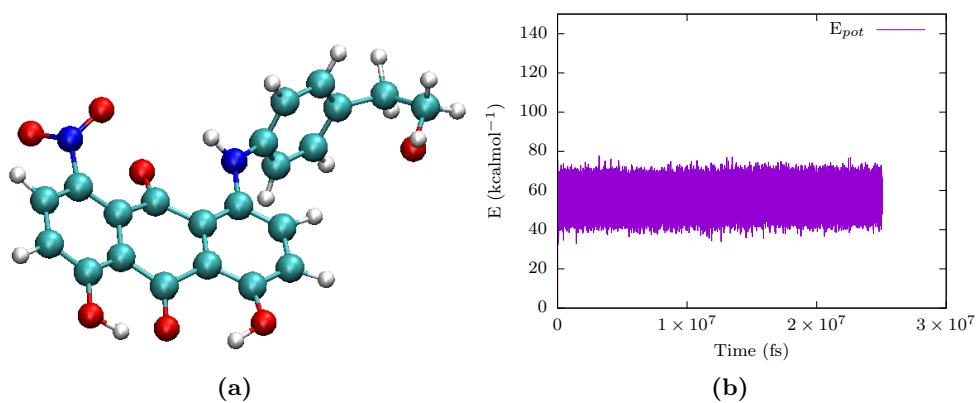


Figure 3.4: NB27 core a) principal conformation and b) E_{pot} profile obtained by FF MD in vacuum.

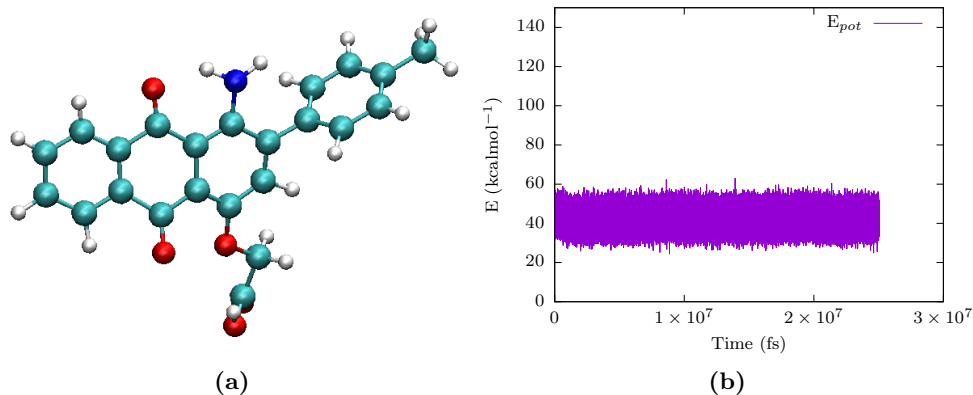


Figure 3.5: NRC1 core a) principal conformation and b) E_{pot} profile obtained by FF MD in vacuum.

had both lateral aniline rings tilted with respect to the central phenyl (Fig. 3.6a). In the second conformation, one of the lateral phenyls and the central ring were coplanar, while the third was tilted, as shown in Fig. 3.6b. In the last conformation, the molecule had a more closed-up conformation, in which the two lateral aniline rings were cofacial (Fig. 3.6c). Despite differences in conformation, NY42 maintained constant its E_{pot} between 80 and 50 kcalmol⁻¹.

3.3 Molecular Dynamics on GDs dimers

The conformational search was then extended to dimers of all GDs to understand how interactions between dye molecules could take place. The two molecules were placed at 30 Å from each other in vacuum and they were allowed to spontaneously assemble during MD. In this MD trajectory, dimers changed conformation on their own accord. The more stable conformations for every dimer were reported here, as preferential conformations. NR202 dimer had at least two preferential conformations. In all cases the two molecules interacted through facial stacking between one of the phenyls. The interaction was equally probable with either of the two ring on each molecule. The main

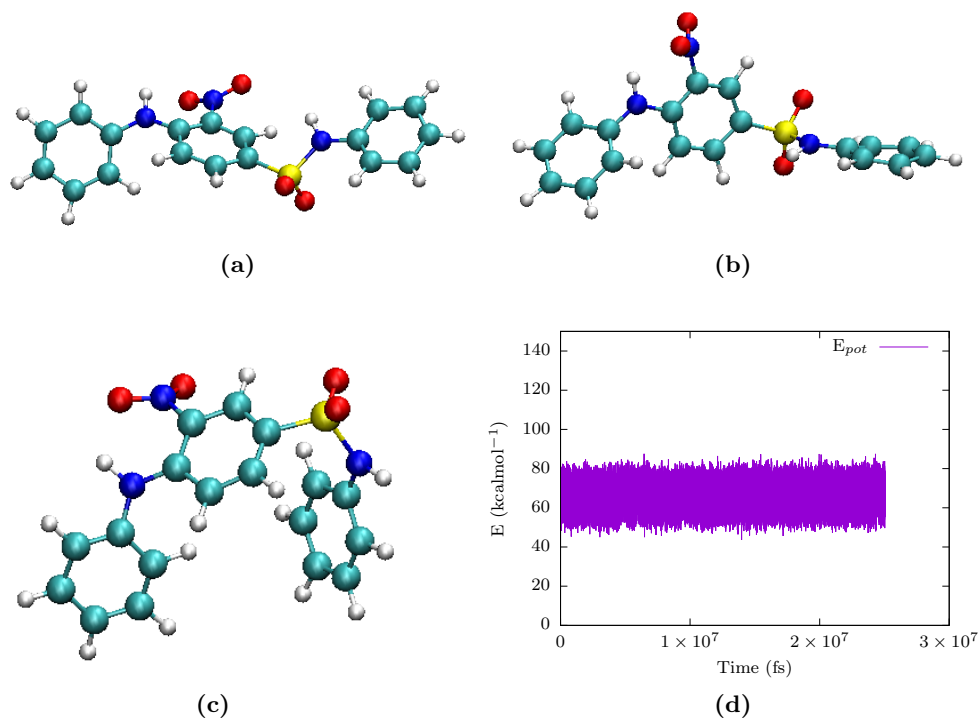


Figure 3.6: NY42 core three conformations (a-c) and d) E_{pot} profile obtained by FF MD in vacuum.

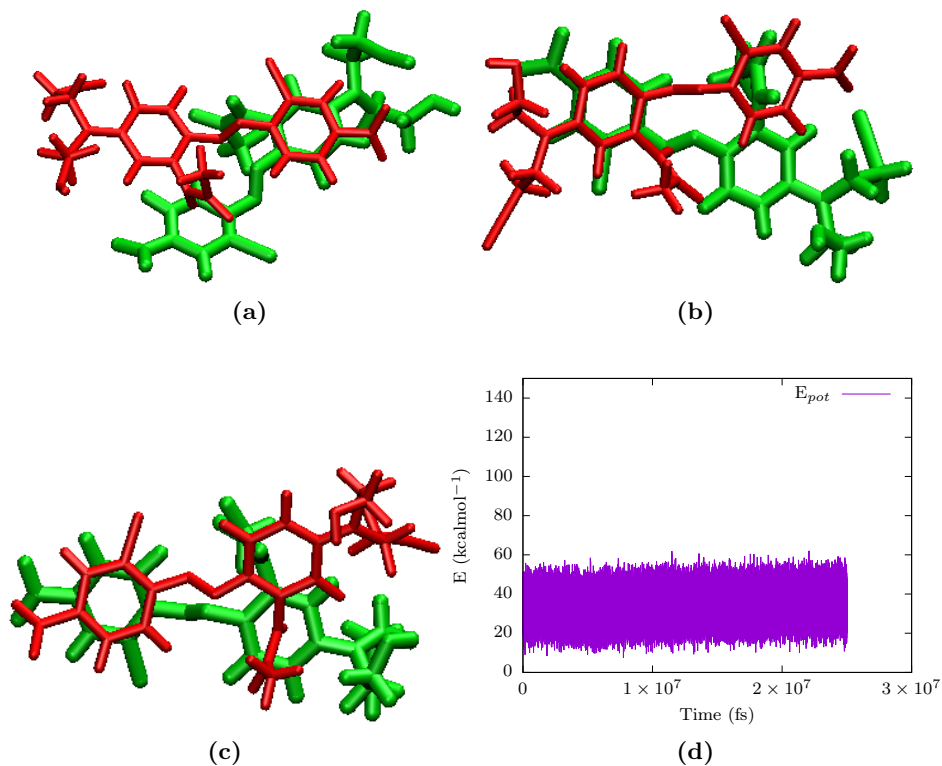


Figure 3.7: NR202 dimers configurations (a–c) and d) E_{pot} profile obtained by FF in vacuum.

difference between the two conformations was the position of the side chains. In one case they were on the same side of the dimer (Fig. 3.7c), while in the other they pointed in opposite directions (Fig. 3.7a and 3.7b). E_{pot} of NR202 dimer oscillated between 50 and 10 kcalmol⁻¹ and no significant energy variation was present, indicating an equal probability for all these dimer conformation to form. Globally, this system was not disordered and could potentially allow elongation of NR202 aggregates up to a certain extent. However, this was not an highly order system either, since azo dyes have some conformational freedom. Therefore, conformational arrangement could interfere with elongation as well. Two molecules of azo dye NO30 could interact in at least two different way. In Fig. 3.8a, a dimer conformation in which the two dye molecules inter-

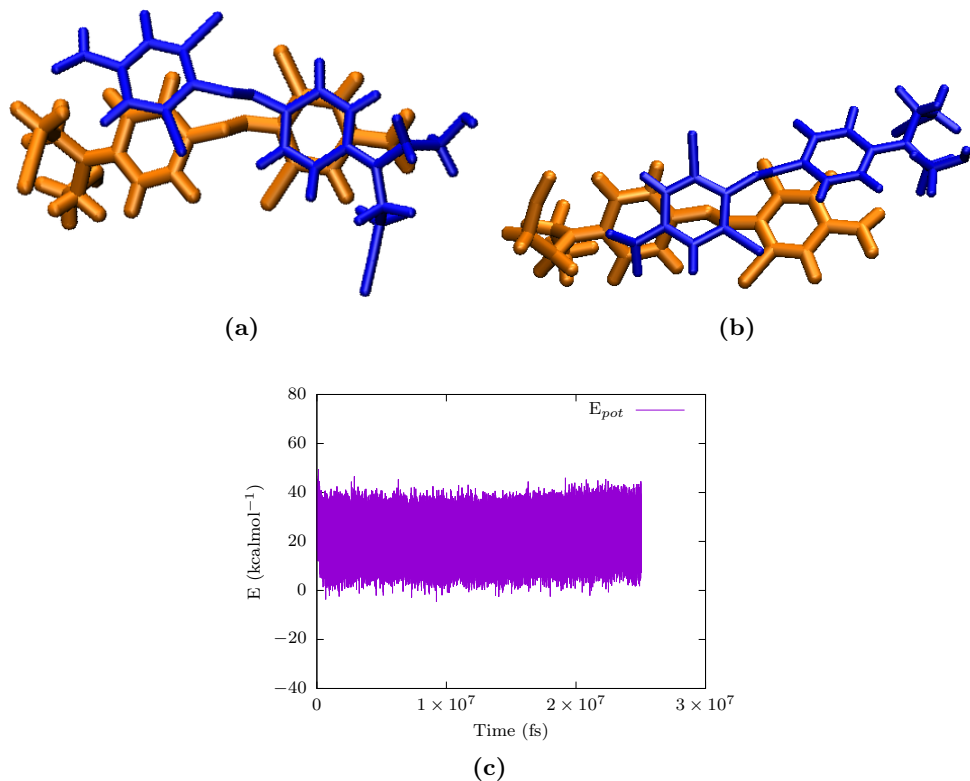


Figure 3.8: NO30 dimers configurations (a–c) and d) E_{pot} profile obtained by FF in vacuum.

acted through facial π stacking was reported. This interaction could take place between either one of the two rings on one molecule, resulting in four possible versions of this conformation. However, the two more stable were those in which the side chains on the two monomers pointed in opposite directions, as in the one reported in this image, with the two molecules slightly tilted. In this disposition, the second couple of phenyls could also interact facially, but only for a brief time. NO30 other preferential conformation was shown in Fig. 3.8b. In this situation, one ring of the monomer interacted with the azo group and the two dye molecules were tilted. These dimer conformations had approximately the same energy, as shown by the E_{pot} , that showed no significant variation in energy and oscillated between 40 and 0 kcalmol⁻¹. Thus, these conformations all had the same probability to form, depicting a rather disordered situation,

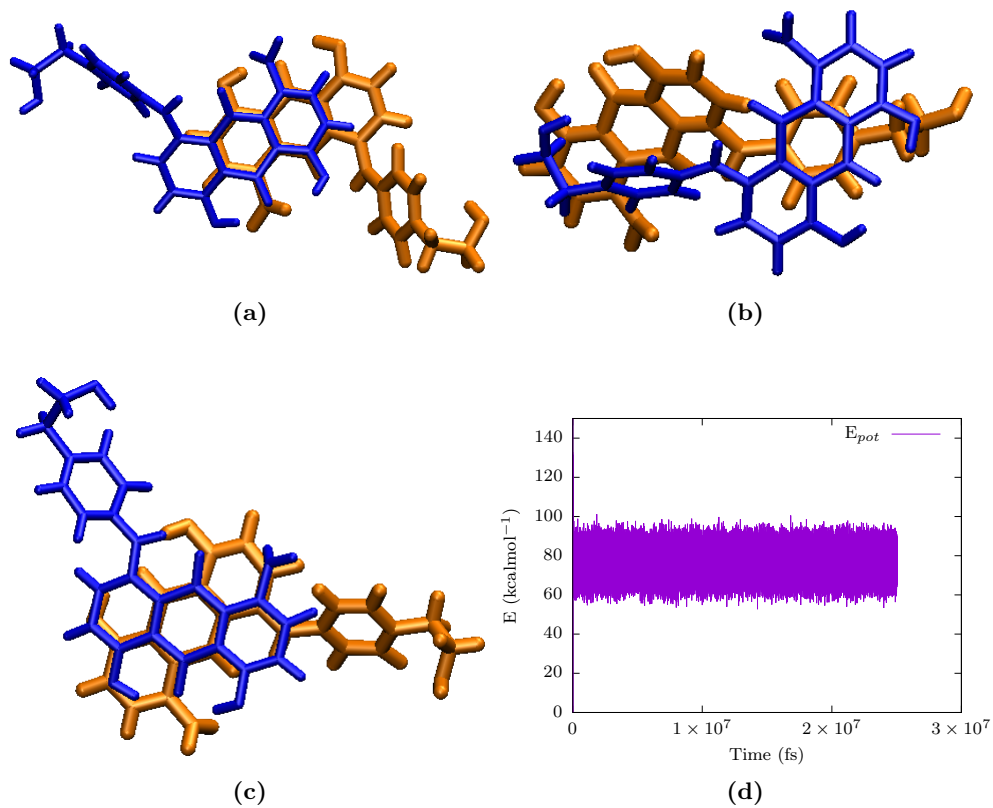


Figure 3.9: NB27 dimers configurations (a–c) and d) E_{pot} profile obtained by FF in vacuum.

in agreement with the experimental data. In fact, while this had no influence on the formation of aggregates, these kind of interaction between molecules did not favor their process of elongation, resulting in disordered and, possibly, spheroidal or discoid objects. Three possible conformations were identified for NB27. The first one showed two molecules interacting facially by stacking between two of the anthracene rings (Fig. 3.9a). The side phenyls for both of them were twisted with respect to anthracene core, and pointed in opposite directions. Another possibility was the anthracene- side phenyl interaction, as shown in Fig. 3.9b. A third preferential conformation was formed by interaction between anthracenes core, that involved all three rings, with side chains pointing in opposite directions (Fig. 3.9c). This last one occurred less frequently than the other two during the MD. However, all these conformations were equally energetic (Fig. 3.9d) and, therefore, equally probable. Even if this system was more ordered than the previous one, this data suggested that elongation of aggregates was disfavored, as well as in NO30. In fact, while the first and third conformations were rather flat, the second one was not, preventing stacking from forming long objects. For NRC1 dimer four different preferential conformation were retraced. All of them involved interaction between anthracene cores. In Fig. 3.10a, molecules interact through stacking between one of each anthracenes cores, with a tilt of approximately 45° and with side phenyls on the same side. A facial interaction between one ring of each core was responsible also for the formation of the second conformation (Fig. 3.10b). In this one though, the tilt between the molecules was higher, around 90° . The third dimer conformation took place again from facial interaction between one ring of each anthracene, but in this case the tilt between molecules was smaller and side phenyls could undergo to facial interaction as well for brief periods (Fig. 3.10c). The last preferential conformation involved a facial interaction between two rings of each core, that were disposed parallel to each other, as shown in Fig. 3.10d. In this case there was no interaction between side phenyls. The transition between these dimer conformations did not induce energy changes, as reported in Fig. 3.11. In fact, E_{pot} oscillated between 80 and 50kcal $^{-1}$ for all MD. These four dimer conformations had all rather flat cores, that could facilitate aggregates elongation, in perfect agreement with its physico-chemical characterization that demonstrated the formation of elongated aggregates and even fibrils in solution for NRC1. The last case was NY42 dimer, for which four preferential conformation were identified.

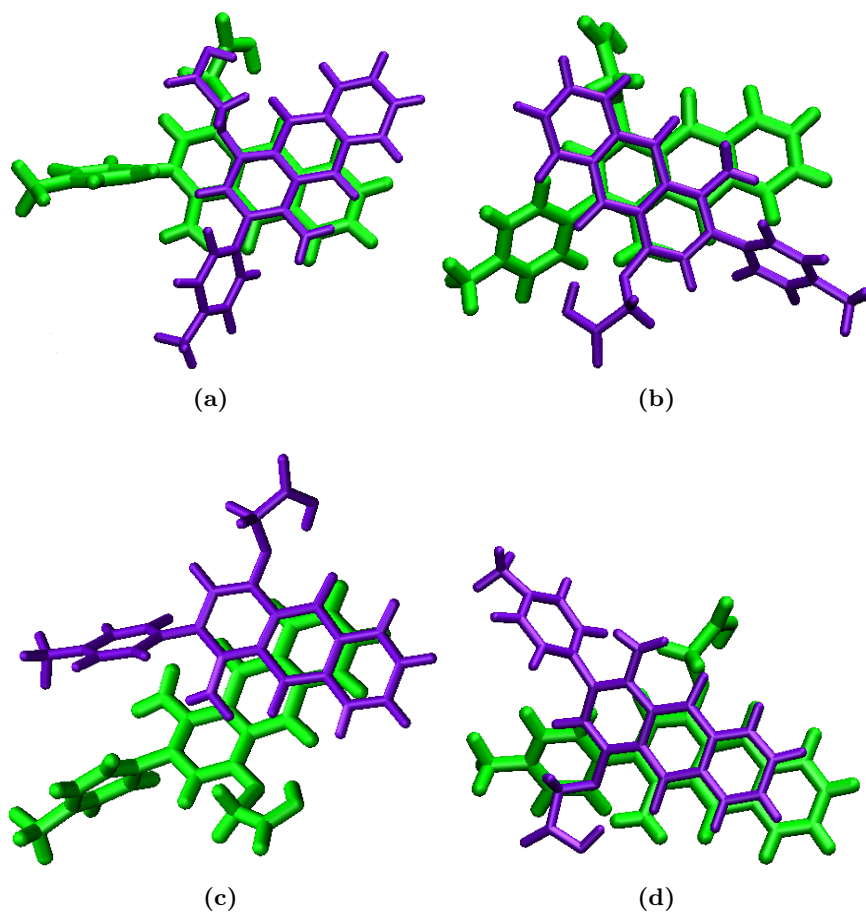


Figure 3.10: NRC1 dimer's configurations (a–d) obtained by FF in vacuum.

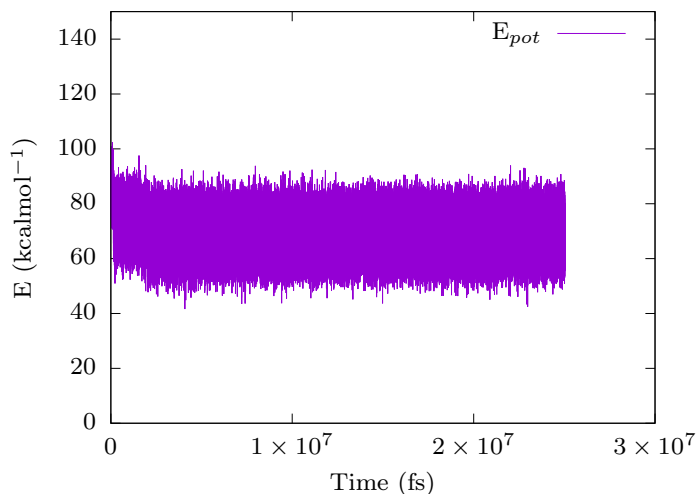


Figure 3.11: E_{pot} profile obtained by FF in vacuum for NRC1 dimer.

The first one formed by interaction between the central rings of each NY42 molecules, tilted of approximately 90° , as shown in Fig. 3.12a. A similar, but not identical, conformation was formed when dye molecules with a lower tilt interacted through their central rings (Fig. 3.12b). In this case, one of the two side phenyl couples could interact briefly and in turn. A facial interaction between the three rings of both molecules led to the second dimer conformation (Fig. 3.12c), that, however, formed less often than the others. The last NY42 conformation took place when molecules, with both phenyls bent on the same side of the central ring, interacted facially by the middle benzene, as shown in Fig. 3.12d. Also in these case all these conformation were equally energetic and, therefore, equally probable. E_{pot} of the system during MD oscillated between 130 and 100 kcalmol $^{-1}$, without important variations. This molecule was the more flexible and these results seemed to point at a situation in which elongation of aggregates was prevented. MD were also performed on GDs trimers. The resulting trajectories were studied and their conformations reflected what previously observed for the corresponding dimers. Thus, their analysis could not add any information. Therefore, considering the very high number of conformations that trimers could assume, they were not evaluated and classified. What would actually be important, as a future perspective,

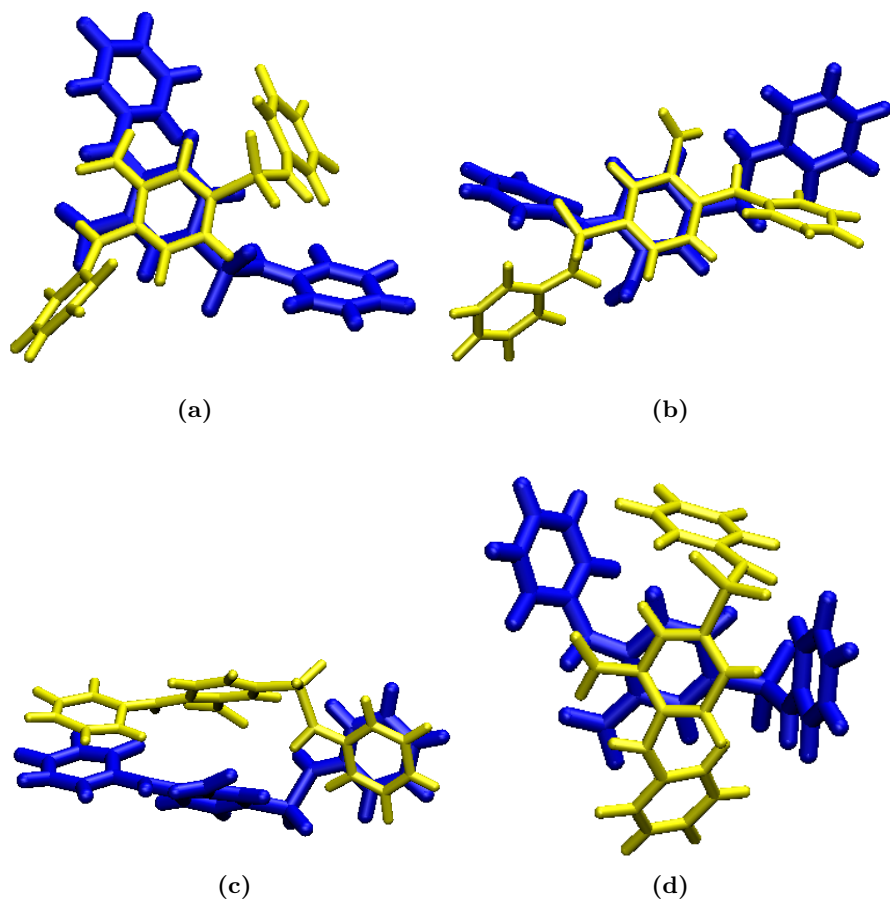


Figure 3.12: NY42 dimers configurations (a-d) obtained by FF in vacuum.

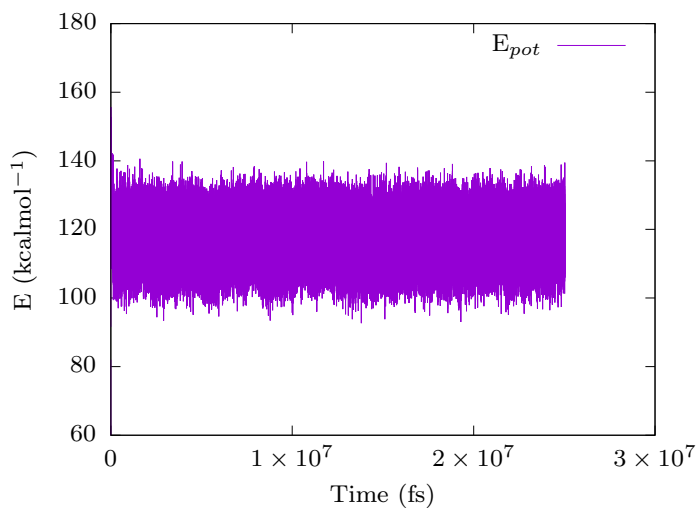


Figure 3.13: E_{pot} profile obtained by FF in vacuum for NY42 dimer.

would be, as already pointed out, taking into account entire GD molecule, including the lactose, for each dye as well as the solvent in the MD calculations, and to obtain their electronic excitation spectra by TD-DFT.

Chapter 4

Bioremediation of glycoconjugated dyes

4.1 Introduction

The dyeing industry among the major causes of water pollution. The remediation of tanneries and textile dyeing wastewaters presents many challenges, one of which is the wide variety of pollutants they contain, e.g. inorganic salts, surfactants and dyes themselves. Synthetic dyes used in dyeing processes are specifically designed to resist at light irradiation, oxidation and high temperatures, therefore conventional wastewaters treatment based either on chemical or physical methods, can be ineffective.[23] Moreover, the degradation of some of these xenobiotic molecules could result in secondary pollution problems.[36, 39] In fact, dyeing industries extensively use azo dyes,[17, 40] whose degradation can result in the production of aromatic amines, molecules recognized as carcinogenic, mutagenic and toxic for humans and the aquatic environment.[49, 59, 67, 68] Bioremediation represents a valid alternative to conventional purification methods, because it is cost effective and employs microorganisms instead of chemicals. The use of active sludge in wastewater treatment plants is widespread, because this approach is effective on a wide variety of pollutants, including many dyes. However, there has been an intensive research in the bioremediation field, always seeking for better performances.

In particular, white-rot fungi had shown great potential in degrading a wide variety of pollutants,[64, 72] thanks to their pool of extra-cellular ligninolytic enzymes, such as manganese dependent peroxidases(MnP), lignin peroxidases and laccases.[50, 67] In this work we present for the first time an evaluation of bioremediation performances on glycoconjugated dyes (GDs). Two different approaches towards bioremediation of GDs solutions were used. The first one concerned the removal of GDs from simulated dyeing effluents using a non standard microorganism, the white-rot fungus *F. trogii*. This microorganism has been reported to be very effective in decolorizing dyeing effluents, thanks to the outstanding activity of its laccase.[14, 22, 23, 40, 73] In the second part of this work, GDs real dyeing effluents, obtained by leather dyeing experiments conducted for the European LIFE project BIONAD, were treated. In this case, since the substrate was a real system, a standard bioremediation approach, involving a highly specialized active sludge, was employed. For both the procedure, bioremediation results on naturalized dyes effluents, simulated and real, were very positive. In fact, both types of microorganisms, white-rot fungus and active sludge, were able of degrading GDs molecules to a high extent. Moreover, mass spectrometry analysis were performed on effluents after remediation with both microorganisms to verify which fragments could remain in solution, referring to molecular peaks of GDs: 923 (NR202), 913 (NB27), 900 (NO30) and 820 (NY42). Moreover, mass spectrometry could allow to detect aromatic amines that could result from GDs degradation, whose exact masses were 93, 172, 206, 293 and 388 (see Section 4.4).

4.2 Simulated effluents: *Funalia trogii*

Bioremediation with *F. trogii* was performed on NR202, NB27, NO30, NY42 and MIX simulated effluents. MIX was considered because, in a real wastewater treatment plant, mixed dyeing effluents are usually treated, rather than single ones. Thus, MIX was more similar to a real case than single dye solutions. To underline any difference in the mechanism of color removal, the microorganism was used in three different conditions: dead fungal biomass (DF), *F. trogii* with (FG) and without (F) glucose as additional nutrition source. Since real effluents had pH around 3, in order to resemble that situation, before the incubation with microorganism the pH of all the samples was adjusted at 4.9, the lowest

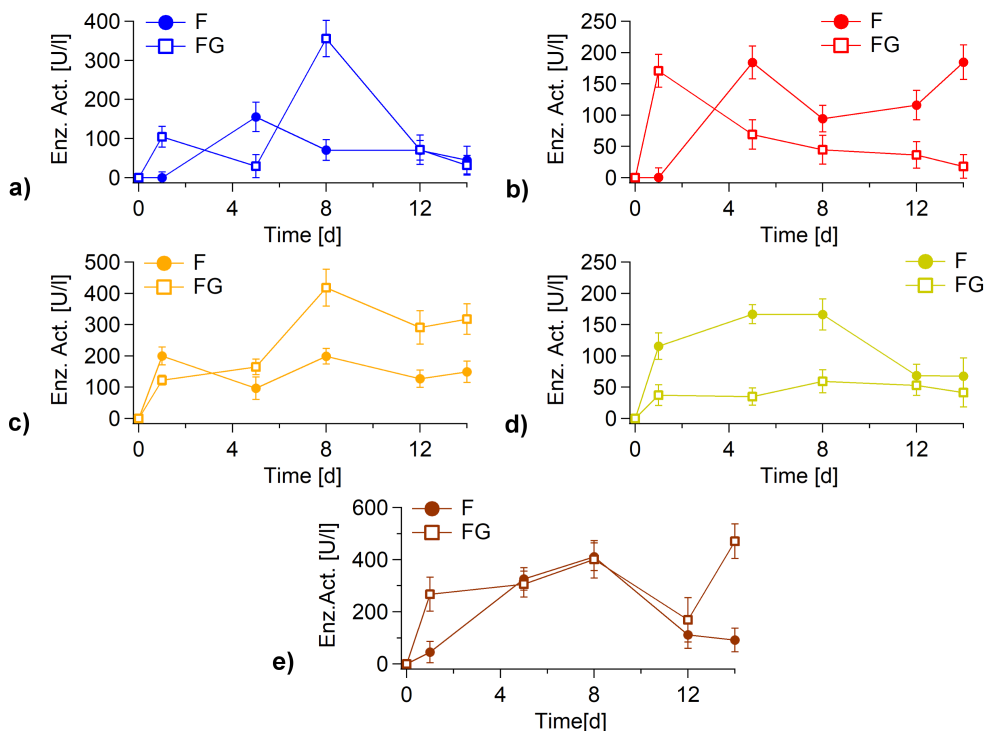


Figure 4.1: Enzyme activity values in U/l profiles for *F. trogii* in presence (FG) and absence (F) of glucose over the 14 days bioremediation experiment of the five GDs simulated effluents.

pH possible to ensure *F. trogii* survivor. However, *F. trogii* acted as a buffer, modifying the pH of all the samples within the first three hours of incubation and maintaining it between 6.5 and 7.5 afterward. Laccase and MnP enzyme activity was also monitored for all the duration of the experiment, to assess the vitality of the microorganism. This tests indicated that *F. trogii* did not produce MnP in that condition, but only Laccases. As expected, Laccase enzyme activity was retraced in those samples containing living microorganism, but not in those incubated with dead biomasses. The detailed profiles of the enzyme activity for living *F. trogii* were reported in Fig. 4.1. Dye removal results, reported in Fig.4.2, revealed that each GD was removed differently from the solution, according to the conditions used. This piece of information confirmed that dye removal took place according to different processes in the three condi-

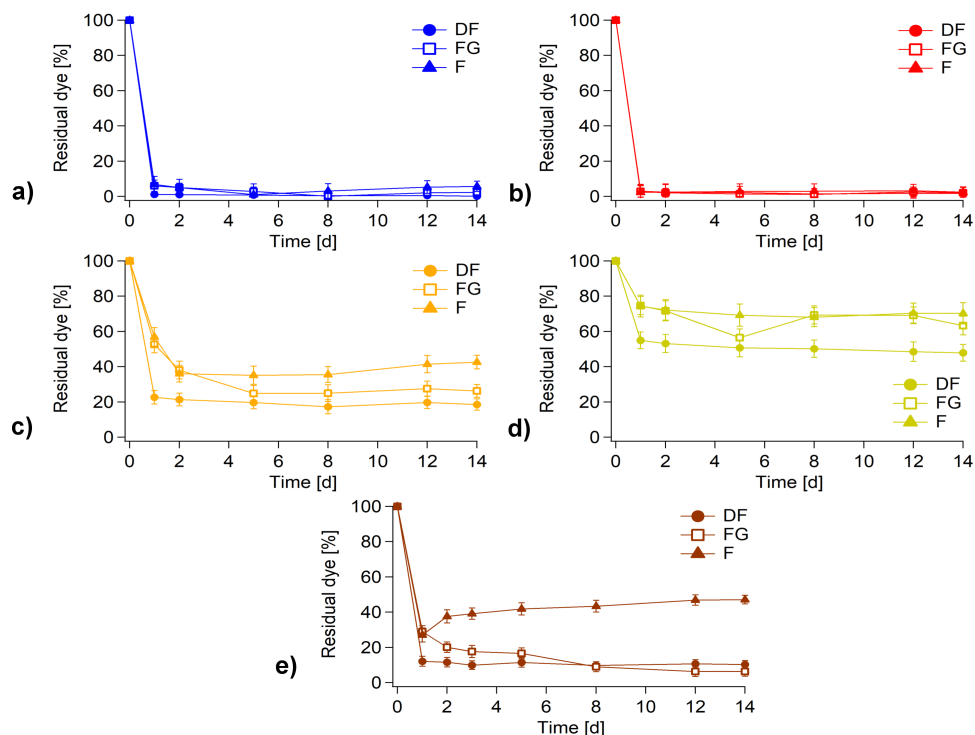


Figure 4.2: Residual dye percentages in time in the three conditions (F, FG, DF) for the five samples: a)NB27, b)NR202, c)NO30, d)NY42, e)MIX.

tions F, FG and DF. Absorption mechanism, always present in bioremediation processes, was the only one active for the dead biomass, while living microorganisms acted through absorption as well as enzymatic degradation,[13, 34] both in presence and absence of nutrient. Moreover, these results also revealed that the efficiency of bioremediation was different for the five simulated effluents. First of all, let's consider the samples treated with dead biomass. The final dye removal percentages for NR202 and NB27 were very high, 98.3 and 99.8% respectively. The decolorization for NO30 was 81.5%, while for NY42 only a 52.1% was reached. Finally, MIX attested for 89.8% of color removal. NY42 resulted quite recalcitrant, while NR202 and NB27 were very easily removed from the solution. After the experiment we analyzed by mass spectrometry all solutions and fungal biomasses, confirming that dye removal with dead

CHAPTER 4. BIOREMEDIATION OF GLYCOCONJUGATED DYES

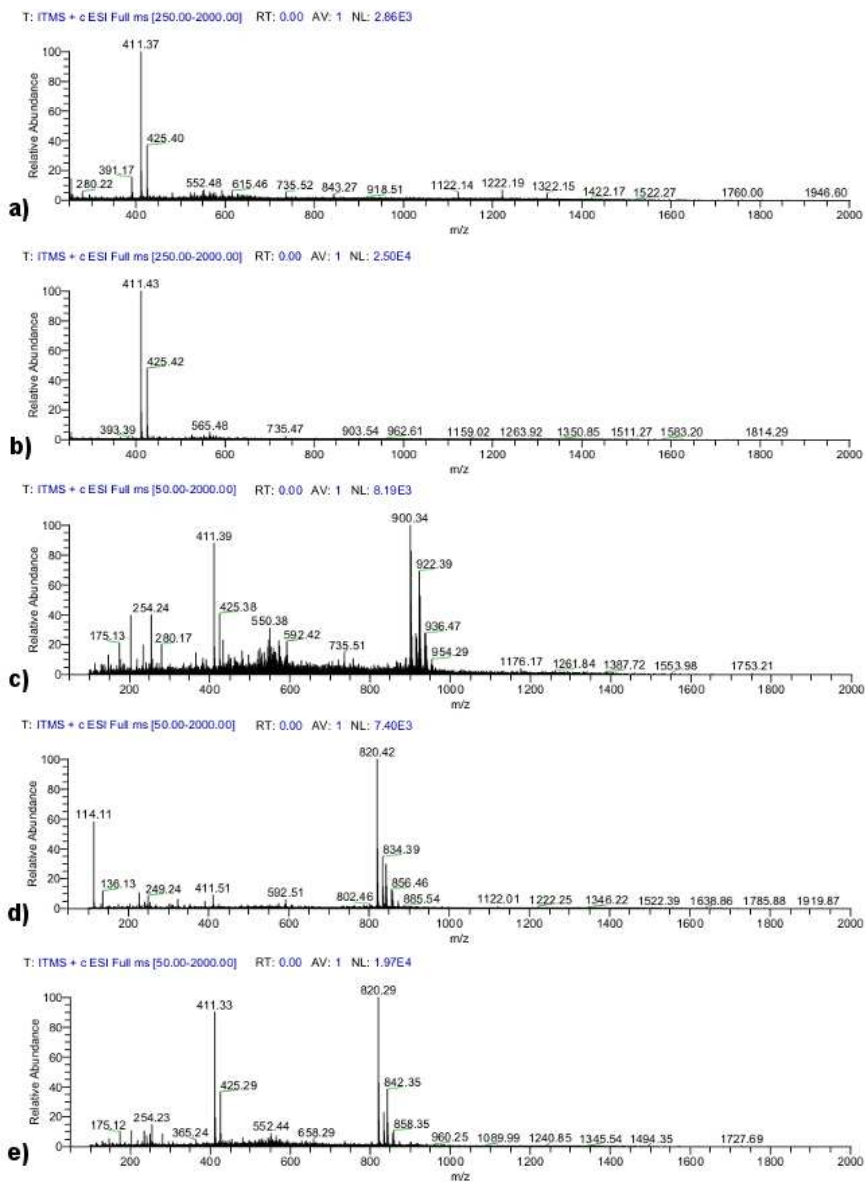


Figure 4.3: Mass spectrometry analysis results for the solutions of the five GDs simulated effluents, a) NB27 b)NR202 c) NO30 d) NY42 e) MIX, after bioremediation with dead *F. troglia* biomass.

CHAPTER 4. BIOREMEDIATION OF GLYCOCONJUGATED DYES

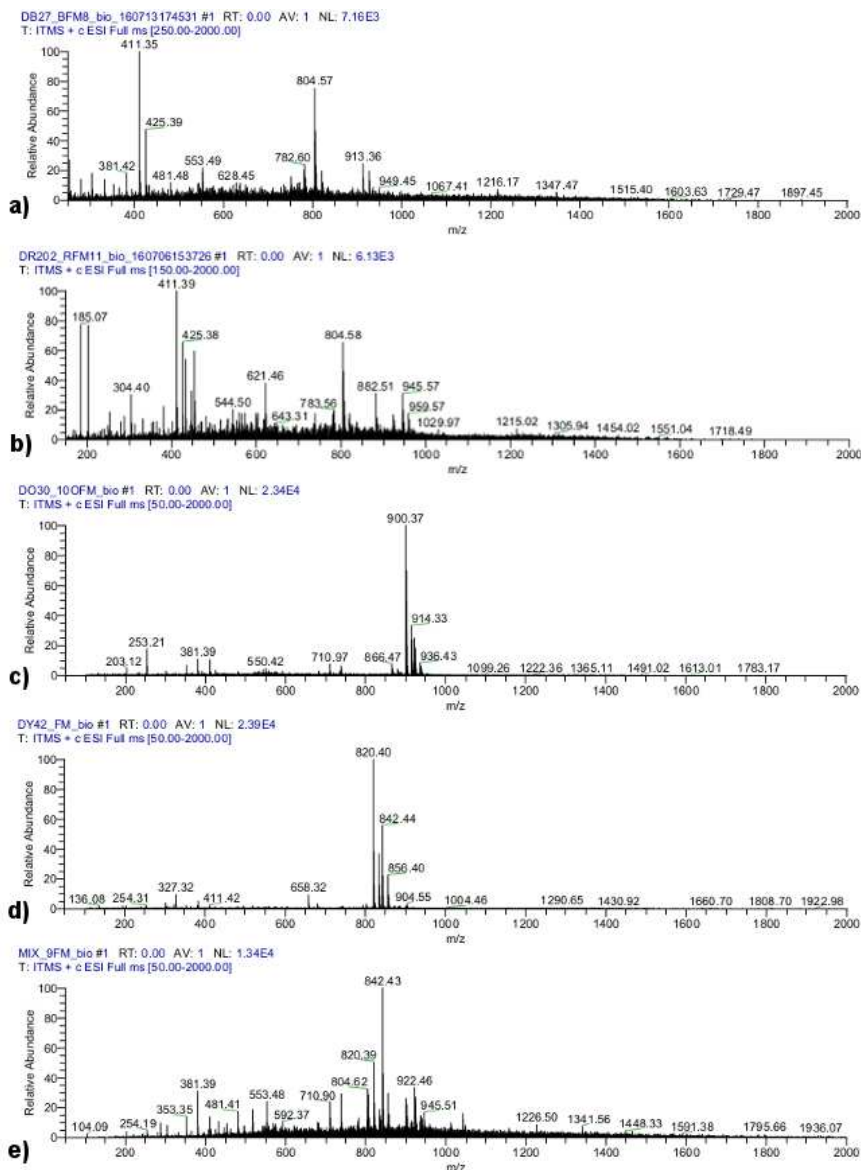


Figure 4.4: Mass spectrometry analysis results for the dead *F.trogl*i biomass after bioremediation of the five GDs simulated effluents: a) NB27 b)NR202 c) NO30 d) NY42 e) MIX.

Table 4.1: Biomass decreases, reported as per cent values (%), that took place after bioremediation experiments in the three conditions (F, FG, DF) for all five GDs simulated effluents.

	NR202	NB27	NO30	NY42	MIX
F	90.2	87.8	91.9	98.4	91.7
FN	56.5	27.3	49.5	69.4	66.8
DF	–	–	1.6	1.2	–

biomass took place only through absorption mechanism (see Table 4.4). On all five biomasses (Fig. 4.4) intact GDs were retraced, while for their corresponding solutions results depended on the sample. For NB27 and NR202, no dye was found in solution, only lactose piperazine (LP), consistently with the high dye removal efficiency (Fig. 4.3a-b). LP in this case could be a residue of the synthetic procedure of the dyes that could not be eliminated. The final solution for NO30 still had some color, and accordingly we could retrace both LP and the intact dye in it (Fig. 4.3c). The only molecule found in the treated solution for NY42 was the unaltered GD (Fig. 4.3d), coherently with the low color removal. Finally, for MIX only intact NY42 and LP were retraced in solution (Fig. 4.3e), in agreement with what was found for the single dyes (see Table 4.2). The second case considered was the incubation of simulated effluents with *F. troglia* without any additional nutrition source. Final dye removal for NR202 and NB27 was high also in this condition, 97.6 and 94.3% respectively. On the other hand, NO30 and NY42 gave poorer results than with DF, with 57.4 and 29.8% of dye removal respectively. MIX was less decolorized as well, with 52.8% of color removal. However, MIX behavior in this case was peculiar. As shown in Fig. 4.2e, initial color removal was very efficient, probably thanks to a synergy between absorption and biodegradation mechanisms. However, afterward the biomass apparently released some of the dye it had absorbed, in particular NO30 and NY42. This release probably took place because *F. troglia* was experiencing autophagy. This phenomenon takes place when a microorganism enters in starvation and, in order to survive, eat itself to recycle the nutrients.[58] This was probably the case the case for *F. troglia* biomass in these samples. This hypothesis was supported by the decrease in biomass that took place in all samples after bioremediation. In fact, the decrease was very pronounced for all F samples, more pronounced than in FN case (Table 4.1).

The reason for that was probably the absence of additional nutrition source

CHAPTER 4. BIOREMEDIATION OF GLYCOCONJUGATED DYES

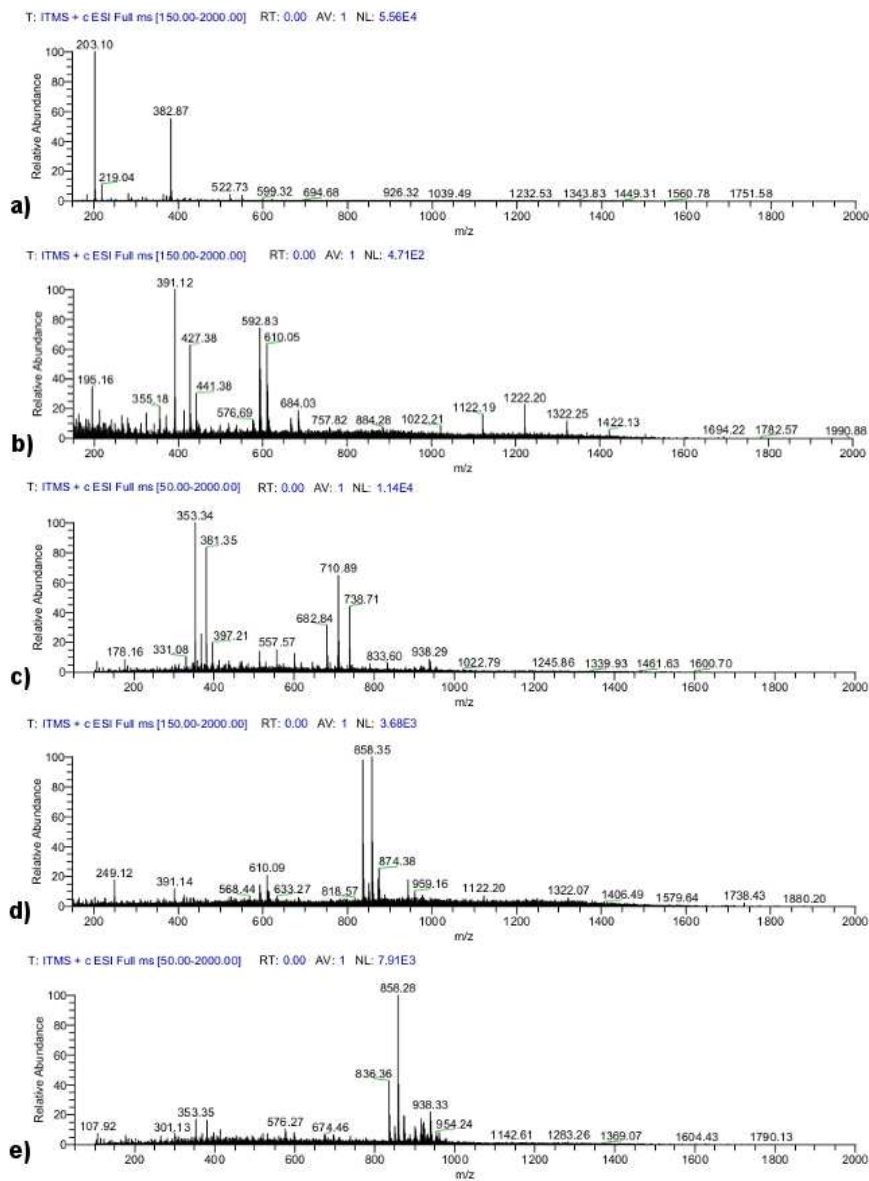


Figure 4.5: Mass spectrometry analysis results for the solutions of the five glycoconjugated dyes simulated effluents, a) NB27 b)NR202 c) NO30 d) NY42 e) MIX, after bioremediation with *F.trogii*.

CHAPTER 4. BIOREMEDIATION OF GLYCOCONJUGATED DYES

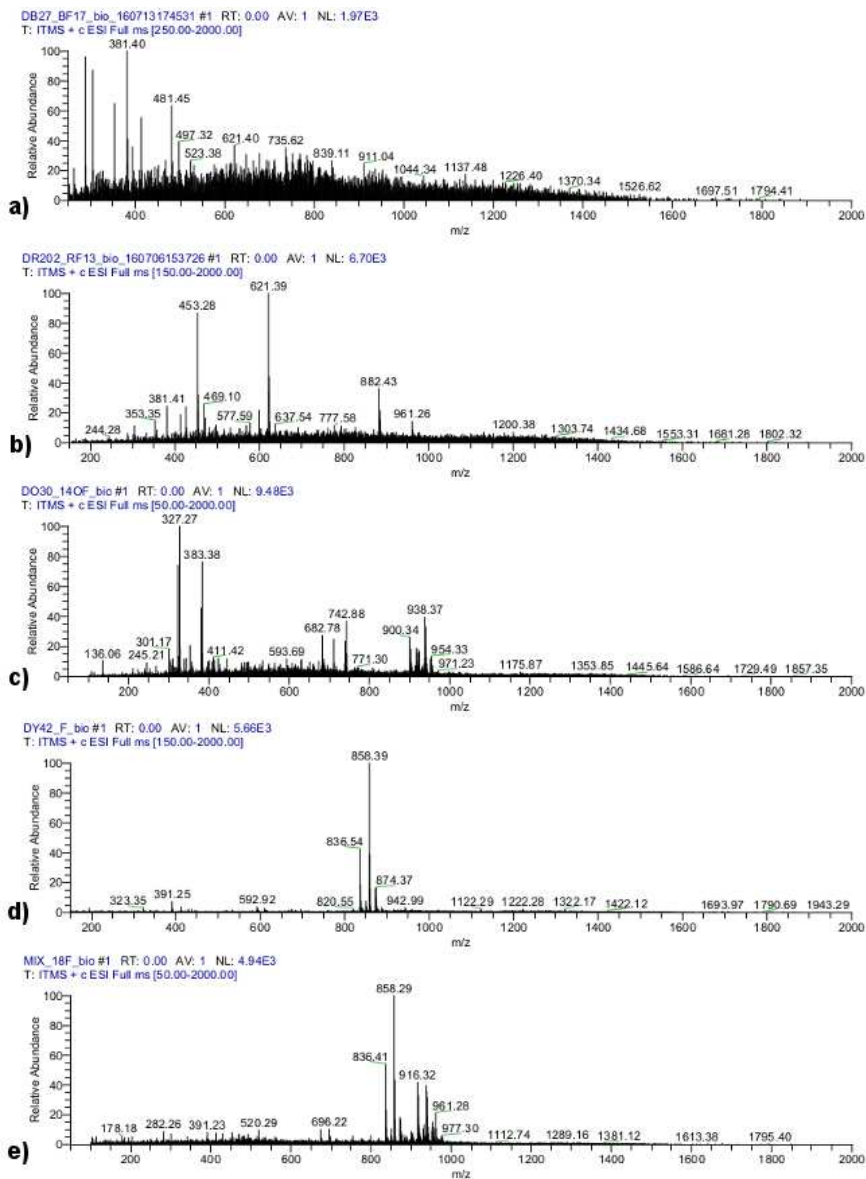


Figure 4.6: Mass spectrometry analysis results for *F.troglia* biomass after bioremediation of the five glycoconjugated dyes simulated effluents: a) NB27 b)NR202 c) NO30 d) NY42 e) MIX.

		Biomasses		Solutions	
F		836.41	ox NY42	858.28	ox NY42 + Na ⁺
		938.30	ox NO30 + Na ⁺	836.36	ox NY42
		961.28	ox NR202 + Na ⁺	938.33	ox NO30 + Na ⁺
MIX	FG	385.32	NO30 metabolite	–	–
		401.32	ox LP + Na ⁺	–	–
DF		842.43	NY42 + Na ⁺	820.29	NY42
		922.46	NR202	411.33	LP
		900.22	NO30	834.35	NY42 + Na ⁺
		945.51	ox NB27	425.29	LP-OCH ₃

Table 4.2: Mass spectrometry analysis of glycoconjugated dyes equimolar mixture (MIX) effluents and biomasses after bioremediation in the three conditions, F, FG, DF.

to sustain the microorganism, as opposite to the case of FG. NB27 and NR202 were easily removed from the solution, as attested from mass spectrometry analysis. No peaks ascribable to any fragmentation of these dyes were found in the treated solution (Table 4.4), confirming that these molecules were degraded by Laccases (Fig. 4.5a-b). A further confirmation was that only degradation products were found on their biomasses (Table 4.4), the chromophore without lactose for NR202 (Fig. 4.6b) and lactose metabolites for NB27 (Fig. 4.6a). For NO30 solution and biomass (Fig. 4.5c and 4.6c), degradation products of both GD and LP were retraced, the first ones being responsible for the residual color of the solution (Table 4.4). Consistently with the low dye removal, for NY42 solution and biomass (Fig. 4.5d and 4.6d), the more abundant species were identified as oxidized forms of the dye (Table 4.4). Mass spectrometry on MIX solution (Fig. 4.5e) revealed that the more abundant molecules were oxidized forms of NY42, while on its biomass (Fig. 4.6e) oxidized forms of both NY42 and NO30 were retraced (Table 4.2). The presence of NY42 and NO30 in MIX after the mycoremediation was consistent with their higher resistance to bioremediation. The presence of oxidized forms of some dyes, specifically NY42 and NO30 (see Table 4.4), after their incubation with *F. trogii* was a further confirmation that enzymatic degradation was active. In agreement with oxidative degradation reported for Laccases,[40, 78] no aromatic amines could be retraced by mass spectrometry analysis after biodegradation of azo-dyes, NR202 and NO30. The last case considered was bioremediation using *F. trogii*

in presence of glucose as additional nutrition source. NR202 and NB27 were, again, very well removed from the solution, respectively 97.9 and 97.7% of final dye removal. Lactose and some of its degradation metabolites were retraced in both their treated effluents (Fig. 4.7a-b) and biomasses (Fig. 4.8a-b), with the difference that also NR202 without lactose was identified on its corresponding biomass (Table 4.4). NO30 attested for 73.7% of decolorization, while only a 36.6% was reached for NY42. Mass spectrometry revealed that in NO30 and NY42 effluents (Fig. 4.7c-d) and biomass (Fig. 4.8c-d) the more abundant molecules were glucose and lactose, together with oxidized forms of both dyes (Table 4.4), consistently with the residual color of the solutions. Therefore, NO30 and, mostly, NY42 resulted quite persistent to bioremediation also in presence of glucose. Surprisingly, they appeared to be well removed from the solution when mixed to the other dyes, as it was the case for MIX. In fact the final dye removal for MIX attested at 93.6%, the highest for this sample. Mass spectrometry analysis of the effluent did not reveal any of the four dyes, nor their degradation products (Fig. 4.7e). Metabolites of NO30 and lactose piperazine were retraced on the biomass (Fig. 4.8c), instead. The main fragments retraced in FG treated effluents for all five GDs samples were summarized in Table 4.3. Also in this case, no aromatic amines were found in effluents nor on biomasses after the bioremediation by mass spectrometry analysis, as expected.[40, 78] The enhancement in the removal of NY42 and NO30 when in MIX was a very peculiar and relevant result. Therefore, MIX UV-Visible absorption water was studied. This spectrum had two main contributions: one from the red-orange component at 460 nm, and the other from the blue dye at 610 nm. The contribution of the yellow dye was not relevant, because it was overwhelmed by that of NR202 and NO30, whose ϵ was considerably higher. Dye removal for MIX two components at 460 and 610 nm were compared in all the three conditions, F, FG and DF. Predictably, DF removal trends for these two components were similar (Fig.4.9a), suggesting that absorption mechanism worked on both components in the same way. This was confirmed by the variation of λ_{max} (Fig.4.9d), that, after an initial decrease from 462 to 422 nm, remained the same for all the duration of the experiment. In F case, the results for 460 nm and 610 nm components were comparable with dye removal trends for NO30 and NB27 respectively (Fig. 4.2b-c). The blue component remained roughly constant after an initial decrease. The 460 nm component, after the initial removal, was gradually released after the first day of incubation

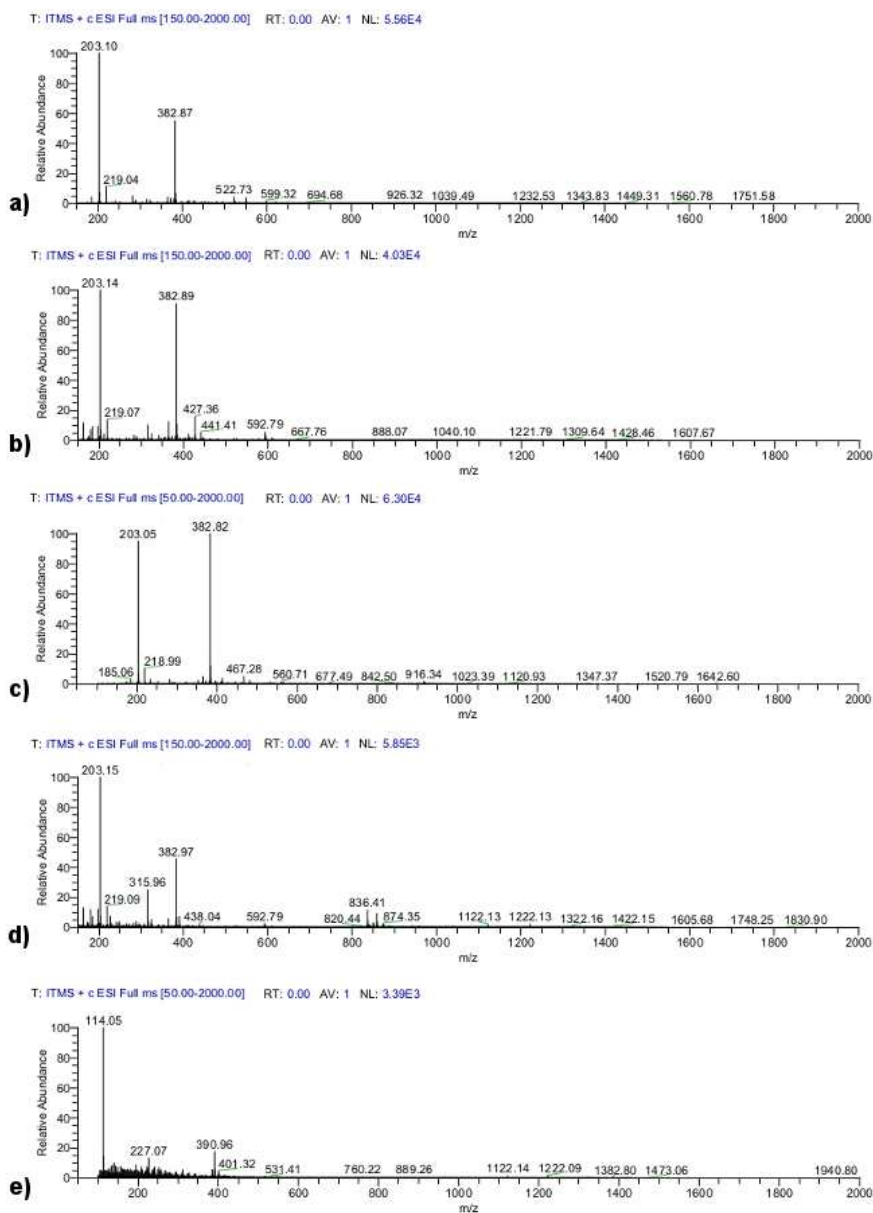


Figure 4.7: Mass spectrometry analysis results for the solutions of the five glycoconjugated dyes simulated effluents, a) NB27 b) NR202 c) NO30 d) NY42 e) MIX, after bioremediation with *F.troglia* in presence of glucose.

CHAPTER 4. BIOREMEDIATION OF GLYCOCONJUGATED DYES

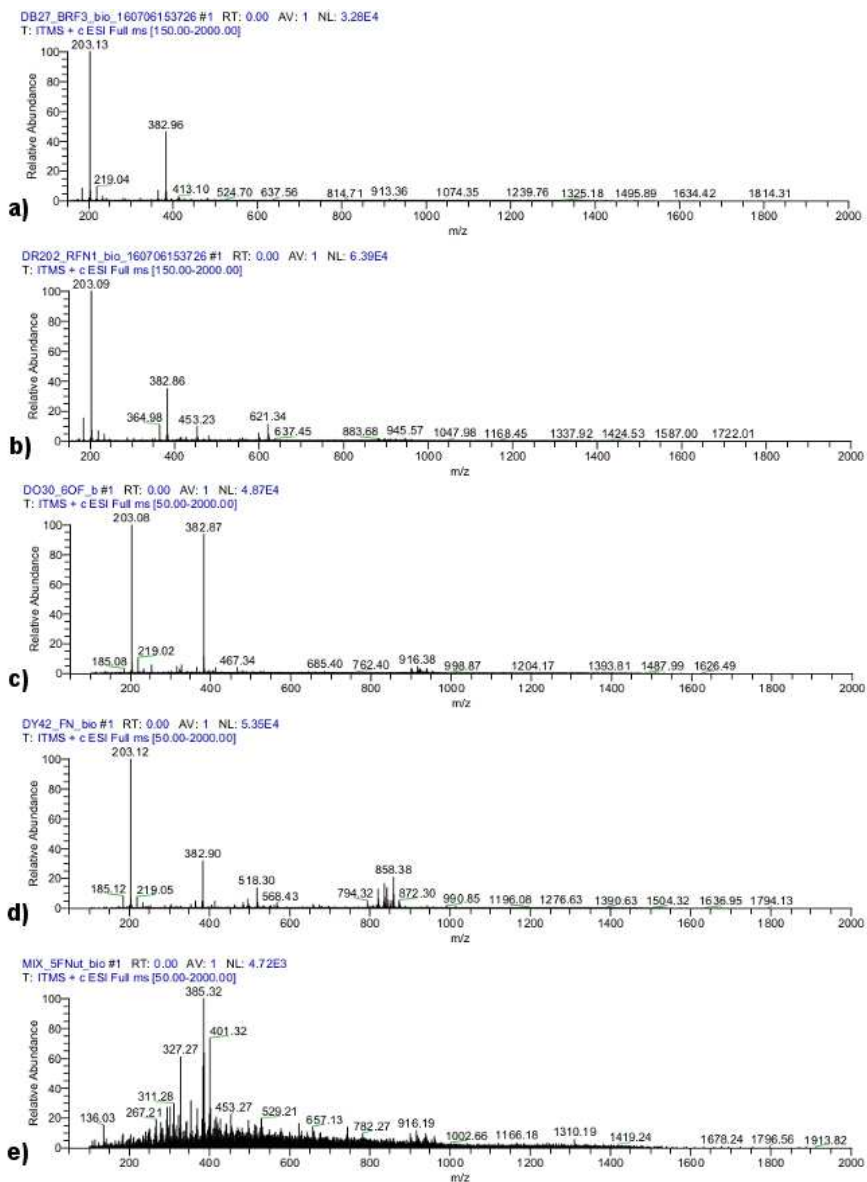


Figure 4.8: Mass spectrometry analysis results for the biomass of *F.trogii* in presence of glucose after bioremediation of the five glycoconjugated dyes simulated effluents: a) NB27 b)NR202 c) NO30 d) NY42 e) MIX.

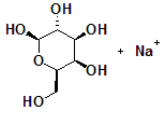
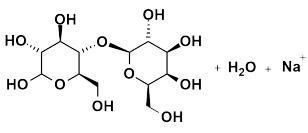
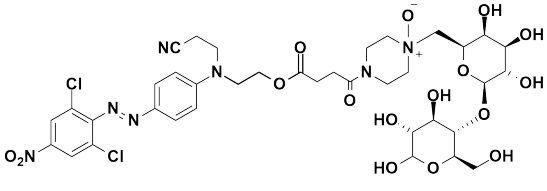
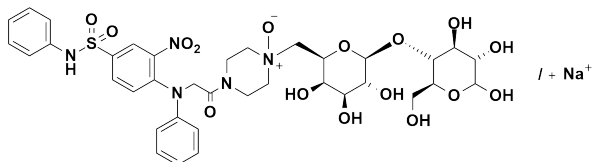
M/Z	Sample	Fragment
203	NB27 NR202 NO30 NY42	
382	NB27 NR202 NO30 NY42	
916	NO30	
836/858	NY42	

Table 4.3: Main fragments retraced by mass spectrometry in the simulated effluents of GDs treated by FG.

(Fig.4.9b), as also testified by the corresponding variation of λ_{max} (Fig.4.9d). Thus, it was surprising to find out that for FG there were two different rate of removal for the blue and the red-orange component (Fig.4.9c). This confirmed a faster and preferential removal for NB27, in agreement with results on single dye effluents. Moreover, the shift in λ_{max} from 462 to 448 nm on the first day of incubation with the microorganism (Fig.4.9d) told us that NR202 (λ_{max} : 462 nm) was removed faster than NO30 (λ_{max} : 442 nm). Then, NO30 started to be degraded, resulting in a further hypsochromic shift to 432 nm on the fifth day. After that the residual color was related to NY42 (λ_{max} : 420 nm) still present in solution. It is particularly important to stress out the differences in the efficacy of bioremediation with FG on the four single dye simulated effluents. The anthraquinone, NB27, was very well removed from the solution. This was an expected result because phenols, and therefore quinones, are laccases'

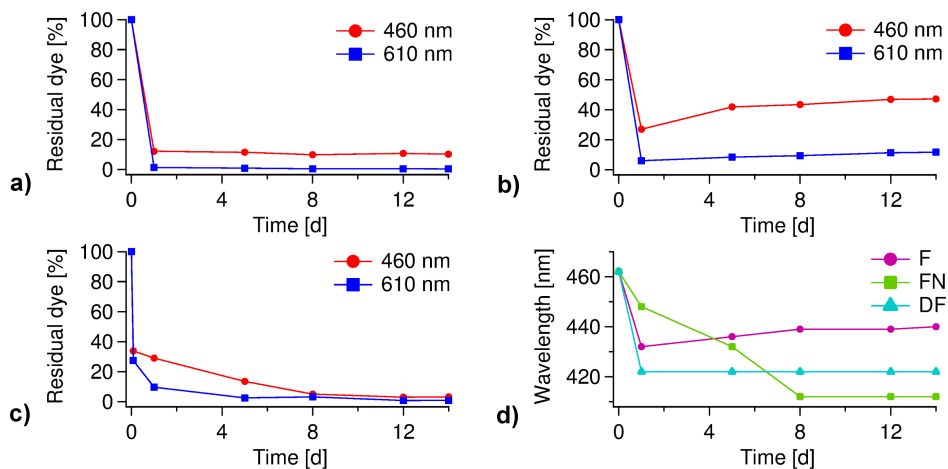


Figure 4.9: Differential removal of red-orange (460 nm) and blue (610 nm) components from MIX in the three bioremediation conditions: a) DF, b) F, c) FG. The maximum wavelength in these three cases changed according to the mechanism of removal, d).

natural substrates.[43, 72] NY42 was the more recalcitrant one and the best result in terms of dye removal was achieved by the absorption mechanism, not by degradation. Apparently this dye was a very poor substrate for the enzyme, resulting in a scarce color removal. This could be ascribable to its molecular structure as well as to the kind of aggregates NY42 formed in solution. That could potentially represent a drawback for biodegradation, possibly because these aggregates did not facilitate an interaction with enzymes. Despite the similarity of the two azo-dyes chemical structures, there was a considerable difference in the results obtained from the bioremediation of NR202 and NO30. In fact, even though the final dye removal for NO30 was good, over 70%, the final solution was still very colored because of its high ϵ value ($\epsilon=17836$). On the contrary, NR202 was clearly more easily degraded by Laccases. Thus, the residual amount of NR202 was so low that the solution appeared transparent by visual inspection. Again, this could be a consequence of the different aggregates they formed in water. In fact, as demonstrated in Chapter 2, NO30 formed spheroidal aggregates, while NR202 elongated ones. Things changed when MIX was taken into account. First of all, degradation mechanism was clearly effective in this case on NY42 and NO30, since they were not detected

Sample		Biomasses		Solutions	
		M/Z	Interpretation	M/Z	Interpretation
NY42	F	858.39	ox NY42 + Na ⁺	858.35	ox NY42 + Na ⁺
		836.54	ox NY42	836.44	ox NY42
	FG	203.12	glucose + Na ⁺	203.15	glucose + Na ⁺
		382.90	ox Lactose + Na ⁺	382.97	ox Lactose + Na ⁺
	DF	820.40	NY42	820.42	NY42
		842.44	NY42 + Na ⁺	834.39	NY42-OCH ₃
NO30	F	323.31	ox LP	353.34	ox LP
		900.34	NO30	710.89	NO30 metabolites
	FG	203.08	glucose + Na ⁺	382.82	ox lactose + Na ⁺
		382.27	ox lactose + Na ⁺	203.05	glucose + Na ⁺
	DF	900.37	NO30	900.34	NO30
		922.45	NO30 + Na ⁺	411.39	LP
NR202	F	621.39	NR202- lactose	–	–
		453.28	NR202- linker& lactose	–	–
	FG	203.09	glucose + Na ⁺	203.14	glucose + Na ⁺
		621.34	NR202- lactose	382.89	ox lactose + Na ⁺
	DF	411.39	LP	411.43	LP
		945.57	NR202 + Na ⁺	425.42	LP-OCH ₃
NB27	F	381.40	part. ox lactose	–	–
		481.45	ox lactose metabolite	–	–
	FG	203.13	glucose + Na ⁺	203.10	glucose + Na ⁺
		382.96	ox lactose + Na ⁺	382.87	ox lactose + Na ⁺
	DF	411.35	LP	411.37	LP
		913.36	NB27	425.40	LP-OCH ₃

Table 4.4: Mass spectrometry analysis of glycoconjugated dyes (NR202, NB27, NO30, NY42) effluents and biomasses after bioremediation in the three conditions, F, FG, DF.

in solution by mass spectrometry analysis (Fig. 4.7e). This was at variance with what observed for their single dye effluents. Moreover, recalcitrant NY42 was not even retraced on the biomass, on which only a metabolite of NO30 was detected (Fig. 4.8e). The enhancement in NY42 and NO30 removal when mixed to other dyes could be ascribable to two different factors, that could have facilitated the action of Laccases. For NO30, this factor could be an interaction with NR202 and NB27, even if no decisive evidence was found of such an interaction was found by physico-chemical characterization. For NY42, removal was definitely not enhanced by action of its aggregation with other GDs, since in Chapter 2 was demonstrated that it assembled only with itself. Therefore, it was likely that lower concentration was the factor that facilitated its removal from MIX effluent by enzymatic degradation.

4.3 Real effluents: Activated sludge

Four GDs real leather dyeing effluents, whose composition was reported in Section 4.4.1, were treated using a highly specialized active sludge. In this case, a different microorganism was used to resemble the real dyeing wastewater remediation procedure employed nowadays. In particular, the efficacy of a sludge conditioned to treat mixed dyes substrates was tested. Moreover, after the bioremediation step, a small portion of each effluent was incubated with active carbon, to remove the residual color from the solution. The efficacy of this bioremediation procedure was evaluated measuring color removal after each of the two steps of the process, incubation with active sludge (AS) and absorption on active carbon (AC). RE3 and RE4 had two absorption maxima, as shown in Fig. 4.10c-d, therefore color removal was calculated for both of them, separately. After the first incubation step, the color of the solution was drastically reduced (Fig. 4.10) and color removal values achieved for the four effluents were reported in Fig. 4.11. The absorption step on AC led to a dye removal above 99.6% for all the four dyeing effluents as shown in Fig. 4.11, reaching an almost complete decolorization of these solutions. The contribution of the two remediation step to final color removal were represented in Fig. 4.12. Results obtained for the bioremediation of real GDs dyeing effluents with AS were very consistent with those achieved by *F.trogii* on simulated dyeing effluents. In fact, even if the microorganisms used in these two cases were different,

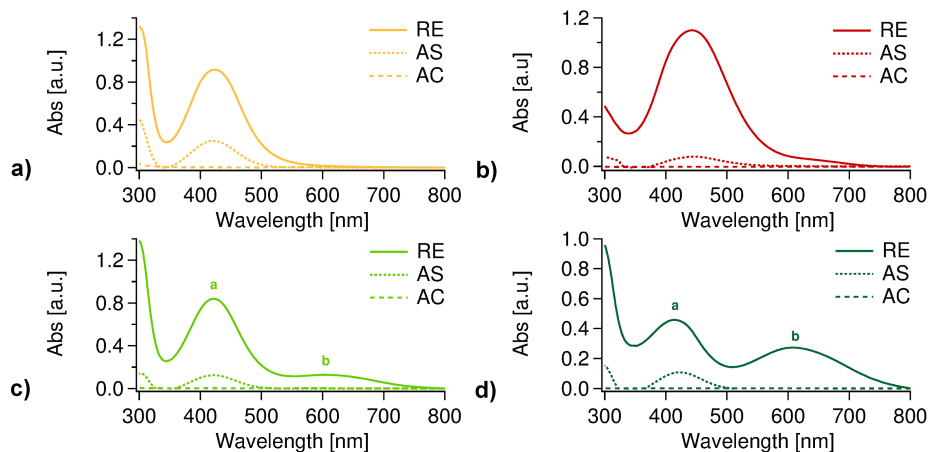


Figure 4.10: UV-Visible absorption of the four real effluents: a)RE1, b)RE2, c)RE3, d)RE4. For each effluent was reported the comparison between the initial absorption (solid line), the absorption after the incubation with active sludge (AS, dotted line) and active carbon (AC, dashed line).

Figure 4.11: Color removal for the four real dyeing effluents after the first (AS) and the second (AC) remediation step.

	AS	AC
RE1	75.7	99.6
RE2	92.8	99.9
RE3	a) 85.2 b) 99.8	a) 99.7 b) 99.8
RE4	a) 76.4 b) 99.7	a) 99.7 b) 99.9

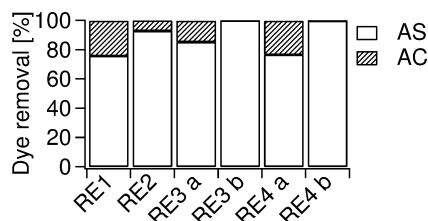


Figure 4.12: Color removal for the four real dyeing effluents (RE1, RE2, RE3 a-b, RE4 a-b) obtained upon subsequent incubation with AS and AC.

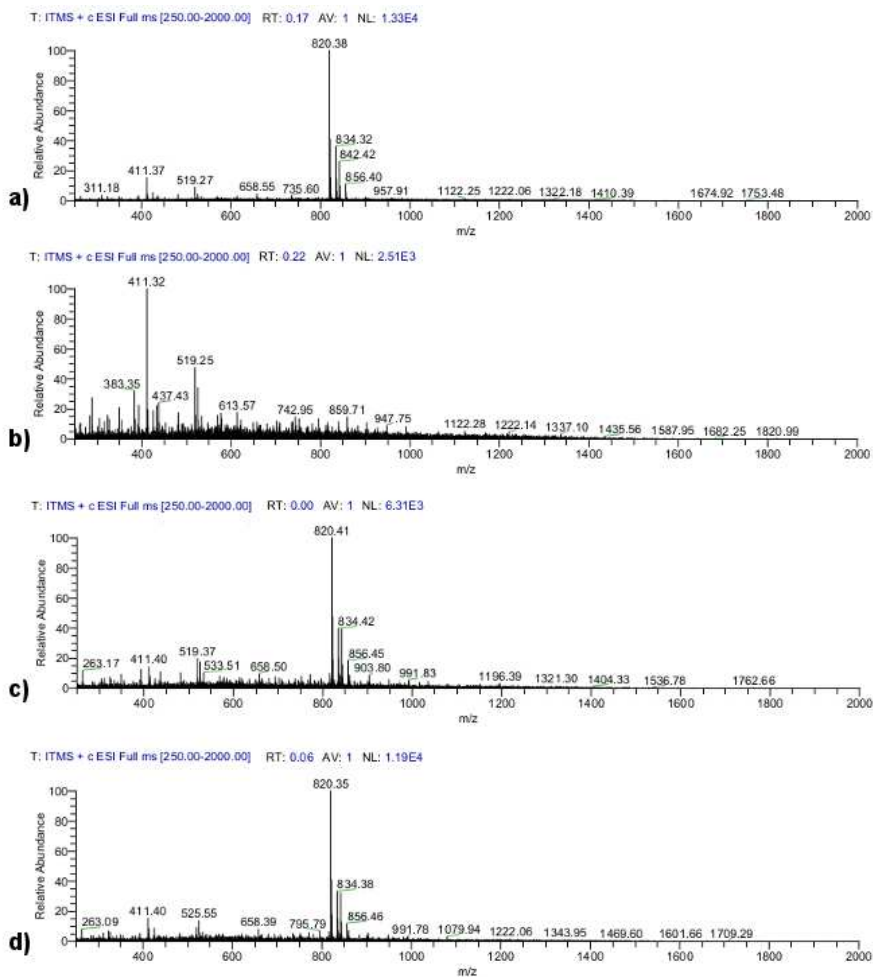


Figure 4.13: Mass spectrometry analysis on the four glycoconjugated dyes real leather dyeing effluents after bioremediation with highly specialized active sludge. a)RE1, b)RE2, c)RE3, d)RE4.

NY42 resulted the more recalcitrant molecule of the four. As demonstrated by mass spectrometry analysis of the solution after the incubation with AS, NY42 could be retraced in RE1, RE3 and RE4 (Fig. 4.13a-c-d). Moreover, none of the other dyes (NB27, NR202, NO30) were identified in the treated effluents after AS, indicating that microorganisms were able to degrade these molecules. However, even if NY42 resulted more resistant than the other dyes to microbial degradation, active sludge proved to be more effective on this molecule compared to *F. trogii* Laccases enzymes. In fact, while the fungus removed only up to 37% of the dye, combining degradation and absorption mechanisms, AS succeeded in degrading 73% of the dye in 36 hours. In all four effluents, also LP

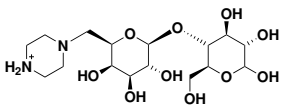
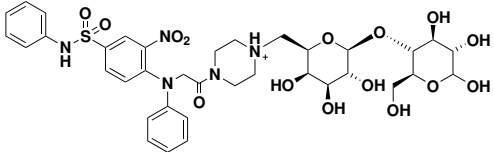
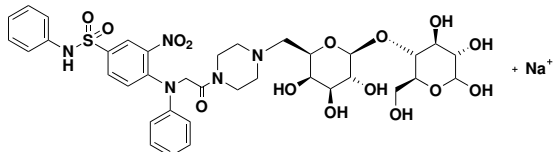
M/Z	Sample	Fragment
411	RE1 RE2 RE3 RE4	
820	RE1 RE3 RE4	
842	RE1 RE4	

Table 4.5: Main fragments retraced in GDs real effluents after bioremediation by highly specialized active sludge.

was retraced after incubation with AS. This molecule could either originate from the GDs degradation process or be a residue from the synthetic procedure itself, as already pointed out in Section 4.2. The main fragment identified in these effluents after AS step were reported in Table 4.5. The results obtained from bioremediation of GDs with AS underlined two important facts. First of all, none of the aromatic amines that could result from GDs degradation (see Section 4.4) were retraced in solution (see Fig. 4.13). Moreover, the almost complete removal of color from the solution suggested that water used for GDs

dyeing processes could be recycled after remediation.

4.4 Experimental

4.4.1 Effluents

Simulated effluents Single dye aqueous solutions of NR202, NB27, NO30, NY42 and their equimolar mixture were prepared adding the dye powder to the water volume. All the samples had a concentration of 0.3 mg/ml, the average concentration of an exhausted leather dyeing bath.

Real effluents Mixtures of the four GDs NR202, NB27, NO30, NY42, were used in a real dyeing process, performed by Biokimica s.p.a. (Santa Croce sull'Arno, Pisa, Italy) for the European project LIFE12 ENV/IT/000352 BIONAD. The four samples presented here were collected from the exhausted dyeing baths. The mixtures had the following initial composition:

RE1 80% NY42, 20% NO30

RE2 5% NR202, 90% NO30, 5% NB27

RE3 72% NY42, 18% NO30, 10% NB27

RE4 40% NY42, 10% NO30, 50% NB27

Fungi culture

The entire fungi culture process was performed under sterile condition, under laminated flow hood, using equipment and glassware that were either sterile or had been sterilized in autoclave at 120°C for 20 min. *F. trogii* was stored at -20°C, therefore it was revived before the use. To do so, it was first incubated at 28°C on a solid growth medium (MEA). Then, the fungus was transferred in liquid medium (BRM) and incubated again at 28°C under stirring at 300 rpm.

MEA

- 20 g/l Malt-extract
- 20 g/l Agar
- 2 g/l Triptone

CHAPTER 4. BIOREMEDIATION OF GLYCOCONJUGATED DYES

- 20 g/l Glucose
- H₂O

Transfer the powders in a screw cap flask, add the water and mix until blended. Sterilize at 120°C for 25 minutes in autoclave. When the solution has cooled down at 60°C, it was poured in Petri dishes (approximately 30 ml in each one) under laminated flow hood to avoid contamination. These dishes were irradiated with UV light for 1 hour and left to dry out under biological hood overnight. After that they were irradiated again with UV light for 30 minutes.

BRM

- 0.6 g/l L-Asparagine
- 1 g/l KH₂PO₄
- 0.5 g/l KCl
- 0.5 g/l Yeast extract
- 10 g/l Glucose
- 10 g/l Triptone
- 3 mg/l MnSO₄
- 10 mg/l Fe SO₄ 7H₂O
- 3 mg/l CuSO₄
- 2 mg/l ZnSO₄ H₂O
- 1 g/l MgSO₄ 7H₂O
- 50 mg/l Ca(NO₃)₂
- H₂O

The solution was sterilized in autoclave at 120°C for 25 minutes.

CZAPEK

- 6 g/l NaNO₃
- 0.52 g/l KCl
- 0.52 g/l MgSO₄ 7H₂O
- 1.52 g/l KH₂PO₄
- 10 mg/l Fe SO₄ 7H₂O
- 3 mg/l CuSO₄
- 2 mg/l ZnSO₄ H₂O
- H₂O

The solution was sterilized in autoclave at 120°C for 25 minutes.

4.4.2 Bioremediation methodology with *Funalia trogii*

Three conditions were used in this study. Samples were treated with *F. trogii* biomass, with (FG) and without (F) a nutrition source. Glucose at a concentration of 10 g/l was used as nutrition source. Moreover, samples were also treated with dead fungal biomass

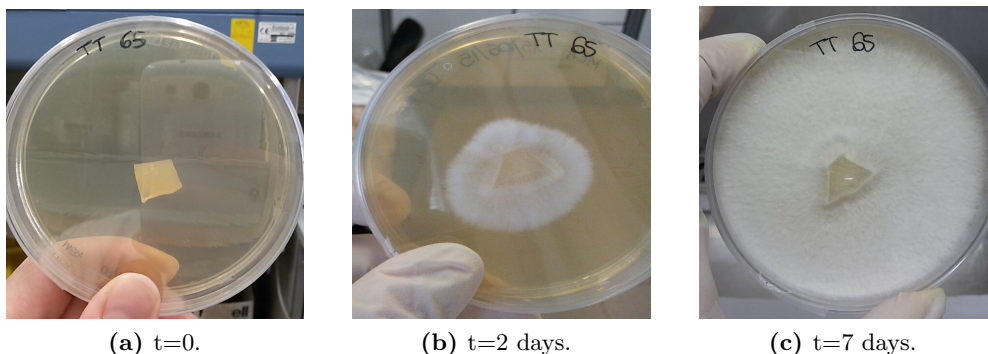


Figure 4.14: *Funalia trogii* regeneration procedure on MEA solid medium.

(DF). The experimental procedure consisted in many steps, including fungal growth in several culture media. Hereafter a description of each stage is reported.

Regeneration *F. trogii* was stored at low temperature (-20°C) and it needed to be revived before use. Thus, it was inoculated on solid medium (MEA) and incubated at 28°C for approximately a week, until it had spread on all the surface of the Petri dish.

Liquid growth Each Petri dish used was divided into 8 identical slices. One of these slices was dried in oven at 60°C in order to obtain the initial quantity of microorganism added to the culture medium. The proportion used for the liquid growth of the fungus was one slice for every 100 ml of sample solution. The slice was divided in 10 smaller pieces and added to the right volume of liquid culture medium (BRM). This stage was carried out in flasks of suitable volume, that has to be at least twofold that of the BRM. That was necessary in order to guarantee the right amount of oxygen to the culture during all the liquid growth step. For the same reason, the flasks should be closed with caps that ensure air penetration, such as cellulose caps. After the addition of *F. trogii*, all flasks were left shaking at 130 rpm at room temperature for 7 to 10 days.

Homogenization and recovery Once the fungus was fully grown, the culture broth was filtered in order to separate the biomass from the medium. Then, the fungus was transferred in CZAPEK and homogenized, to guarantee a homogeneous distribution

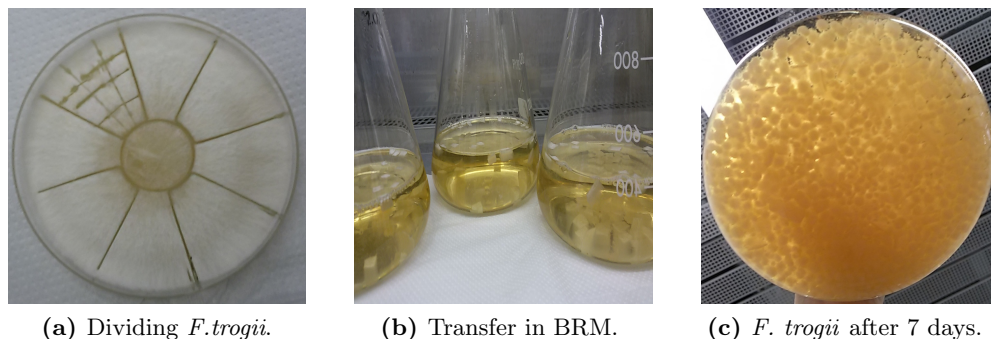


Figure 4.15: *Funalia trogii* growth procedure in BRM liquid medium.

of the microorganism in all the volume. CZAPEK is different from BRM, as it doesn't contain carbon source. This step has to be carried out in the same volume and oxygen conditions as those reported for the liquid growth stage. All flasks were left shaking at 130 rpm at room temperature for 3 days, in order to allow *F. trogii* to recover after the blending. This whole step was skipped to obtain the dead fungal biomass. In this case, after the liquid growth stage in BRM, the micro-organism was heated in autoclave at 120°C for 25 minutes.

Incubation The culture broth (100 mL) recovered from the sterilizing step was filtered and added to 100 ml of sample. This procedure was followed for both the living and dead biomasses. Then the samples were incubated at room temperature shaking at 130 rpm for 20 days. One batch of 100 ml culture broth was dried in oven at 60°C and then weighted, to evaluate the initial biomass inoculated with GDs effluents.

Monitoring During all the experiment color removal and enzyme activity levels were monitored, collecting 1 ml of solution from each sample at regular time intervals. The absorbance of these samples was measured and compared to the initial one. Enzyme activity was monitored with the assays described in Section 4.4.3. The biomass recovered at the end of the experiment was dried in oven at 60°C and then weighted to evaluate biomass decrease percentage by comparison with inoculated biomass.

4.4.3 Enzyme activity test

To verify the vitality of the revived microorganism, enzyme activity tests were performed for Laccases and Manganese Peroxidases.

Laccases

- 800 μ l sodium citrate buffer 0.1 M (pH=3)
- 180 μ l sample
- 20 μ l ABTS 100 mM

The components should be added in this order. The cuvettes were shaken vigorously and the measurement readily started.

Conditions: $\lambda = 420$ nm, $T = 25^\circ\text{C}$, $t = 1$ minute

The enzyme activity (EA) was calculated as:

$$EA\left(\frac{U}{ml}\right) = \frac{\text{slope}}{6.48} \quad (4.1)$$

Manganese Peroxidases

- 720 μ l succinate lactate buffer 100 mM (pH=4.5)
- 100 μ l DMAB
- 50 μ l MBTH
- 100 μ l sample
- 25 μ l MnSO_4
- 5 μ l H_2O_2

The components should be added in this order. The cuvettes were shaken vigorously and the measurement readily started.

Conditions: $\lambda = 590$ nm, $T = 25^\circ\text{C}$, $t = 1$ minute

The enzyme activity was calculated as:

$$EA\left(\frac{U}{ml}\right) = \frac{\text{slope}}{3.29} \quad (4.2)$$

4.4.4 Bioremediation procedure with activated sludge

The active sludge was kindly provided by Cuoidepur s.r.l. (Santa Croce sull'Arno, Italy). The biomass was kept under oxygenation for 24 hours to allow the degradation



Figure 4.16: Activated sludge bioremediation procedure.

of any existing dye residues before the incubation with our real effluents. The activity of the sludge was then verified at pH 3, measuring the O_2 consumption for 6 minutes, which was $XXX \text{ mg l}^{-1}$ per hour. Then, in a 250 ml flask, 60 ml of each effluents were added to 30 ml of active sludge. These samples were stirred at 130 rpm at r.t. for 24 hours. To 15 ml of each sample 280 mg of active carbon were, then, added and the solutions were left under stirring at 130 rpm for 24 hours.

4.4.5 Color removal

The initial absorbance A_0 of each sample was measured in order to calculate the percentage of color removal (% C.R.) along the incubation. To monitor the process of color removal the absorbance (A) of each sample was measured and compared to its A_0 . To do so, Equation 4.3 was used.

$$\%C.R. = \frac{A_0 - A}{A_0} \times 100 \quad (4.3)$$

4.4.6 Aromatic Amines

GDs degradation, in particular degradation of azo dyes NR202 and NO30, as well as aniline dye NY42, could result in the production of aromatic amines, especially in AS case. Here were reported structures and exact masses for aromatic amines that could be obtained.

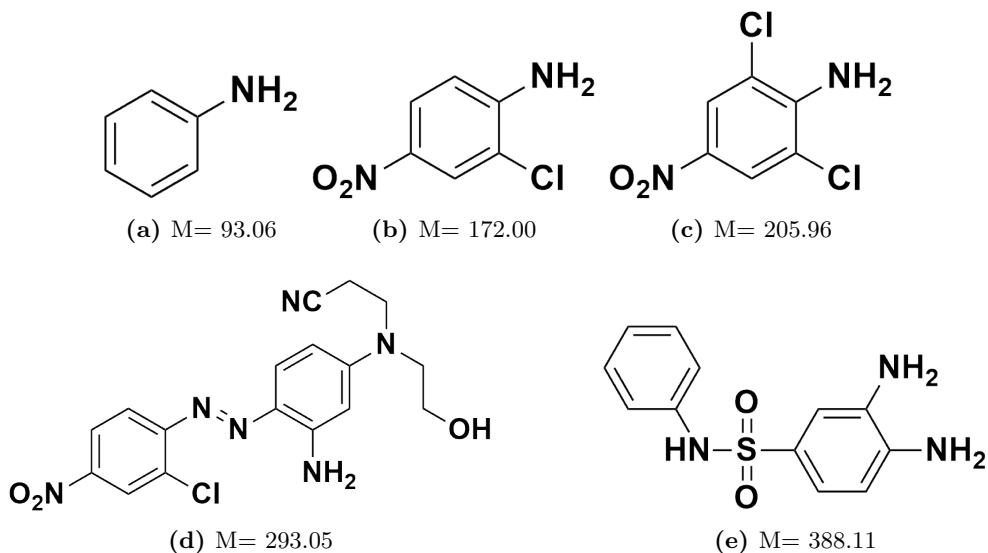


Figure 4.17: Exact mass for the five aromatic amines that could originate from GDs degradation.

4.4.7 Materials

D-(+)-Glucose 99.5%, KCl, MnSO_4 , $\text{FeSO}_4 \cdot 7\text{H}_2\text{O}$ >99.0%, CuSO_4 , L-Asparagine >98%, H_2O_2 (solution), 2,2'-Azino bis (3-Ethylbenzothiazoline 6 Sulphonic acid) diammonium salt >98%, 3-Methyl 2-Benzothiazoline hydrazone hydrochloride hydrate >99%, Citric acid monohydrate >99%, Succinic acid >99% and HCOOH 98-100% were purchased by Sigma-Aldrich (St. Louis, MO, USA). ZnSO_4 monohydrate >99%, $\text{MgSO}_4 \cdot 7\text{H}_2\text{O}$ >99%, Tryptone, Malt-extract, Agar, 3-(Dimethylamino) Benzoic acid >95%, and Lactic acid were supplied by Fluka Analytical (.). KH_2PO_4 and NaH_2PO_4 were purchased by ACROS (Geel, Belgium). Yeast extract and Peptone (buffered peptone water) were supplied by OXOID (Basingstoke, UK) while CaNO_3 and ultrapure MilliQ[®] water by Merck (Darmstadt, Germany).

4.4.8 UV-Visible spectrophotometry

UV-Visible measurements were carried out with a Perkin-Elmer Lambda EZ 201 (Waltham, Massachusetts, USA) in 1 cm disposable cuvettes. Spectra were regis-

tered in the wavelength range 300-800 nm.

4.4.9 Mass spectrometry

A 0.5 ml aliquot of each fungal treated and untreated dyeing effluent was diluted with 1 ml of HPLC grade methanol (Fisher Scientific, Leicestershire, UK) and then filtered on Titan2[®] Syringe Filter. The filtrate was analyzed using a ThermoScientific LCQ-Fleet mass spectrometer under electrospray ionization (ESI, +c technique) (Thermo Scientific, Austin TX, USA) by direct infusion with a 500 KL Hamilton micro-syringe and using a 10 $\mu\text{l min}^{-1}$ flow. The mass spectrometer parameters used were: sheet gas flow=10, spray voltage=5.00 kV, capillary tube temperature=270°C, capillary voltage=10.0 V and tube lens=75.0 V.

Chapter 5

Conclusion

In this work, five GDs of different nature were studied: azo dyes NR202 and NO30, anthraquinone dyes NB27 and NRC1 and aniline dye NY42. The amphiphilicity of these molecules, given by the presence of hydrophilic lactose and hydrophobic cores, allowed their self-assembly in solution. The presence of aggregates in water was confirmed for all five GDs by spectroscopic and scattering techniques. For three of these dyes, NRC1, NR202 and NY42, supramolecular chirality of their assemblies was verified by ECD. The influence of solvents on GDs self-assembly was investigated, revealing that aggregation did not take place in organic solvents and that their addition to GDs water solutions caused the disruption of preexisting objects. Mixtures of GDs in solution were also studied, underlining relevant interactions between NR202 and NB27, as well as between NRC1 and NO30. Particularly interesting were GDs interaction with three surfactants of different nature: non ionic TX, cationic CTAB and anionic SDS. All these molecules caused gradual disruption of dye aggregates, but at low concentration they perturbed GDs behavior, resulting in variations of the optical activity for NR202 and NY42 and helicity inversion for NRC1. Still at low surfactant concentrations, SDS case was particularly intriguing. In a specific range of surfactant concentration, reentrant condensation took place for all GDs, resulting in their precipitation. Interestingly, scattering investigations revealed that this condensation led to the formation of what appeared to be an ordered lamellar crystalline phase. Computational modeling of the cores of these five GDs, in particular their MD, revealed that these molecules interacted mainly by facial stacking interactions between their aromatic cores. The conformational search performed on GDs dimers underlined the possibility of elongation of the aggregates for NRC1, while it indicated that for NB27 and NO30 the system seemed to be too disordered for that. In both cases this was in perfect agreement with the information obtained by their physico-chemical charac-

terization. NY42 also resulted as a rather disordered system while the situation was intermediate for NR202, that appeared sufficiently ordered to elongate up to a certain extent. Biotechnological remediation of GDs effluents was attempted using two different approaches: non standard bioremediation of simulated effluents by *F. troglia* and standard bioremediation of real effluents by highly specialized activated sludge. The overall dye removal performances for both methodologies were rather good. Moreover, the results of both these procedures were in perfect agreement, underlining an easier removal from the solution for NR202 and NB27 and resistance toward biodegradation for NY42. In addition, mass spectrometry analysis on effluents after bioremediation revealed that aromatic amines were not produced by degradation of GDs in any case. GDs physico-chemical characterization allowed to identify some parameters that influenced their behavior in solution, such as solvent or presence of surfactants. These information are crucial and represent the foundation to refine GDs dyeing processes. For instance, knowing their behavior in solution, their solubility could be increased for dyeing purposes or their moiety could be modified to facilitate their deposition on a specific substrate. Further investigations on the interaction between GDs and anionic surfactant would be of interest, to understand if variations in surfactant's polar head or in its hydrophobic tail could have consequences on GDs behavior and reentrant condensation. Alkyl benzene sulfonates, sodium laureth sulfate and sodium decyl sulfate would all be very interesting candidates for this purpose. For the same reason, the effects of salts addition could be investigated. To better understand the atomistic interactions that took place between GDs during aggregation in solution, a fundamental step would be to extend the computational study on these molecules. In particular, MD should be performed on the entire GD molecule and also include the solvent. This would allow to obtain more realistic results and, with an additional TD-DFT analysis, could also provide simulated UV-Visible and ECD spectra. Moreover, MD calculations on interactions between GDs and surfactants or other additives could be a useful support for a refinement of dyeing conditions. The preliminary dye removal experiments presented in this work were relevant in light of GDs application in industrial dyeing. This is especially true for the standard bioremediation procedure with highly activated sludge. In fact, treating real GDs leather dyeing effluents with this simplified procedure gave good color removal results, regardless of the complex composition of this matrix. Pairing microorganisms action to a simple step, such as incubation with active carbon, led to complete removal of color from the solution. These results suggest that a more sophisticated and well-structured remediation procedure, as those employed in wastewater treatment plants, would be even more effective on GDs dyeing effluents. Therefore, using these dyes in industrial dyeing could allow to recycle the water employed in dyeing processes, that would be an excellent result. In fact, this would ensure not only lower costs for dyeing processes, but also decrease their environmental impact. Further bioremediation experiments could also be performed. The natural extension of this work would be to scale up the process for both

procedures, to resemble even more a real remediation case. In particular, it would be interesting to understand if the efficacy of *F. troglia* would change working out of sterile environment, or if working in a continuous system could enhance dye removal from GDs effluents for both the sludge and the white-rot fungus.

Bibliography

- [1] Shigehisa Akine, Shiho Sairenji, Takanori Taniguchi, and Tatsuya Nabeshima. Stepwise Helicity Inversions by Multisequential Metal Exchange. *Journal of the American Chemical Society*, 135(35):12948–12951, 2013.
- [2] Roi Asor, Orly Ben-nun-Shaul, Ariella Oppenheim, and Uri Raviv. Crystallization, Reentrant Melting, and Resolubilization of Virus Nanoparticles. *ACS Nano*, 11(10):9814–9824, 2017.
- [3] Francesco Babudri, Donato Colangiuli, Lorenzo Di Bari, Gianluca M. Fariola, Omar Hassan Omar, Francesco Naso, and Gennaro Pescitelli. Synthesis and chiroptical characterization of an amino acid functionalized dialkoxypoly(p-phenyleneethynylene). *Macromolecules*, 39(16):5206–5212, 2006.
- [4] Priya R. Banerjee, Anthony N. Milin, Mahdi Muhammad Moosa, Paulo L. Onuchic, and Ashok A. Deniz. Reentrant Phase Transition Drives Dynamic Substructure Formation in Ribonucleoprotein Droplets. *Angewandte Chemie International Edition*, 56(38):11354–11359, 2017.
- [5] Nina Berova, Lorenzo Di Bari, and Gennaro Pescitelli. Application of electronic circular dichroism in configurational and conformational analysis of organic compounds. *Chem. Soc. Rev.*, 36(6):914–931, 2007.
- [6] R. Bianchini, M. Corsi, and M. Bonanni. Coloring agents naturalised with the 6'-deoxy-6'-(piperazinyl)lactose moiety, November 2014.
- [7] Roberto Bianchini, Massimo Rolla, Jalal Isaad, Giorgio Catelani, Lorenzo Guazzelli, Massimo Corsi, and Marco Bonanni. Efficient double glycoconjugation to naturalize high molecular weight disperse dyes. *Carbohydrate Research*, 356(Supplement C):104–109, 2012.
- [8] Victor A. Bloomfield. DNA condensation by multivalent cations. *Biopolymers*, 44(3):269–282, 1997.

BIBLIOGRAPHY

- [9] Uwe H. F. Bunz. Poly(aryleneethynylene)s: Syntheses, properties, structures and applications. *Chemical Reviews*, 100(4):1605–1644, 2000.
- [10] Uwe H. F. Bunz. Poly(aryleneethynylene)s. *Macromolecular Rapid Communications*, 30(9-10):772–805, 2009.
- [11] Max Burian, Francesco Rigodanza, Heinz Amenitsch, László Almásy, Ivan Khalakhan, Zois Syrgiannis, and Maurizio Prato. Structural and optical properties of a perylene bisimide in aqueous media. *Chemical Physics Letters*, 683:454–458, 2017. Ahmed Zewail (1946-2016) Commemoration Issue of Chemical Physics Letters.
- [12] L. Calugi, M. Bonanni, M. Corsi, S. Chimichi, and R. Bianchini. Suzuki and Heck Processes for the Synthesis of New Anthraquinone-Based Glycoconjugated Dyes. *ChemistrySelect*, 3(8):2235–2239, 2018.
- [13] Si Hui Chen and Adeline Su Yien Ting. Biosorption and biodegradation potential of triphenylmethane dyes by newly discovered *Penicillium simplicissimum* isolated from indoor wastewater sample. *International Biodeterioration & Biodegradation*, 103(Supplement C):1–7, 2015.
- [14] Ilaria Ciullini, Silvia Tilli, Andrea Scozzafava, and Fabrizio Briganti. Fungal laccase, cellobiose dehydrogenase, and chemical mediators: Combined actions for the decolorization of different classes of textile dyes. *Bioresource Technology*, 99(15):7003 – 7010, 2008.
- [15] Matthew Clark. *Handbook of textile and industrial dyeing: principles, processes and types of dyes*. Elsevier, 2011.
- [16] Wendy D Cornell, Piotr Cieplak, Christopher I Bayly, Ian R Gould, Kenneth M Merz, David M Ferguson, David C Spellmeyer, Thomas Fox, James W Caldwell, and Peter A Kollman. A second generation force field for the simulation of proteins, nucleic acids, and organic molecules. *Journal of the American Chemical Society*, 117(19):5179–5197, 1995.
- [17] S. Rodríguez Couto. Decolouration of industrial azo dyes by crude laccase from *Trametes hirsuta*. *Journal of Hazardous Materials*, 148(3):768–770, 2007.
- [18] Piya Das Ghatak, Shomita S. Mathew-Steiner, Priyanka Pandey, Sashwati Roy, and Chandan K. Sen. A surfactant polymer dressing potentiates antimicrobial efficacy in biofilm disruption. *Scientific Reports*, 8(1):873, 2018.

- [19] K. Dirian, S. Bauroth, A. Roth, Z. Syrgiannis, F. Rigodanza, M. Burian, H. Amenitsch, D. I. Sharapa, M. Prato, T. Clark, and D. M. Guldi. A water-soluble, bay-functionalized peryleneimide derivative – correlating aggregation and excited state dynamics. *Nanoscale*, 10(5):2317–2326, 2018.
- [20] Rainer Fiesel, Carrie E. Halkyard, Mary E. Rampey, Lioba Kloppenburg, Shannon L. Studer-Martinez, Ullrich Scherf, and Uwe H. F. Bunz. Aggregation and chiroptical behavior of a high molecular weight chirally substituted dialkylpoly(p-phenyleneethynylene). *Macromolecular Rapid Communications*, 20(3):107–111, 1999.
- [21] Dengwei Fu, Juntao Li, Jie Wei, and Jinbao Guo. Effects of terminal chain length in hydrogen-bonded chiral switches on phototunable behavior of chiral nematic liquid crystals: Helicity inversion and phase transition. *Soft Matter*, 11(15):3034–3045, 2015.
- [22] Anna Maria Garzillo, Maria Chiara Colao, Vincenzo Buonocore, Romina Oliva, Lucia Falcigno, Michele Saviano, Anna Maria Santoro, Riccardo Zappala, Raffaele Pietro Bonomo, Carmelina Bianco, Paola Giardina, Gianna Palmieri, and Giovanni Sannia. Structural and kinetic characterization of native laccases from *pleurotus ostreatus*, *rigidoporus lignosus*, and *trametes trogii*. *Journal of Protein Chemistry*, 20(3):191–201, 2001.
- [23] Emanuel Grassi, Pablo Scodeller, Nestor Filiel, Romina Carballo, and Laura Levin. Potential of *Trametes trogii* culture fluids and its purified laccase for the decolorization of different types of recalcitrant dyes without the addition of redox mediators. *International Biodeterioration & Biodegradation*, 65(4):635–643, 2011.
- [24] Sibao Guo, Hiroki Kamite, Nozomu Suzuki, Laibing Wang, Asuka Ohkubo, and Michiya Fujiki. Ambidextrous Chirality Transfer Capability from Cellulose Tris(phenylcarbamate) to Nonhelical Chainlike Luminophores: Achiral Solvent-Driven Helix-Helix Transition of Oligo- and Polyfluorenes Revealed by Sign Inversion of Circularly Polarized Luminescence and Circular Dichroism Spectra. *Biomacromolecules*, 19(2):449–459, 2018.
- [25] Ian W. Hamley, Ashkan Dehsorkhi, Valeria Castelletto, Jani Seitsonen, Janne Ruokolainen, and Hermis Iatrou. Self-assembly of a model amphiphilic oligopeptide incorporating an arginine headgroup. *Soft Matter*, 9:4794–4801, 2013.
- [26] Boualem Hammouda. Probing nanoscale structures-the sans toolbox. *National Institute of Standards and Technology*, pages 1–717, 2008.

BIBLIOGRAPHY

- [27] Heiko Heerklotz. Interactions of surfactants with lipid membranes. *Quarterly Reviews of Biophysics*, 41(3-4):205–264, 2008.
- [28] Derek L. Ho, Boualem Hammouda, Steven R. Kline, and Wei-Ren Chen. Unusual phase behavior in mixtures of poly(ethylene oxide) and ethyl alcohol. *Journal of Polymer Science Part B: Polymer Physics*, 44(3):557–564, 2006.
- [29] Pai-Yi Hsiao. Overcharging, Charge Inversion, and Reentrant Condensation: Using Highly Charged Polyelectrolytes in Tetravalent Salt Solutions as an Example of Study. *The Journal of Physical Chemistry B*, 112(25):7347–7350, 2008.
- [30] Yongwei Huang, Jianchen Hu, Wenfeng Kuang, Zhixiang Wei, and Charl F. J. Faul. Modulating helicity through amphiphilicity—tuning supramolecular interactions for the controlled assembly of perylenes. *Chem. Commun.*, 47(19):5554–5556, 2011.
- [31] Yongwei Huang, Junchao Wang, and Zhixiang Wei. Modulating supramolecular helicity and electrical conductivity of perylene dyes through an achiral alkyl chain. *Chem. Commun.*, 50(61):8343–8345, 2014.
- [32] Zhegang Huang, Seong-Kyun Kang, Motonori Banno, Tomoko Yamaguchi, Dongseon Lee, Chaok Seok, Eiji Yashima, and Myongsoo Lee. Pulsating Tubules from Noncovalent Macrocycles. *Science*, 337(6101):1521–1526, 2012.
- [33] Klaus Hunger, Peter Mischke, Wolfgang Rieper, and Shufen Zhang. *Azo Dyes, 3. Direct (Substantive) Dyes*, pages 1–14. American Cancer Society, 2018.
- [34] Anna Jasińska, Sylwia Różalska, Przemysław Bernat, Katarzyna Paraszkiwicz, and Jerzy Dhugoński. Malachite green decolorization by non-basidiomycete filamentous fungi of *Penicillium pinophilum* and *Myrothecium roridum*. *International Biodeterioration & Biodegradation*, 73(Supplement C):33–40, 2012.
- [35] Xuan Jiang, Young-Kwan Lim, Bong June Zhang, Elizabeth A. Opsitnick, Mu-Hyun Baik, and Dongwhan Lee. Dendritic Molecular Switch: Chiral Folding and Helicity Inversion. *Journal of the American Chemical Society*, 130(49):16812–16822, 2008.
- [36] Akhil N. Kabra, Rahul V. Khandare, and Sanjay P. Govindwar. Development of a bioreactor for remediation of textile effluent and dye mixture: A plant–bacterial synergistic strategy. *Water Research*, 47(3):1035–1048, 2013.
- [37] Jisung Kim, Jinhee Lee, Woo Young Kim, Hyungjun Kim, Sanghwa Lee, Hee Chul Lee, Yoon Sup Lee, Myungeun Seo, and Sang Youl Kim. Induction and control of supramolecular chirality by light in self-assembled helical nanostructures. *Nature Communications*, 6:6959, 2015.

- [38] Ryou Kubota, Shohei Tashiro, and Mitsuhiko Shionoya. Chiral metal–macrocycle frameworks: Supramolecular chirality induction and helicity inversion of the helical macrocyclic structures. *Chem. Sci.*, 7(3):2217–2221, 2016.
- [39] Mayur B. Kurade, Tatoba R. Waghmode, and Sanjay P. Govindwar. Preferential biodegradation of structurally dissimilar dyes from a mixture by *Brevibacillus laterosporus*. *Journal of Hazardous Materials*, 192(3):1746–1755, 2011.
- [40] Laura Levin, Emanuel Grassi, and Romina Carballo. Efficient azoic dye degradation by *Trametes trogii* and a novel strategy to evaluate products released. *International Biodeterioration & Biodegradation*, 75(Supplement C):214–222, 2012.
- [41] Guofeng Liu, Xin Li, Jianhui Sheng, Pei-Zhou Li, Wee Kong Ong, Soo Zeng Fiona Phua, Hans Ågren, Liangliang Zhu, and Yanli Zhao. Helicity Inversion of Supramolecular Hydrogels Induced by Achiral Substituents. *ACS Nano*, 11(12):11880–11889, 2017.
- [42] Guofeng Liu, Jianhui Sheng, Hongwei Wu, Chaolong Yang, Guangbao Yang, Yongxin Li, Rakesh Ganguly, Liangliang Zhu, and Yanli Zhao. Controlling Supramolecular Chirality of Two-Component Hydrogels by J- and H-Aggregation of Building Blocks. *Journal of the American Chemical Society*, 140(20):6467–6473, 2018.
- [43] Josée-Anne Majeau, Satinder K. Brar, and Rajeshwar Dayal Tyagi. Laccases for removal of recalcitrant and emerging pollutants. *Bioresource Technology*, 101(7):2331–2350, 2010.
- [44] Tzenka Miteva, Liam Palmer, Lioba Kloppenburg, Dieter Neher, and Uwe H. F. Bunz. Interplay of thermochromicity and liquid crystalline behavior in poly(p-phenyleneethynylene)s: π - π interactions or planarization of the conjugated backbone? *Macromolecules*, 33(3):652–654, 2000.
- [45] Mozhgan Nazari, Mustafa Kurdi, and Heiko Heerklotz. Classifying Surfactants with Respect to Their Effect on Lipid Membrane Order. *Biophysical Journal*, 102(3):498–506, 2012.
- [46] Frank Neese. Prediction of molecular properties and molecular spectroscopy with density functional theory: From fundamental theory to exchange-coupling. *Coordination Chemistry Reviews*, 253(5):526 – 563, 2009.
- [47] Frank Neese. The orca program system. *Wiley Interdisciplinary Reviews: Computational Molecular Science*, 2(1):73–78, 2012.
- [48] Frank Neese. Software update: the orca program system, version 4.0. *Wiley Interdisciplinary Reviews: Computational Molecular Science*, 8(1):e1327, 2018.

BIBLIOGRAPHY

- [49] Čeněk Novotný, Nicolina Dias, Anu Kapanen, Kateřina Malachová, Marta Vándrovcová, Merja Itävaara, and Nelson Lima. Comparative use of bacterial, algal and protozoan tests to study toxicity of azo- and anthraquinone dyes. *Chemosphere*, 63(9):1436–1442, 2006.
- [50] Cristiane Ottoni, Luis Lima, Cledir Santos, and Nelson Lima. Effect of Different Carbon Sources on Decolourisation of an Industrial Textile Dye Under Alkaline–Saline Conditions. *Current Microbiology*, 68(1):53–58, 2014.
- [51] Daniele Padula, Fabrizio Santoro, and Gennaro Pescitelli. A simple dimeric model accounts for the vibronic ecd spectra of chiral polythiophenes in their aggregated states. *RSC Adv.*, 6:37938–37943, 2016.
- [52] Fang Pan, Zongyi Li, Haoning Gong, Jordan T. Petkov, and Jian R. Lu. Membrane-lytic actions of sulphonated methyl ester surfactants and implications to bactericidal effect and cytotoxicity. *Journal of Colloid and Interface Science*, 531:18–27, 2018.
- [53] John P. Perdew, Matthias Ernzerhof, and Kieron Burke. Rationale for mixing exact exchange with density functional approximations. *The Journal of Chemical Physics*, 105(22):9982–9985, 1996.
- [54] Gennaro Pescitelli, Lorenzo Di Bari, and Nina Berova. Application of electronic circular dichroism in the study of supramolecular systems. *Chem. Soc. Rev.*, 43(15):5211–5233, 2014.
- [55] Gennaro Pescitelli, Omar Hassan Omar, Alessandra Operamolla, Gianluca M. Farinola, and Lorenzo Di Bari. Chiroptical Properties of Glucose-Substituted Poly(p-phenylene-ethynylene)s in Solution and Aggregate State. *Macromolecules*, 45(24):9626–9630, 2012.
- [56] Dirk Pijper, Mahtild G. M. Jongejan, Auke Meetsma, and Ben L. Feringa. Light-Controlled Supramolecular Helicity of a Liquid Crystalline Phase Using a Helical Polymer Functionalized with a Single Chiroptical Molecular Switch. *Journal of the American Chemical Society*, 130(13):4541–4552, 2008.
- [57] Steve Plimpton. Fast parallel algorithms for short-range molecular dynamics. *Journal of Computational Physics*, 117(1):1 – 19, 1995.
- [58] Judith K. Pollack, Steven D. Harris, and Mark R. Marten. Autophagy in filamentous fungi. *Fungal Genetics and Biology*, 46(1):1–8, 2009.
- [59] Valeria Prigione, Valeria Tigini, Cinzia Pezzella, Antonella Anastasi, Giovanni Sannia, and Giovanna Cristina Varese. Decolourisation and detoxification of textile effluents by fungal biosorption. *Water Research*, 42(12):2911–2920, 2008.

- [60] Stephen W. Provencher. A constrained regularization method for inverting data represented by linear algebraic or integral equations. *Computer Physics Communications*, 27(3):213–227, 1982.
- [61] Guangyan Qing, Xingxing Shan, Wenrui Chen, Ziyu Lv, Peng Xiong, and Taolei Sun. Solvent-Driven Chiral-Interaction Reversion for Organogel Formation. *Angewandte Chemie International Edition*, 53(8):2124–2129, 2014.
- [62] Claudio Resta, Sebastiano Di Pietro, Maja Majerić Elenkov, Zdenko Hameršak, Gennaro Pescitelli, and Lorenzo Di Bari. Consequences of Chirality on the Aggregation Behavior of Poly[2-methoxy-5-(2'-ethylhexyloxy)-p-phenylenevinylene] (MEH-PPV). *Macromolecules*, 47(15):4847–4850, 2014.
- [63] Claudio Resta, Gennaro Pescitelli, and Lorenzo Di Bari. Natural α -Amino Acid-Functionalized Poly(phenyleneethynylene)s (PPEs): Synthesis and Chiroptical Characterization of Aggregate States. *Macromolecules*, 47(20):7052–7059, 2014.
- [64] Susana Rodríguez Couto. Dye removal by immobilised fungi. *Biotechnology Advances*, 27(3):227–235, 2009.
- [65] Shiho Sairenji, Shigehisa Akine, and Tatsuya Nabeshima. Response speed control of helicity inversion based on a “regulatory enzyme”-like strategy. *Scientific Reports*, 8(1):137, 2018.
- [66] S. Sennato, F. Bordi, and C. Cametti. On the phase diagram of reentrant condensation in polyelectrolyte-liposome complexation. *The Journal of Chemical Physics*, 121(10):4936–4940, 2004.
- [67] Ram Lakhan Singh, Pradeep Kumar Singh, and Rajat Pratap Singh. Enzymatic decolorization and degradation of azo dyes – A review. *International Biodeterioration & Biodegradation*, 104(Supplement C):21–31, 2015.
- [68] Astha Sinha and W. Jabez Osborne. Biodegradation of reactive green dye (RGD) by indigenous fungal strain VITAF-1. *International Biodeterioration & Biodegradation*, 114(Supplement C):176–183, 2016.
- [69] Daniel Soraruf, Felix Roosen-Runge, Marco Grimaldo, Fabio Zanini, Ralf Schweins, Tilo Seydel, Fajun Zhang, Roland Roth, Martin Oettel, and Frank Schreiber. Protein cluster formation in aqueous solution in the presence of multivalent metal ions – a light scattering study. *Soft Matter*, 10(6):894–902, 2014.
- [70] Charles Tanford. *The hydrophobic effect: formation of micelles and biological membranes 2d ed.* J. Wiley., 1980.

BIBLIOGRAPHY

- [71] Junmei Wang, Romain M. Wolf, James W. Caldwell, Peter A. Kollman, and David A. Case. Development and testing of a general amber force field. *Journal of Computational Chemistry*, 25(9):1157–1174, 2004.
- [72] Dirk Wesenberg, Irene Kyriakides, and Spiros N Agathos. White-rot fungi and their enzymes for the treatment of industrial dye effluents. *VI International Symposium on Environmental Biotechnology*, 22(1):161–187, 2003.
- [73] Jinping Yan, Jiezhen Niu, Daidi Chen, Yuhui Chen, and Chagan Irbis. Screening of *Trametes* strains for efficient decolorization of malachite green at high temperatures and ionic concentrations. *International Biodeterioration & Biodegradation*, 87(Supplement C):109–115, 2014.
- [74] Steffen Zahn and Timothy M. Swager. Three-Dimensional Electronic Delocalization in Chiral Conjugated Polymers. *Angewandte Chemie*, 114(22):4399–4404, 2002.
- [75] F. Zhang, M. W. A. Skoda, R. M. J. Jacobs, S. Zorn, R. A. Martin, C. M. Martin, G. F. Clark, S. Weggler, A. Hildebrandt, O. Kohlbacher, and F. Schreiber. Reentrant Condensation of Proteins in Solution Induced by Multivalent Counterions. *Phys. Rev. Lett.*, 101(14):148101, 2008.
- [76] Fajun Zhang, Sophie Weggler, Michael J. Ziller, Luca Ianeselli, Benjamin S. Heck, Andreas Hildebrandt, Oliver Kohlbacher, Maximilian W. A. Skoda, Robert M. J. Jacobs, and Frank Schreiber. Universality of protein reentrant condensation in solution induced by multivalent metal ions. *Proteins: Structure, Function, and Bioinformatics*, 78(16):3450–3457, 2010.
- [77] Li Zhang and Minghua Liu. Supramolecular Chirality and Chiral Inversion of Tetraphenylsulfonato Porphyrin Assemblies on Optically Active Polylysine. *The Journal of Physical Chemistry B*, 113(42):14015–14020, 2009.
- [78] Xueheng Zhao, Yiping Lu, Dennis R. Phillips, Huey-Min Hwang, and Ian R. Hardin. Study of biodegradation products from azo dyes in fungal degradation by capillary electrophoresis/electrospray mass spectrometry. *Mass Spectrometry: Innovation and Application. Part V: Capillary Electrophoresis - Mass Spectrometry*, 1159(1):217–224, 2007.
- [79] Heinrich Zollinger. *Color chemistry: syntheses, properties, and applications of organic dyes and pigments*. John Wiley & Sons, 2003.

Acknowledgements

My deepest gratitude goes to Prof. Roberto Bianchini, who believed in me and gave me the opportunity to work on this project. My heartfelt thanks goes also to Prof. Debora Berti, that with her patience and kindness guided me through this work, helping me as much as she could. I would like to thank also Prof. Piero Baglioni and CSGI group, that provided funding for this project. For the financial support of the bioremediation part of this work, included in LIFE project BioNaD, I thank the European Community. For their help with SAXS measurements, I deeply thank Prof. Emiliano Fratini and Dr Paolo Tempesti, as well as Dr Claudio Resta for his patience and advice on ECD analysis. Thanks to Prof. Andrea Scozzafava and Silvia Tilli, that allowed me to use their laboratories and guided me when I approached biotechnological remediation for the first time. I also would like to thank Dr Marco Bonanni and Dr Massimo Corsi for the advices they gave me in this three years. For all the time we brainstormed, fought, helped and supported each other, I also thank my colleague Lorenzo Calugi, with whom I shared this journey. My gratitude goes to Dr Alessandro Lunghi, that patiently guided me along when I was learning how to use computational tools. All my love goes to my father, that supported me all along, believing in me and loving me no matter what. Thanks to all my friends, Roberta, Martina, Marco and Alessandro, that with their presence helped me to get through this time. A special mention goes to Irene and Giulia, that not only were friends to me, but also colleagues and kindly shared their knowledge with me when I needed advice. Finally, from the bottom of my heart, my gratitude goes to my best friend of all, Alessandro, who supported me, encouraged me and shared with me the worst and the best parts of this time. Thanks for being always there for me. You gave me the strength to do this.